Applied Catalysis B: Environment and Energy 348 (2024) 123683

Contents lists available at ScienceDirect

Applied Catalysis B: Environment and Energy

journal homepage: www.elsevier.com/locate/apcatb

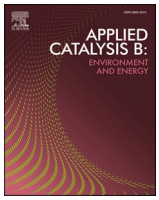

Atomic-level coordination structures meet graphitic carbon nitride (g-C_3N_4) for photocatalysis: Energy conversion and environmental remediation

Haiwei Su [1], Haibo Yin [1], Rong Wang, Yunlong Wang, William Orbell, Yue Peng, Junhua Li [*]

State Key Joint Laboratory of Environment Simulation and Pollution Control, School of Environment, Tsinghua University, Beijing 100084, PR China

ARTICLE INFO

Keywords:
Carbon nitride
Single atom catalyst
Photocatalysis
Energy conversion
Environmental remediation

ABSTRACT

Up to date, the single-atom catalysts (SACs) have provided a sustainable solution for mitigating the energy crisis and improving environmental quality. The enhanced efficiency and selectivity in various chemical reactions relies on the rational design of metal atom coordination environments and a deep understanding of the underlying mechanisms. The atomic-level coordination between metal species and graphitic carbon nitride (g-C_3N_4) support offers potential unique characteristics and advantages. This review summarizes and provides insights into the recent progress of g-C_3N_4-based SACs. We discuss the principles and benefits of introducing atomic-level metal sites on g-C_3N_4, as well as essential preparation methods and characterization techniques. We also explore the applications of g-C_3N_4-based SACs in photocatalytic energy conversion and environmental remediation to gain a comprehensive understanding of how single-metal sites impact activity, selectivity, and stability. Finally, we highlight both the opportunities and challenges for development of g-C_3N_4-based SACs in the future.

1. Introduction

The energy crisis and environmental pollution are formidable challenges facing our society today [1–5]. To combat these issues, scientists are constantly seeking new methods and technologies. Among these, photocatalysis has attracted widespread attention as an environmentally friendly and efficient technology for energy conversion and environmental remediation [6–8]. Numerous photocatalytic materials have been extensively researched and developed, including titanium dioxide (TiO_2) [9], zinc oxide (ZnO) [10], cadmium sulfide (CdS) [11], bismuth vanadate ($BiVO_4$) [12], metal-organic framework materials (MOF) [13], and graphitic carbon nitride (g-C_3N_4) [14], etc, which exhibit excellent photocatalytic performance under visible or ultraviolet light. The key steps of photocatalysis include light absorption [15], electron-hole pairs generation [16], and charge separation and transfer [17]. Initially, photons must have energy equal to or higher than the bandgap energy (E_g) of the photocatalyst, enabling semiconductor catalysts to absorb photons and reach an excited state [18]. Subsequently, the generated electrons and holes from the light excitation undergo internal conduction processes for charge separation, yielding free electrons and holes that migrate across the catalyst surface and participate in specific chemical reactions [19]. For example, the photo-generated electrons can be engaged in reduction reactions with substances like oxygen and water in the photocatalytic system, while the holes can engage in oxidation reactions. These redox reactions contribute to the formation of active species on the catalyst surface, thereby facilitating the progression of the desired chemical reactions.

Unfortunately, catalysts currently suffer from low utilization efficiency of solar energy and severe charge carrier recombination [20–22]. Furthermore, the selectivity and stability still need to be improved for the complex reactions. To tackle these challenges, researchers primarily focus on improving the performance of semiconductors through synthesis control [23], junction engineering [24], and structural optimization [25]. One common strategy for accelerating the charge separation is achieved by loading highly conductive nanoparticles, including noble metals (Au [26], Ag [27], Pt [28], etc.), sulfides (CdS [29], MoS_2 [30], CuS [31], etc.), carbonaceous quantum dots [32], etc. An emerging type of catalyst, single atom catalysts (SACs), possess several notable advantages compared to traditional nanoparticle catalysts. SACs are cost-effective and provide controllable active site density, high selectivity, and excellent catalytic stability [33–35]. With its high specific surface area and abundant C and N elemental content, g-C_3N_4 holds the

* Corresponding author.
E-mail address: lijunhua@tsinghua.edu.cn (J. Li).
[1] These authors contributed equally to this work.

https://doi.org/10.1016/j.apcatb.2023.123683
Received 16 November 2023; Received in revised form 28 December 2023; Accepted 29 December 2023
Available online 3 January 2024
0926-3373/

potential to form stable binding with isolated metal atoms [36]. Additionally, g-C_3N_4 features rich functional groups and modulated vacancies, enabling the adjustment of atomic size, composition, and dispersion. By tuning the species, anchoring position and coordination mode of single metal atoms, the electronic binding states can be modulated, thereby improving the charge dynamics [37]. Coordinating single metal atoms on the surface of g-C_3N_4 results in additional active sites and enhanced chemical reactivity, leading to higher catalytic efficiency and selectivity towards the target reaction. These advantages make g-C_3N_4-based SACs an ideal choice in the fields of energy and catalysis.

This review aims to systematically summarize and discuss the recent research progress of g-C_3N_4-based SACs in the field of photocatalysis in recent years. We will delve into the application of single atom coordination strategies on g-C_3N_4, including catalyst preparation, characterization methods, charge separation and transfer mechanisms, as well as optimization of photocatalytic performance. In addition, we explore the application prospects of SACs in various fields, such as water splitting, organic synthesis, pollutant degradation, CO_2 reduction, CH_4 conversion, etc. By conducting comparative studies across multiple domains, we can gain a better understanding and evaluation of the role of single atom coordination strategies in photocatalysis. Furthermore, we provide suggestions and prospects for their sustainable development in practical applications.

1.1. Graphitic carbon nitride (g-C_3N_4)

Graphitic carbon nitride (g-C_3N_4) is a two-dimensional material with unique structure and excellent properties. It consists of C and N elements, and the structure is similar to graphene with a honeycomb arrangement of hexagons [38–40]. Moreover, the g-C_3N_4 layers are stacked together through van der Waals forces, forming a porous three-dimensional structure as shown in Fig. 1. The conduction band (CB) of g-C_3N_4 is primarily formed by C 2p and N 2p orbitals, while the valence band (VB) is formed by N 2p orbitals [41,42]. As a result, the band structure exhibits a relatively narrow band gap, typically between 2.6–2.9 eV [43], enabling it to absorb light in the visible range.

In 2009, Wang et al. discovered that high-quality g-C_3N_4 could be synthesized through a simple thermal polymerization method [44], which sparked rapid developments in its applications in photocatalytic energy conversion and environmental remediation. Currently, g-C_3N_4 are primarily synthesized using methods such as thermal polymerization [45–47], hydrothermal synthesis [48], and chemical vapor deposition [49], etc. Researchers have been exploring the diversity of g-C_3N_4 materials and have discovered that in addition to crystalline g-C_3N_4, amorphous g-C_3N_4 has also attracted significant attention. For example, Xu et al. developed an O-doped amorphous g-C_3N_4 photocatalyst, exhibiting significantly enhanced photocatalytic activity for CO_2 reduction and methylene blue degradation [50]. Furthermore, g-C_3N_4 has also demonstrated potential in electrocatalysis [51–54], sensors [55], and optoelectronic devices [56]. Based on the high reactivity, tunable chemical composition, abundant defect structures and contribution to excellent performance, we hope that more attention and research efforts could generate towards g-C_3N_4.

1.2. Single atom catalysts (SACs) for photocatalysis

Single atom catalysts (SACs) represent an emerging research direction in the field of catalysis, wherein atomically dispersed metal sites (with no neighboring metal atoms) are utilized as active centers for efficient catalytic reactions [57–59]. In comparison to traditional nanoparticle catalysts, SACs offer unique advantages. The high catalytic activity of SACs is ensured due to the efficient utilization of each isolated atomic site [60]. Furthermore, SACs can avoid the activity loss caused by surface defects and aggregation, thereby enhancing the stability of the catalyst. Additionally, the single metal atoms are influenced by their specific electronic structures and coordination environments [61–63], enabling selective control over specific reaction pathways.

In 2011, Zhang et al. successfully prepared and characterized FeO_x-supported single Pt atoms [64], which initiated the research fervor in SACs. Initially, SACs were proposed to enhance the utilization of precious metal atoms due to their high cost [65,66]. Impressively, transition metal atoms possess complex electronic structures, including different d orbitals and energy levels, enabling their participation in various activation and transformation reactions [67,68]. This rich electronic structure allows transition metal atoms to exhibit remarkable performance in SACs. Thanks to advanced synthesis methods and characterization techniques, various types of SACs samples have been successfully synthesized, including Ir_1/TiO_2 [69], Rh/CeO_2 [70], PdPSA-CdS [71], Pd@MOF [72], Au/Cu single atom alloy [73], Ru_1/C_3N_4 [74], etc. Currently, SACs have demonstrated outstanding performance in many important photocatalytic reactions. For example, Wu et al. achieved remarkable results by constructing a highly active Pt_1-TiO_2 photocatalyst decorated with single Pt atoms [75]. They confirmed that hydrogen species were more readily induced into the sub-surface of the oxide support during the photocatalytic process, leading to the formation of a stable amorphous thin layer and significantly enhancing the photocatalytic H_2 evolution performance. In addition, Chen et al. reported for the first time the use of mesoporous g-C_3N_4 supported Pd single atoms for photocatalytic water transfer hydrogenation, enabling the visible light-driven hydrogenation of styrene to ethylbenzene [76]. SACs have found applications in various fields such as CO_2 reduction [77–79], organic synthesis [80,81], NH_3 production [82,83], and wastewater purification [84–86]. In summary, SACs, as a promising catalytic strategy, possess advantages including high activity, stability, and controllability, thereby offering new avenues and opportunities for achieving low-cost, high-efficiency and highly selective catalytic reactions.

1.3. Recent achievements of g-C_3N_4-based SACs

With the optimization of preparation methods and the improvement of sophisticated instruments, scientists have gained a deeper understanding and mastery of the preparation and characterizations of g-

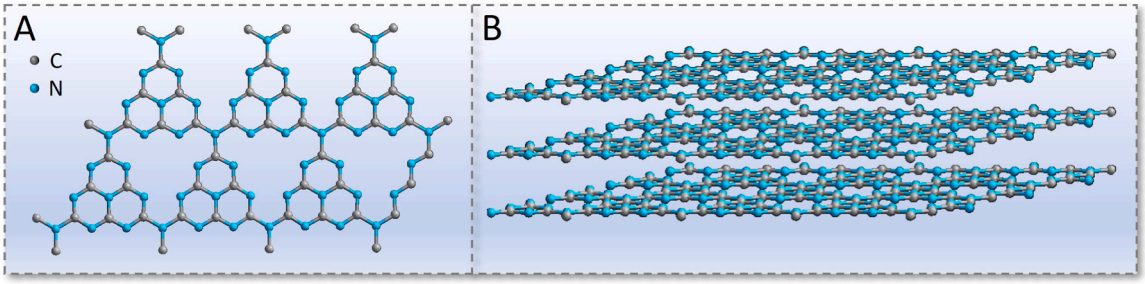

Fig. 1. The (A) plan and (B) interlayer structure diagram of g-C_3N_4.

C_3N_4-based SACs, which has made the research more feasible and generated increasing interest [87–90]. As displayed in Fig. 2**a**, the research hotspots in g-C_3N_4-based SACs have been identified as focusing on atomic-level coordination engineering, energy, and environment in recent years. In Fig. 2**b**, we have investigated the number of research publications and citations related to g-C_3N_4-based SACs from 2016 to the present. Impressively, the research interest in g-C_3N_4-based SACs has experienced an exponential surge. In 2022, the citations of publications on g-C_3N_4-based SACs have already exceeded 7000. Due to the delayed effect of publication and time, the data for 2023 is not yet complete. However, we believe that the research enthusiasm for g-C_3N_4-based SACs will not wane. Fig. 3 depicts a timeline of recent achievements and features related to the metal atoms coordination structures in g-C_3N_4-based SACs. To the best of our knowledge, Wu et al. first characterized the Pt-C_2N_3 coordination structure on g-C_3N_4 in 2016 and applied it for photocatalytic H_2 evolution [91]. In this work, the turnover frequency (TOF) of the Pt-CN sample with an optimized Pt loading of 0.16 wt% reached 775 h^{-1}, which is approximately 9 times higher than that of Pt nanoparticles. In 2017, Zhong et al. proposed that Pt-N_2 coordination improved the photocatalytic multifunctionality of g-C_3N_4 [92]. Apart from the application in H_2 evolution, it could also photo-oxidize the gaseous pollutant nitrogen monoxide (NO) into nitrate (NO_3^-). Furthermore, transition metals have gained attention and are being utilized in g-C_3N_4-based SACs. In 2018, Xie et al. discovered that the Cu-N_3 coordination structure could accelerate photocatalytic nitrogen fixation under ambient conditions, resulting in a NH_3 evolution rate of 186 μmol g^{-1} h^{-1} [93]. As expected, the construction of bi-heterogeneous single atom coordination has been emerged. Guo's group achieved stabilization of neighboring Pt-Ru monomers by constructing Pt-C and Ru-N bonds in 2019 [94]. The bridging O_2 adsorption induced by Pt-O and Ru-O bonds facilitated O_2 activation, thus promoting CO oxidation reaction. The research efforts have significantly increased since 2020, as evident from Fig. 2. For example, Xiang et al. introduced isolated Cu-N_6 sites into crystalline g-C_3N_4, enabling efficient selective CO_2 photo-reduction to CO [95]. In addition, different coordination structures of the same metal atom have been investigated. Zou et al. anchored Ag-N_4 and Ag-C_2N_2 structures onto g-C_3N_4, respectively [96]. As a result, the Ag-C_2N_2 coordination exhibits remarkable advantages in photocatalytic H_2 evolution reaction due to its faster charge transfer capability. In recent years, more precise and intricate metal atom coordination structures have been designed and applied in functionalized reactions, including Ni-O_6 [97], Sb-N_4 [98], intercalated Pd-N_3 [99], Fe-C_2N_1 [100], Co-C_2N_2 [101], Ga-N_5 [102] coordination environments, etc. Building upon the tremendous achievements made in the past few years, the introduction of atomic-level metal coordination structures on g-C_3N_4 has been demonstrated as a promising strategy for efficient energy conversion and environmental remediation. Some significant advancements in this regard will be specifically discussed in Section 4.

2. The advantages and mechanisms of atomic coordination structure anchored on g-C_3N_4

g-C_3N_4-based SACs have become a research hotspot in the field of catalysis due to their high catalytic activity, high selectivity, high stability, resource utilization efficiency and fine structure controllability, which have demonstrated extensive potential applications in numerous attractive reactions [103,104]. In this section, we attempt to present the characteristics and advantages of isolated metal species in g-C_3N_4-based SACs, based on some significant recent advancements (Fig. 4).

Some previous excellent works have demonstrated that atomically dispersed metal species can effectively act as active catalytic centers due to their high utilization and density [60]. Zhang et al. loaded single Co-N_4-O active site onto the heptazine cavity of crystalline g-C_3N_4, achieving rapid directional extraction of photogenerated holes and showing significantly enhanced photocatalytic HER activity [105]. Zhou and colleagues enhanced the CO_2 adsorption and activation capability by utilizing high-density single dispersed Co-N_2C active sites [106], and further selectively photo-reduced to liquid solar fuel methanol. For g-C_3N_4-based SACs, the metal atoms coordinate with the C/N atoms on g-C_3N_4 surface to ensure the isolated reaction sites. This case avoids the interaction between metal atoms, reducing the non-target side reactions and achieving a high reaction selectivity.

Furthermore, g-C_3N_4 has been regarded as an emerging visible-light-responsive semiconductor photocatalyst [107–109]. Rational band engineering could prolong the photogenerated charges lifetime and suppress the electron-hole pairs recombination, enabling the full utilization of solar energy [110]. Thereinto, the loading of single atoms can introduce additional electronic states or levels in the bandgap position for promoting charge separation. For example, Li et al. found that the doping of single Mo atoms led to the introduction of dopant levels within the bandgap of g-C_3N_4 [111]. The dopant levels enable the capture of holes, prolonging the charge separation of electrons and holes. The modification of single atom band engineering provides more opportunities to participate in catalytic reactions for g-C_3N_4, while enhancing the light absorption capacity. In contrast, Liu's group pointed out that the confined single Pt atoms would reduce the bandgap by positiveizing the VB potential instead of introducing impurity levels via the spin-polarized DFT calculation results [112]. The isolated Pt sites have improved the HER kinetics and enhance the light responsiveness of g-C_3N_4.

The local structure (coordination environment) of the metal atoms in g-C_3N_4-based SACs can affect the adsorption mode of reactants and modulate the interaction between the reactants and g-C_3N_4-based SACs,

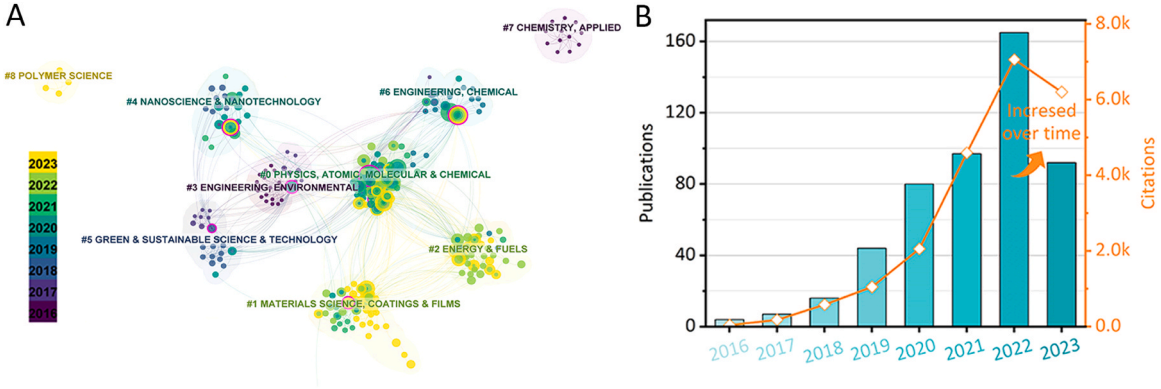

Fig. 2. (A) The subject categories of research hotpots in g-C_3N_4-based SACs by searching the keyword of "carbon nitride" and "single atom photocatalysis" on *Web of Science* (obtained on 2023–11-05). (B) The number of publications and citations by searching the keyword of "carbon nitride single atom photocatalysis" or "g-C_3N_4 single atom photocatalysis" on *Web of Science* (obtained on 2023–11-05). Time line: from 2016 to 2023.

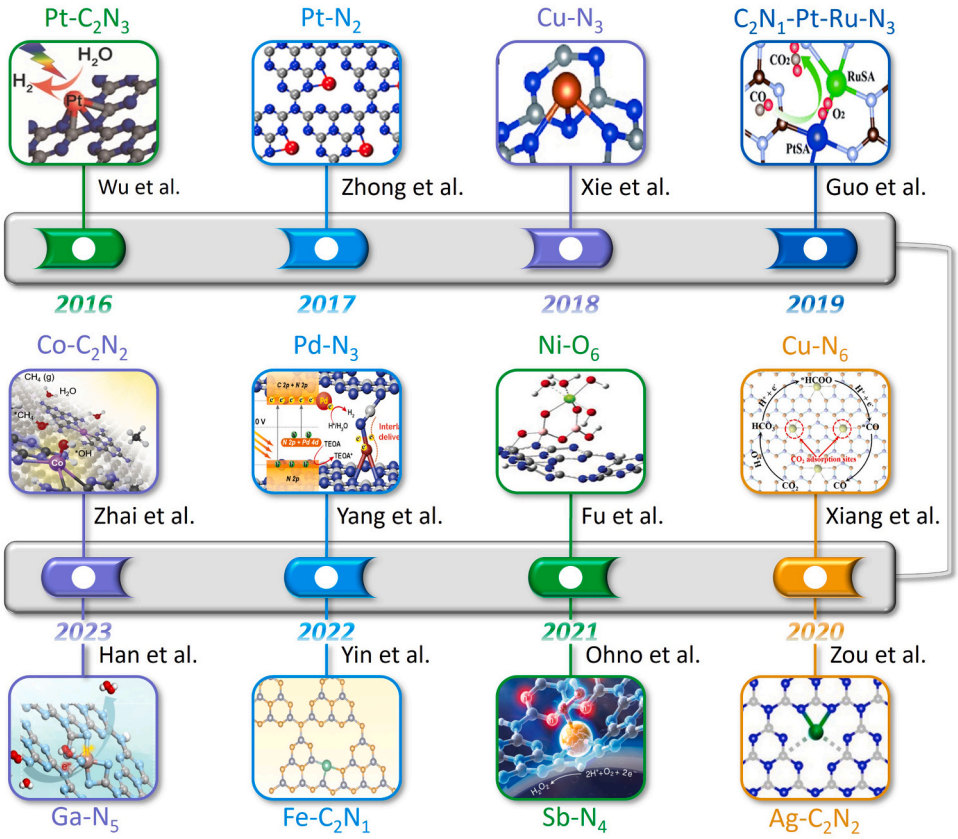

Fig. 3. Timeline of g-C_3N_4-based SACs with atomic-level coordination structures features from 2016 to 2023.

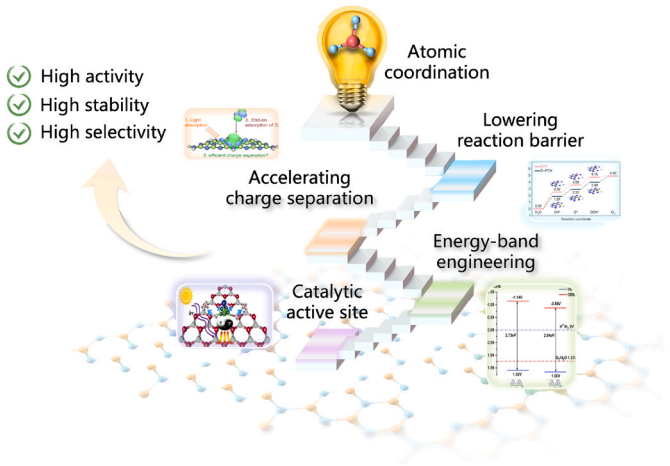

Fig. 4. The schematic core advantages of single metal atoms anchored on g-C_3N_4 [107,113,118,120].

during the catalytic process [113]. The mode relies on the theoretical calculations, especially for CO_2 photoreduction [114], organic synthesis [115] and H_2O oxidation reaction [116]. Impressively, single Zn atom coordinates with six N atoms of g-C_3N_4 in the central position, enhancing the adsorption and activation of H_2O molecules [117]. To further elaboration, the intermediate energy barriers for H* and OH* are lowered to make H_2O more prone to splitting into H_2 and O_2 under irradiation. That is, the optimization of the interfacial effect between reactants and g-C_3N_4-based SACs is an effective strategy for lowering the reaction activation energy and reaction pathway controllability.

To be emphasized, the interaction between single metal atom and g-C_3N_4 can result in electron redistribution [118]. The electron rearrangement properties can change the electronic environment of single metal atoms (or generate a polarized electric field in g-C_3N_4), which regulate the electron density and catalytic activity. Ohno et al. observed that photogenerated electrons tend to accumulate to the positions of atomically dispersed metal species (In and Sn) by molecular orbital simulations [119]. As a result, the highly coalesced electron region presents a desirable electronic configuration for attracting electrophilic oxygen and promotes the oxygen reduction reaction. It can be explained that, the formation of a stable coordination structure supported by single metal atoms with g-C_3N_4 leads to the electrons transfer from g-C_3N_4 to metal atoms, which favors the filling of the density of states of metal atoms. Moreover, the rare earth Dy atoms are believed to serve as an interface charge transfer bridge to provide an alternative means for promoting the charge separation in g-C_3N_4 composite [120]. The intermediate excited state energy level of Dy^{3+} aligns precisely between the CB of g-C_3N_4 and the VB of CdS, causing an electron cascade from g-C_3N_4 to CdS. Simultaneously, the electron cloud density around single Dy sites undergoes alterations to facilitate CO_2 molecule adsorption.

3. Synthesis and characterizations of g-C_3N_4-based SACs

3.1. Synthetic strategies

Although g-C_3N_4-based SACs possess numerous advantages and promising application prospects, the incorporation of single metal atoms onto g-C_3N_4 faces several challenges and difficulties. Currently, comprehensive synthesis strategies for SACs have been well summarized in some excellent reviews [103]. Here, we primarily focus on the metal atoms anchoring pathways and atomic-level active sites activation during the preparation process of g-C_3N_4-based SACs, which aims to enhance the control over metal atom dispersion and loading efficiency. Due to the interactions and energy characteristics of g-C_3N_4 surface,

single metal atoms tend to aggregate rather than being uniformly dispersed. Moreover, single metal atoms may not be fully accommodated within the g-C_3N_4 network owing to the unique arrangement (or interaction force) of C/N atoms in g-C_3N_4, resulting in lower loading efficiency. In short, the synthesis of g-C_3N_4-based SACs faces challenges such as stability issue, dispersion control, loading amount limitation, active sites understanding and catalytic performance optimization. In this section, some innovative strategies and successful experiences to prepare g-C_3N_4-based SACs are briefly presented, partitioned into single atom anchoring and activation, which are crucial for the development of efficient catalysts.

3.1.1. *Dispersal and anchoring strategies of single metal atoms*

3.1.1.1. Supramolecular self-assembly. The fabrication of SACs using supramolecular self-assembly involves the orderly assembly of individual metal atoms into atomic-scale structures through specific supramolecular interactions, thereby creating highly active catalysts [121,122].

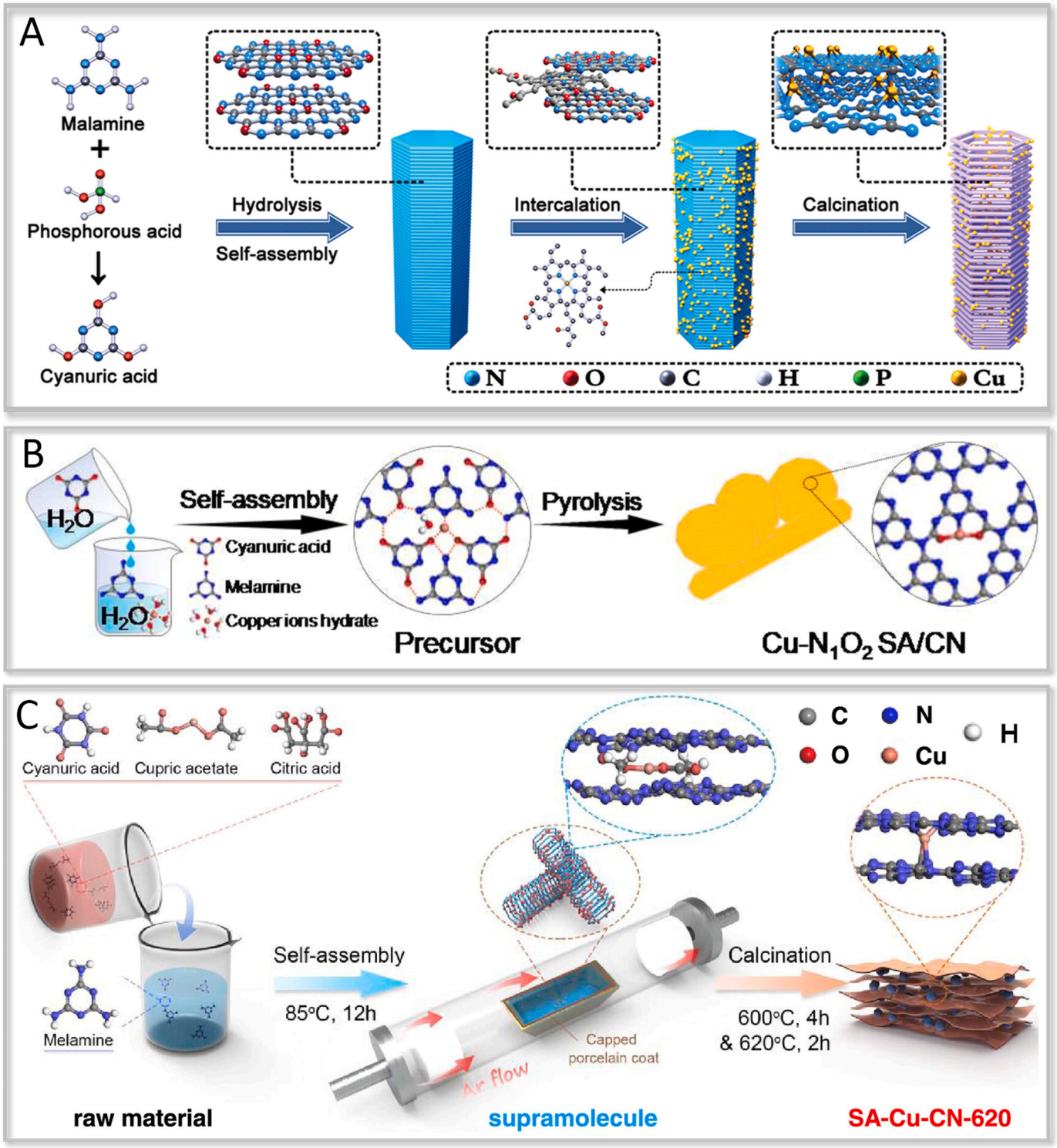

Fig. 5. The Cu atom is anchored to g-C_3N_4 via supramolecular self-assembly strategies [124,128,129].

For g-C_3N_4-based SACs, stable coordination compounds are formed by suitable ligand molecules with metal atoms, and the interaction forces such as hydrogen bonding, π-π stacking, and electrostatic interactions are employed to spontaneously arrange or coordinate the single metal atoms to generate precursor materials. The precursors are further processed (generally by thermal polymerization) to produce g-C_3N_4 while the single metal atoms are anchored. When employing supramolecular self-assembly for g-C_3N_4-based SACs preparation, the appropriate ligand molecules are selected to form highly stable coordination compounds with the metal atoms [123]. Meanwhile, the ligand molecules should possess the potential to either co-generate g-C_3N_4 or bind to g-C_3N_4 support. Additionally, by adjusting factors such as reaction conditions, solvent environment and molecular structure, it is possible to control the ligand molecules arrangement and metal atoms dispersion, thereby achieving precise synthesis of g-C_3N_4-based SACs. To date, the preparation of g-C_3N_4-based SACs through supramolecular self-assembly involves various metal atoms, including Ag [96], Cu [124], Fe [125], Co [126], etc. Notably, the interactions between different metal atoms and g-C_3N_4 support may be different. In this discussion, we will focus on the anchoring of Cu atoms as a representative example.

Cu, as one of the abundant metals in the earth crust, which is readily available as a raw material [127]. Furthermore, it is relatively affordable and possesses a tunable electronic structure and dynamic surface reconstruction capabilities. Fu et al. proposed a layered supramolecular precursor generated by melamine hydrolysis and then combined with Cu salt molecules (copper sodium chlorophyll) (Fig. 5**A**) [124]. After heat treatment, a tubular accordion-like structure of C_3N_4 with intercalated single Cu atoms is obtained, which greatly facilitates the separation and transfer of charges within the plane and between layers. As shown in Fig. 5**B**, Zhao and colleagues improved the method for preparing Cu single-atom g-C_3N_4-based SACs (Cu-N_1O_2 SA/CN) by replacing dimethyl sulfoxide (DMSO) with H_2O as the solvent [126]. They found that in DMSO solvent, the coordination ability of the -OH group of melamine molecules is extremely weak, resulting in minimal coordination between melamine molecules and Cu ions. Due to the weak alkaline nature of melamine aqueous solution, the -O- groups of melamine molecules may form Cu-O coordination with Cu ions. Therefore, in a mixed aqueous solution containing copper nitrate, melamine and melamine uric acid, a supramolecular precursor with Cu coordination is obtained. Furthermore, through FTIR spectra, they observed hydrogen bonding supramolecular structures formed between melamine and cyanuric acid through N-H···O and N-H···N interactions. Finally, thermal polymerization was carried out at 600 ℃ under a nitrogen atmosphere, resulting in the formation of Cu-N_1O_2 SA/CN. When selecting the source of single metal atoms, it is necessary to consider the stability and solubility under reaction conditions, as well as their impact on catalytic activity and selectivity. Using a similar preparation approach, Liu et al. obtained a rod-shaped supramolecular structure self-assembled through hydrogen bonding (Fig. 5**C**) [129]. However, acetic copper was chosen as the Cu precursor, which was believed to provide a stable metal center and prevent the aggregation of Cu atoms. The organic ligands from the organic copper compound itself can provide spatial barriers, preventing excessive proximity between Cu atoms and reducing the possibility of aggregation. Indeed, the advantages of supramolecular self-assembly method are highly controllable and sustainable. Of note, the source of single metals and ligands should be focused on, while the interaction of the metal atoms with g-C_3N_4 support should be understood, which constitute the key steps toward achieving highly active catalysts.

3.1.1.2. Impregnation method. Different from supramolecular self-assembly methods, the impregnation method does not require suitable ligand molecules. These two methods have essential differences in terms of operation process and structure control. The impregnation method is relatively simple and no complex synthesis steps or special equipment are required. In this method, g-C_3N_4 support is directly immersed in a solution containing metal precursors to adsorb metal ions. Subsequently, it undergoes treatment steps such as calcination and reduction to obtain g-C_3N_4-based SACs. Indeed, the impregnation method is not favorable for achieving high loading of single atoms, which may result in clusters or nanoparticle aggregations. For example, Chen et al. synthesized a single-atom palladium catalyst (Pd_1-mpg-C_3N_4) via a simple impregnation treatment [76]. They observed the atomic dispersion of Pd species on C_3N_4 by high-angle annular dark field scanning transmission electron microscope (HAADF-STEM) and X-ray absorption fine structure (XAFS). The results showed that Pd_1-mpg-C_3N_4 exhibited excellent catalytic activity for hydrogenation transfer reaction involving various unsaturated bonds. However, in the HAADF-STEM images (Fig. 6**A**) of samples with Pd loading exceeding 0.8 wt%, some nano-clusters and nanoparticles were observed. Moreover, the samples with Pd loading of 1.54 wt% and 2.76 wt% exhibited a linear decrease in hydrogenation activity, (Fig. 6**B**) highlighting the advantages of atomic dispersion sites over traditional nanoparticle catalysts. The key point to the impregnation method lies in controlling the concentration of the metal precursor solution and the dispersion of metal ions, such as increasing the immersion time and using appropriate support can enhance the adsorption of the metal precursor onto the surface of g-C_3N_4. Meanwhile, with appropriate impregnation conditions, a higher degree of dispersion for metal single atoms would be achieved. Wang et al. successfully anchored different amount of Ag single atoms onto a hollow porous polyhedral tubular structure g-C_3N_4 support using a simple "impregnation + pyrolysis" process (Fig. 6**C**) [130]. This is mainly due to that the porous tubular g-C_3N_4 support was chosen to provide more active sites for the adsorption and dispersion of Ag. The maximum actual content of Ag in the synthesized photocatalysts up to 1.12 wt% was determined by inductively coupled plasma optical emission spectroscopy (ICP-OES). Alternatively, surfactants or complexing agents may be required to modulate the adsorption and dispersion processes of the metal precursors with the aim of precisely controlling the coordination structure of single metal atoms. In Fig. 6**D**, Jing and colleagues employed boronic acid as the source of boron and utilized a low-temperature hydrothermal method to modify ultra-thin porous C_3N_4 nanosheets through B-N coordination (bCN) [131]. Then, five O-coordinated single Co sites were synthesized by dropwise addition of $Co(NO_3)_2$ aqueous solution to the bCN suspension under continuous stirring and sonication. Here, the Co-O_5 coordination is actually obtained by ion exchange between Co^{2+} and the protons of loaded borate species. In conclusion, despite the current challenges in the preparation of g-C_3N_4-based SACs by impregnation, it is still possible to move towards the goal of higher metal loading and more precisely controlled atomic coordination structures.

3.1.1.3. Morphology construction and defect introduction strategy. Indeed, the morphological construction can change the specific surface area of g-C_3N_4 support and the exposure of metal anchoring sites, thereby capturing single metal atoms. Meanwhile, the introduction of C/N defects may change the surface structure of g-C_3N_4, generating a large number of localized electrons [132]. Due to the confinement effect, the metal species are successfully anchored at single defect sites (interacting with surrounding C/N atoms) and prevented from aggregation. Typically, this strategy requires the preparation of modified g-C_3N_4 support precursors in advance. In recent years, the defect engineering anchoring single-atom strategy has been widely applied in the synthesis of g-C_3N_4-based SACs, playing a crucial role in improving photocatalytic performance. In this regard, Wang et al. fabricated g-C_3N_4 (Cv-CN, Fig. 7**A**) with large specific surface area and C defect modification by secondary calcination of g-C_3N_4 in an air atmosphere [133]. Notably, the presence of C defects could be verified by electron paramagnetic resonance (EPR) spectra (Fig. 7**B**) due to the lower Lorentz line intensity of Cv-CN. Next, Pd species were in-situ anchored on the Cv-CN surface by photo-deposition at atomic-level (Pd-Cv-CN). The Pd atoms further took the place of C defects, leading to the formation of the Pd-N_3

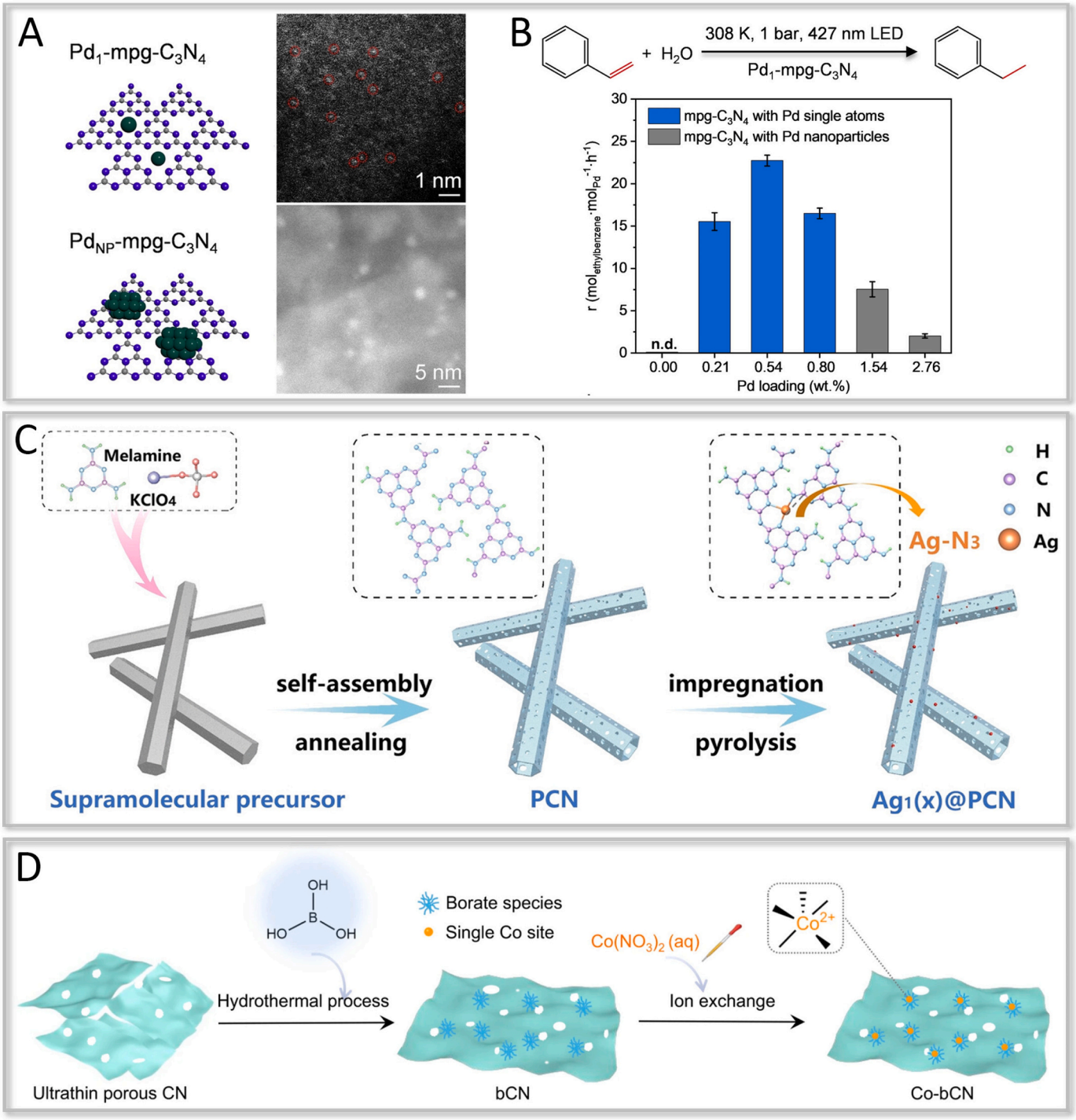

Fig. 6. (A) HAADF-STEM images of Pd_1-mpg-C_3N_4 and Pd_1-mpg-C_3N_4. (B) The hydrogenation activity of Pd_1-mpg-C_3N_4 with different Ag content [76]. The synthetic diagram of g-C_3N_4-supported (C) Ag and (D) Co single-atom catalysts via impregnation procedure [130,131].

structure (Fig. 7**C**). On the other hand, Zhai et al. introduced C defects in C_3N_4 via a steam reforming strategy [$C(s) + H_2O(g) \rightarrow CO(g) + H_2(g)$]. The presence of additional unpaired electrons and charge localization around the C vacancies further confined the Sb single atoms to the Cv-C_3N_4 network, forming the unique Sb-N_5 structure (Fig. 7**D**) [134]. As a result, the Sb-N_5 sites promote efficient electron transfer for efficient oxygen photo-reduction to hydrogen peroxide (H_2O_2). In summary, the defect engineering strategy is considered as an innovative way that can manipulate the electronic configuration of g-C_3N_4-based SACs.

3.1.2. *Activation of atomic-level active sites*

3.1.2.1. Co-polymerization. The activation of single atoms on g-C_3N_4 by co-polymerization allows the new functional sites introduction, which largely changes the surface properties and electronic structure of g-C_3N_4, providing additional chemical reactivity and electron transport paths. That is, the formation of chemical bonds between single metal atoms and g-C_3N_4 under high temperature allows the single atoms to be firmly embedded in the g-C_3N_4 network. This is a way to activate the metal species, unlike supramolecular self-assembly (a way of dispersing

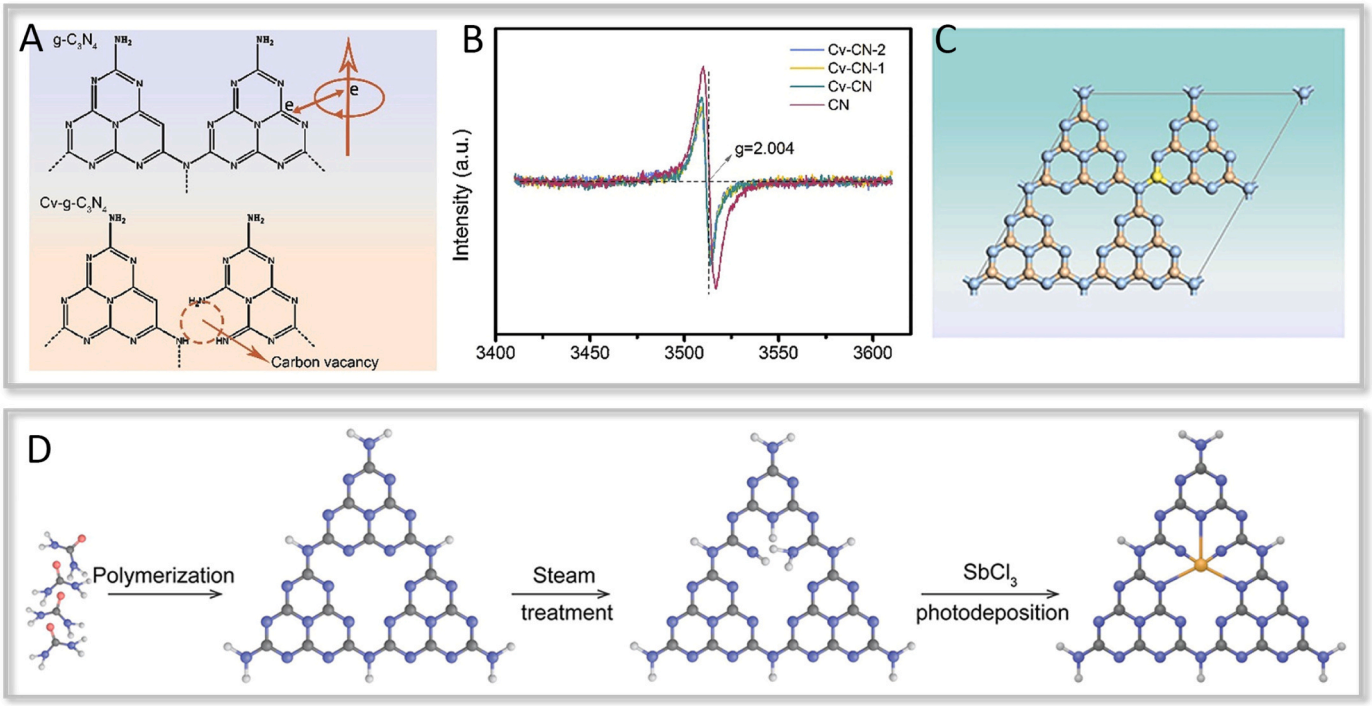

Fig. 7. (A) Structure of Cv-g-C_3N_4 with C defect. (B) EPR spectra of different samples. (C) Schematic model of Pd-Cv-CN [133]. (D) Schematic illustration to synthesize Sb_1/Cv-C_3N_4 [134].

the metal species). In addition, the calcined metal species are generally anchored to g-C_3N_4 through covalent interactions, since the destabilizing interactions have been disrupted. The co-polymerization process can be achieved through various techniques, such as thermal decomposition [135] and vapor-phase deposition [136]. Typically, the precursor of g-C_3N_4 (such as melamine, urea, thiourea, etc.) is directly mixed with metal salts (nitrate salts, chloride salts, organometallic salts, etc.) and further subjected to sintering.

In this regard, Pérez-Ramírez et al. reported the synthesis of Cu, Fe, and CuFe single atom-modified C_3N_4 materials via a one-pot polymerization reaction using metal nitrates and dicyandiamide as precursors (Fig. 8**A**) [137]. Zou et al. employed the co-polymerization strategy by placing a mixture of uniformly mixed indium chloride ($InCl_3$) and urea into a muffle furnace to prepare atomically dispersed In species photocatalysts (Fig. 8**B**) [138]. As a result, this single atom-assisted thermal polymerization process successfully achieved a reduced interlayer distance in g-C_3N_4, thereby significantly influencing the carriers transfer during the photocatalytic process. In addition, suitable calcination atmosphere is required for the preparation of g-C_3N_4-based SACs. As demonstrated in Fig. 8**C**, Shi and co-workers

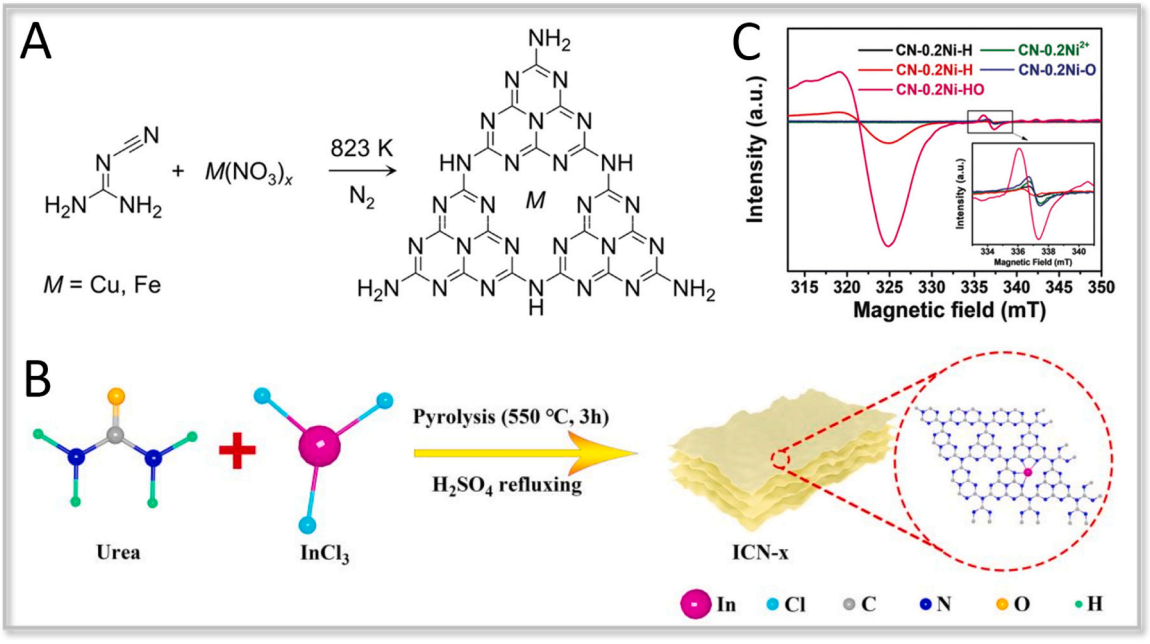

Fig. 8. (A) Approach to synthesize Cu or Fe atoms doped g-C_3N_4 [137]. (B) Schematic diagram of ICN-x synthesis [138]. (C) EPR spectra of different samples [139].

sonicated and lyophilized the synthesized bulk g-C_3N_4 in $NiCl_2$ solution to obtain the precursor sample with atomically dispersed Ni^{2+} (CN-xNi^{2+}) [139]. Subsequently, the samples were treated by calcination in H_2, O_2 and H_2/O_2, respectively. They claimed that there is a significant difference in the unpaired electrons concentration of synthesized single atom samples, which is one of the important factors affecting the catalytic activity. To sum up, the copolymerization method is mainly used to achieve single atom localization and control on the g-C_3N_4 surface by introducing appropriate metal precursor materials. Currently, the preparation of g-C_3N_4-based SACs by copolymerization has been extended to various metal species, while some recent works with specifics are provided in Table 1. Among them, factors such as reaction temperature and gas atmosphere should be noted for the activation effect.

3.1.2.2. Photochemical deposition. In a typical photochemical deposition process, a solution containing metal ions is commonly employed as the precursor, primarily based on the photochemical reactions occurring on the g-C_3N_4 surface to achieve atomic-level deposition of metal species. Furthermore, the photochemical deposition process for the preparation of SACs is highly rapid and no post-treatment step is required, thereby resulting in high coordinative selectivity and efficiency. For semiconductor catalysts, the photoexcited active species such as holes and electrons could be transferred to the metal precursor for redox reactions. For instance, Yao et al. successfully introduced single Pt species onto g-C_3N_4 by irradiating an aqueous solution of chloroplatinic acid ($[PtCl_6]^{2-}$) using a Xe lamp, where Pt species coordinated with four N atoms (Fig. 9**A**) [152]. In addition, with an increase in the concentration of $[PtCl_6]^{2-}$, Pt nanoparticles gradually formed. In this regard, Yu and colleagues have proposed an effective method to enhance the photocatalytic activity by adding hole scavengers in aqueous solution [153], which can promote the full separation of photogenerated charges of g-C_3N_4 and accelerate the reduction of Ag species. They used triethanolamine (TEOA) as a hole scavenger to consume the holes on the VB of g-C_3N_4 in the precursor solution containing metal ions. Interestingly, DFT calculations revealed that TEOA can easily capture Ag^+ to form $[Ag(TEOA)_2]^+$ complex (Fig. 9**B**), leading to a significant decrease in the reduction potential and providing a favorable activation environment for the atomically dispersed metal species. Similarly, Bi et al. successfully prepared Pt single atom catalyst (Pt/C_3N_4) in a chloroplatinic acid solution containing TEOA [154], demonstrating the universal advantage of electron donor sacrificial agents in g-C_3N_4-based SACs synthesis via photochemical deposition. Due to the visible light responsiveness of g-C_3N_4, it offers a wider range of options for light sources. Of note, different wavelengths of light carry different energy levels, and an appropriate range of light wavelengths can affect the formation rate and atomic coordination structure of single dispersed metal species. Shi et al. proposed the deposition of the same amount of H_2PtCl_6 onto g-C_3N_4 in the form of single Pt atoms and bulk Pt species under near-infrared (NIR) and visible light (Vis) region, respectively (Fig. 9**C**) [155]. Indeed, with an increasing deposition time from 3 h to 6 h, the Pt content in the optimized single atom samples increased from 0.0988 wt% to 0.2248 wt%.

In summary, the preparation of g-C_3N_4-based SACs involves two steps: dispersion of metal species and activation of single active sites. Furthermore, some researchers have employed sulfuric acid washing to remove unanchored metal clusters/aggregates, which is distinct from the dispersion or activation of metal atoms [150,156]. Furthermore, we have also summarized that metal species could be dispersed through strategies such as atomic confinement [157], atomic layer deposition (ALD) [158], ball milling [159], mechanical grinding [143,156] and electrostatic adsorption [111]. In the activation stage of single metal sites, techniques such as electrochemical deposition [160], microwave-assisted method [161] and solvent-thermal method [162] are commonly employed.

Table 1
Recent works in the synthesis of g-C_3N_4-based SACs via co-polymerization process.

Year	Catalyst	Coordination structure	Metal salt precursors	Calcination conditions	Reference
2020	Mn-C_3N_4	Mn-N_3	Mn $(COOH)_2{\cdot}4\ H_2O$	N_2, 600 ℃, 1 h	Zhang et al. [140]
2020	Cu_1/HCNS	Cu-N_3	Cu $(NO_3)_2{\cdot}3\ H_2O$	550 ℃, 4 h	Zhao et al. [141]
2020	Co-pCN	Co-N_2O_2	$Co(acac)_2$	550 ℃, 2 h	Zhang et al. [142]
2020	Ag-N_2C_2/CN Ag-N_4/CN	Ag-N_2C_2 Ag-N_4	$AgNO_3$	Ar, 600 ℃, 4 h	Zou et al. [96]
2021	GCN	Ga-N_4	$GaCl_3$	Air, 550 ℃, 3 h	Kang et al. [143]
2021	Sb-SAPC15	Sb-N_4	$NaSbF_6$	N_2, 560 ℃, 4 h	Ohno et al.[98]
2021	WSA-CN-PUNS	W-N_1O_2	Phosphotungstic acid	Air, 500 ℃, 2 h	Zhang et al. [144]
2021	Fe_1-N_v/CN	Fe-N_4	$FeCl_3{\cdot}6\ H_2O$	Ar, 620 ℃, 4 h	Zhan et al. [145]
2022	Co/C_3N_4-C	Co-N_4	$Co(OAc)_2$	N_2, 550 ℃, 4 h	Qu et al. [146]
2022	CNFe_2-0.6	Fe-N_5	$Fe(acac)_3$	Ar, 600 ℃, 1 h	Liu et al. [147]
2022	MO-PCN (M= Mo, W)	M-N_4O_2	$(NH_4)_2MoO_4$ $Na_2WO_4 0.2\ H_2O$	N_2, 580 ~ 640 ℃, 2 h	Li et al. [111]
2022	Co-CN	Mixed Co-N and Co-N_3	Cobalt salen complex	Ar, 600 ℃	Liu et al. [148]
2022	CuACs/PCN	Cu-N_4	$CuCl_2$	N_2, 550 ℃, 4 h	Huang et al. [149]
2023	FeSA/CN	Fe-N_2O_2	$Fe(acac)_2$	550 ℃, 2 h	Lai et al. [150]
2023	$Pt_{0.21}$/CN	Pt-N_3	$H_2PtCl_6{\cdot}6\ H_2O$	5% Ar/H_2, 550 ℃, 2 h	Peng et al. [151]
2023	SC-Co_1/PCN AC-Co_1/PCN	Co-N_4 Co-N_2C_2	$CoCl_2$	Air, 550 ℃, 2 h Ar, 500 ℃, 2 h	Zhai et al. [101]

3.2. Morphological and structural characterizations

When researchers attempt to design novel catalysts, they often face the challenge of comprehensively and accurately characterizing their structures and properties. Traditional experimental methods have certain limitations in revealing the single atom structure on the surface of SACs and elucidating the catalytic reaction mechanisms. Therefore, the utilization of advanced characterization techniques, primarily relying on aberration-corrected scanning transmission electron microscopy (AC-HAADF-STEM) and X-ray absorption spectroscopy (XAS), has become a key approach to understand the structures of single metal atoms and probing the reaction mechanism. Scientists are able to observe information such as atomic distribution, crystal structure, and electronic states on the surface of SACs, thereby gaining a deeper understanding of the catalytic active sites and reaction processes [83,163,164]. The precise and comprehensive characterization of the structure of single metal atoms, as well as their interactions with the g-C_3N_4 support, holds significant importance in gaining a profound understanding of their catalytic performance, modulating active sites and

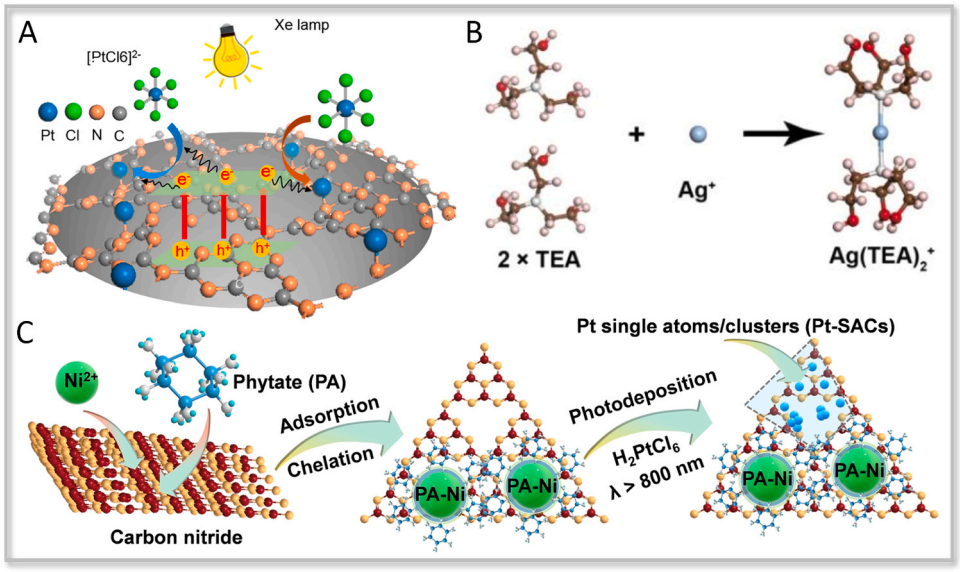

Fig. 9. (A) Illustration of the synthesis for Pt single atoms anchored on g-C_3N_4 by photo-deposition [152]. (B) The formation process of $[Ag(TEOA)_2]^+$ complex [153]. (C) Schematic illustration of the synthesis process for PA-Ni@PCN/Pt-SAC [155].

optimizing catalytic reactions. With the ongoing advancements and innovations in characterization techniques, we anticipate unveiling further mysteries of g-C_3N_4-based SACs, thereby establishing a robust basis for their applications in energy conversion, environmental remediation and sustainable chemistry.

3.2.1. *Electron microscope techniques*

In recent years, with the rapid development of SACs, scientists have sought to enhance catalytic performance by controlling the distribution and size of surface atoms on catalysts, which has necessitated more sophisticated characterization techniques [165]. The characterizations of SACs using electron microscopy techniques can be challenging due to the extremely small size and low atomic concentration. The advanced electron microscopy techniques provide us with important tools to intuitively observe particle distribution and behavior at the micro/-nanoscale, such as nanoparticles or single atoms. Generally, due to the imperfect magnetic lens structure of conventional transmission electron microscopes (TEM), they suffer from low resolution (approximately 0.8 nm), which is insufficient for observing the atomic-level distribution of metallic species. The AC-HAADF-STEM could precisely determine the presence of isolated metal atoms and their spatial distribution on the support. In 2011, Zhang and colleagues introduced the concept of SACs [64]. Prior to that, although SACs may have existed, they could not be directly defined due to the limitations in electron microscopy technology. Fig. 10 illustrates the images of different metal single-atom loaded g-C_3N_4 catalysts determined by AC-HAADF-STEM. The bright white atomic-scale spots indicated the presence of single metal atoms. Especially in Fig. 10**A**, we can clearly distinguish between Pd nanoclusters and single Pd atoms (indicated by yellow circles) [166]. Typically, the size of single metal atoms is characterized between 0.1–0.2 nm, such as Ag (Fig. 10**B**) [153], In (Fig. 10**C**) [119], and Co (Fig. 10**D-E**) [167] atoms. Furthermore, the elemental composition of atomically dispersed metal species can be characterized using energy dispersive X-ray spectroscopy (EDS), which provides information about their energy distribution. As displayed in Fig. 10**F-G**, Wang et al. verified the presence and uniform distribution of Cu single atoms on S-doped g-C_3N_4 through mapping analysis [168]. In addition to that, there are several advanced electron microscopy techniques, which will not be elaborated on here. For instance, electron energy loss spectroscopy (EELS) reveals the chemical composition and oxidation state of individual atoms [98,169]; selected area electron diffraction (SAED) is employed to determine the crystal structure and symmetry of single-atom photocatalysts [170,171]; scanning tunneling microscopy (STM) is utilized to observe the arrangement of single atoms on the catalyst surface [172].

3.2.2. *Spectroscopy technologies*

Through spectroscopic techniques, we can delve into the atomic-scale details of catalysts, enabling precise control and understanding of SACs. Due to the high activity and selectivity exhibited by g-C_3N_4-based SACs, spectroscopic methods provide crucial structural and characterization information, particularly XAFS [173]. The energy range of measured XAFS spectra can be divided into two regions: X-ray absorption near edge structure (XANES) and extended X-ray absorption fine structure (EXAFS) [174–176].

XANES primarily focuses on the pre-edge region near the X-ray absorption edge, providing information about the atomic oxidation state, charge distribution, and bonding properties in catalysts. For example, Zhang et al. loaded single Co atoms in a penta-coordinated (Co-N_4-O) configuration onto the pyridinic sites of crystalline g-C_3N_4 nanorods (CCN-Co) [105]. Through XANES analysis, the near-edge absorption energy of the Co single atom was found to lie between that of metallic Co foil and Co_3O_4, indicating a positive charge on the Co component in CCN-Co (Fig. 11**A**). Xiang et al. observed that the initial white line of the prepared Cu single-atom sample (Cu-CCN) exhibited a small shoulder at 8989.3 eV and an absorption edge energy at 8996.3 eV, which is consistent with the typical characteristics of Cu^{2+} (Fig. 11**B**) [95]. Furthermore, Shen's group successfully synthesized g-C_3N_4 SACs (Zn-PCN) with a Zn-N_6 electron-deficient configuration using an intermediate coordination strategy [117]. From the Zn K-edge XANES spectrum (Fig. 11**C**), it can be observed that the absorption threshold of Zn-PCN is even higher than that of ZnO, indicating that the Zn single atom in Zn-PCN is in a higher oxidation state compared to Zn^{2+}. This suggests that the Zn single atom in Zn-PCN possesses more unoccupied states than Zn^{2+}.

The analysis of XAFS data is a complex process that typically involves the utilization of various mathematical and physical models to interpret experimental results. For SACs, Fourier transform (FT) and wavelet transform (WT) techniques, including radial distribution functions and polycrystalline structure simulations, are commonly employed to determine structural parameters, atomic displacements, vibrations, and chemical environments of the prepared catalysts [177,178]. Notably, FT-EXAFS analysis allows for the extraction of valuable information

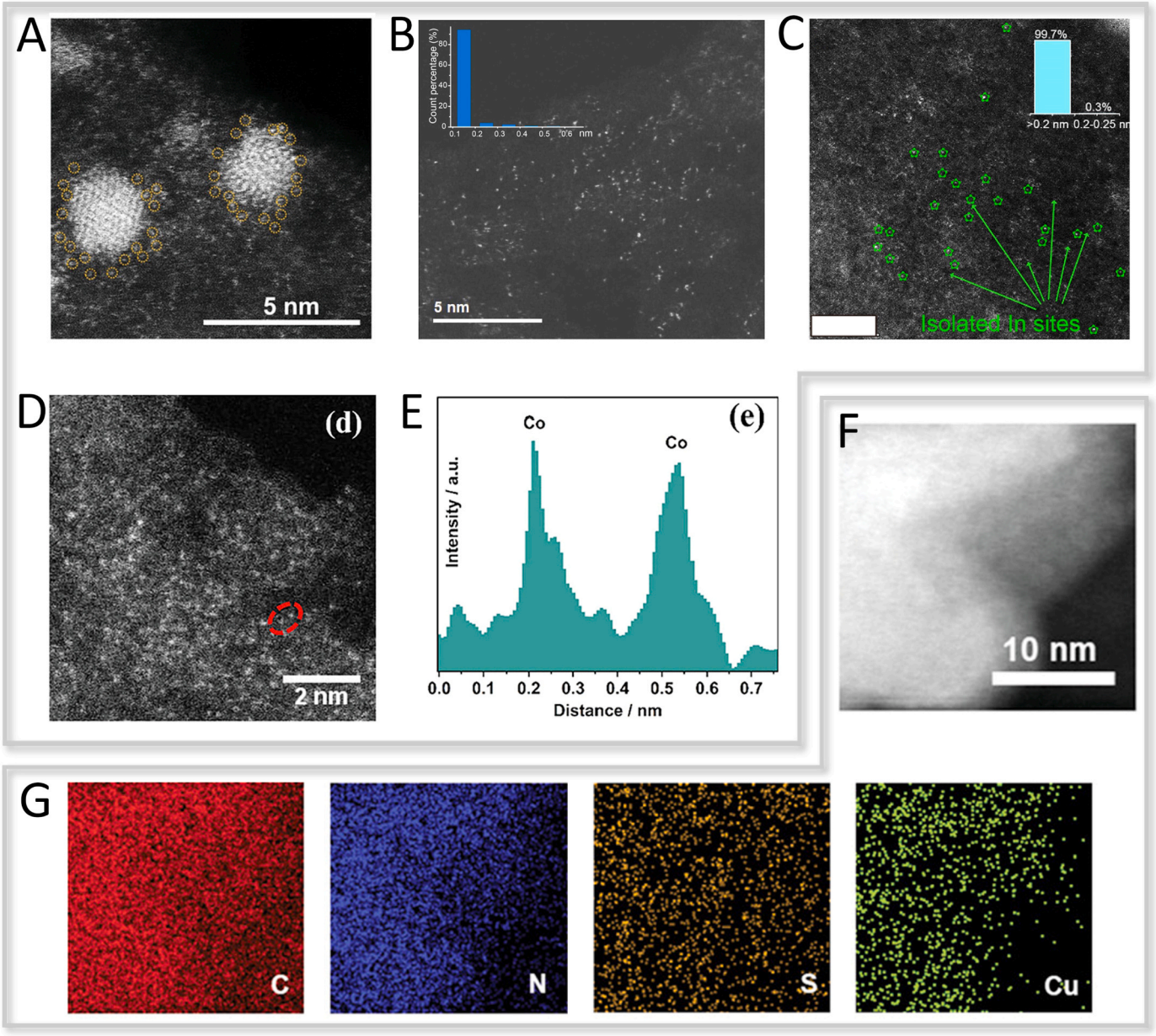

Fig. 10. AC-HAADF-STEM images of (A) Pd_{1+NPs}/C_3N_4 [166], (B) Ag-N_3S_1 [153], (C) In-SAPCs [119]. (D) AC-HAADF-STEM image and (E) the corresponding line-scanning intensity profile of Co/CNNS [167]. (F) AC-HAADF-STEM image of Cu SAs/pCNS and (G) Elemental maps [168].

such as interatomic distances, coordination numbers, and atomic species by analyzing the scattering signals generated during X-ray absorption processes. For instance, Zou et al. investigated the FT-EXAFS spectrum of Fe_1/CN (Fig. 11**D**) and observed a prominent peak at ~1.7 Å [125], attributed to the Fe-N bond. In comparison to Fe foil, FeO, and Fe_2O_3, no Fe-Fe or Fe-O peaks were observed, indicating the absence of Fe clusters or oxides in Fe_1/CN. In Fig. 11**E**, Dong et al. demonstrated the coordination information of La single atoms on g-C_3N_4 [169]. They explained that each La atom forms six La-N and four La-C coordination in the first and second coordination shells, respectively. However, considering their distances from the central absorbing ion, the isolated La atoms are found to preferentially anchor with N atoms. Furthermore, Yu et al. elucidated the coordination environment of single atom Ag loaded on S-doped g-C_3N_4 (AgSA-SCN) (Fig. 11**F**) [153]. Apart from a negligible peak corresponding to Ag-Ag bonding at around ~2.6 Å, a composite peak appeared at < 2 Å. The results indicated that the peaks formed at ~1.5 Å and ~1.9 Å could be attributed to Ag-N and Ag-S neighboring coordination, respectively. Further data fitting confirmed the Ag-N_3S_1 coordination at the Ag sites. Additionally, taking defective g-C_3N_4 loaded with single Pt atoms as an example (Fig. 11**G**), Xiong et al. observed through WT analysis that, in contrast to Pt foil (Fig. 11**H**) and PtO_2 (Fig. 11**I**), it exhibited only one dominant peak at 3.9 $Å^{-1}$, indicating the Pt-N/C/O coordination [179].

Besides XAFS, there are several other non-destructive spectroscopic techniques available for characterizing g-C_3N_4-based SACs, including X-ray photoelectron spectroscopy (XPS), Raman spectroscopy, X-ray diffraction (XRD) patterns, and Mössbauer spectroscopy, etc. The comprehensive application of these techniques can provide multidimensional information about the catalyst structure and properties, aiding in a comprehensive understanding and optimization of the performance of g-C_3N_4-based SACs. XPS can effectively provide information about the elemental composition and chemical states of the sample surface. It is worth noting that Ohno et al., while investigating the high-resolution XPS N 1 s spectrum of Sb-SAPC15 (isolated Sb sites dispersed

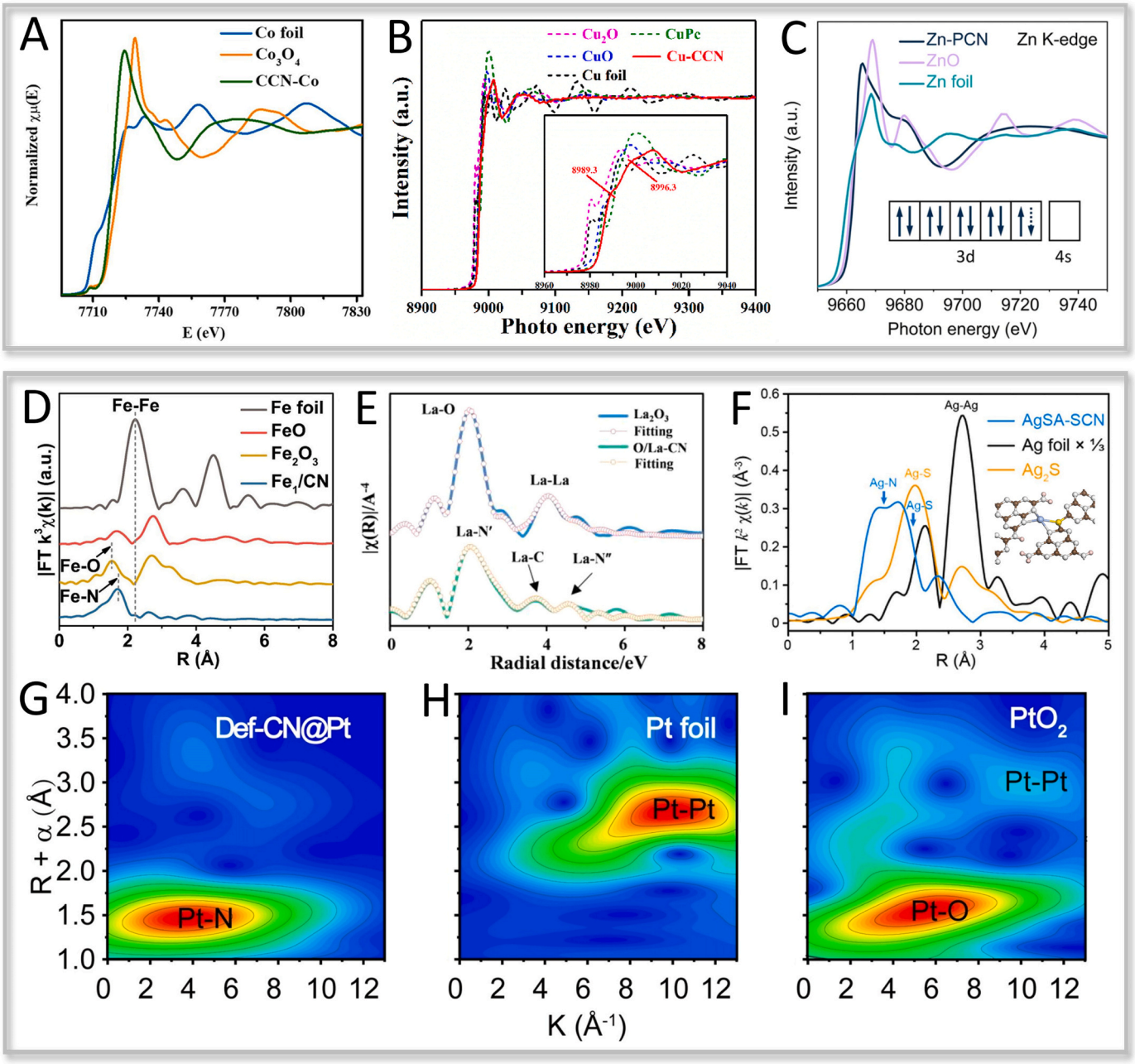

Fig. 11. XANES spectra at the (A) Co K-edge [105], (B) Cu L_3-edge and [95] (C) Zn K-edge [117]. FT-EXAFS spectra for (D) Fe_1/CN [125], (E) O/La-CN [169], (F) Ag-N_3S_1 [153], and the corresponding reference samples, respectively. (G-I) WT contour map of Pt@Def-CN, Pt foil and PtO_2 [179].

on g-C_3N_4), observed a new peak at 398.1 eV (Fig. 12**A**) [98]. The new peak was attributed to the Sb-N bond, directly demonstrating the presence of Sb-N coordination. Meanwhile, Yang et al. discovered that when investigating the highest loading of single Pd atoms on g-C_3N_4 [99], two small peaks belonging to metallic Pd^0 particles appeared at 336.0 and 341.2 eV of high-resolution XPS Pd 3d spectrum (Fig. 12**B**). Indeed, XPS could be employed to differentiate between the zero-valent state of nanoparticles and the positive valence of isolated metal species. Raman spectroscopy, which can be employed to investigate the vibrational modes and chemical bonding characteristics of SACs, possesses advantages such as high sensitivity and good chemical adaptability. In this regard, Zbořil et al. observed Ru-N/C and Ru-O vibrational signals through Raman spectra (Fig. 12**C**) [161], confirming the presence of Ru bonding at two distinct sites, in accordance with XAFS results. Generally, metal active sites on g-C_3N_4-based SACs exist in atomic-level dispersion. XRD measurement can detect the dispersion of metal atoms on g-C_3N_4 support, aiding in confirming whether the metal atoms exist in a single-atom rather than as clusters or particles. In Fig. 12**D**, Fu et al. surprisingly discovered through XRD that Cu single atoms are embedded in the interlayers of g-C_3N_4, without the peaks of Cu aggregations [124]. The introduction of trace amounts of Cu leads to broadening of the (002) crystal plane peak and a shift towards smaller angles. We consider this finding as a groundbreaking advancement in exploring the structural aspects of g-C_3N_4-based SACs using conventional characterization methods. In addition, Mössbauer spectroscopy could measure the changes in energy levels and line widths of surface atomic nuclei in catalysts by the nuclear resonance absorption effect. It can reveal valuable information about the structure, nanoscale positioning, and electronic environment of atomic catalysts. In this regard, Xie et al. utilized Mössbauer spectroscopy to infer the transformation of Fe^{3+}-N_x

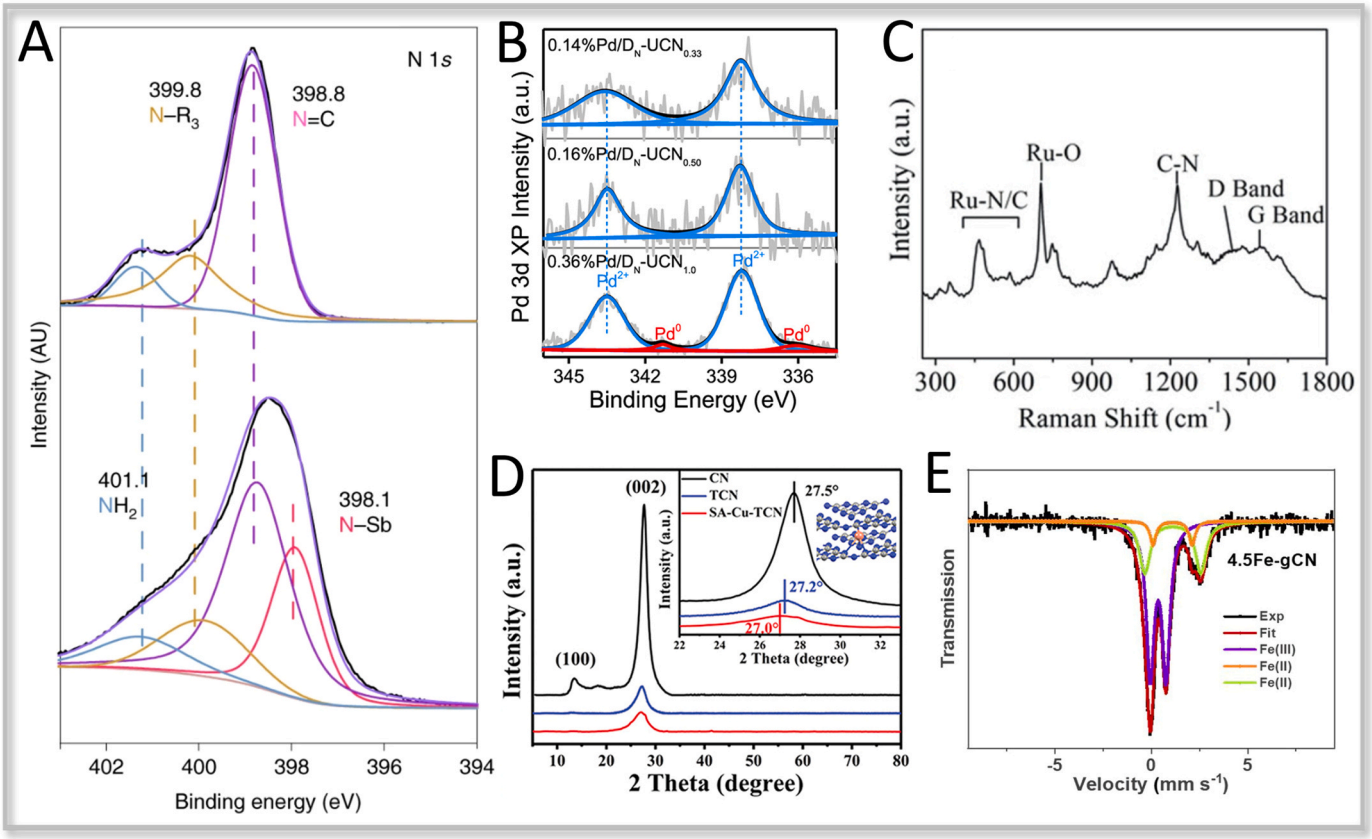

Fig. 12. XPS spectra in (A) N 1 s of Sb-SAPC15 [98] and (B) Pd 3d of 0.36 wt%Pd/D_N-$UCN_{1.0}$ [99], respectively. (C) Raman spectrum of RuSA-mC_3N_4 [161]. (D) XRD patterns of SA-Cu-TCN and reference samples [124]. (E) Mössbauer spectroscopy of 4.5Fe-gCN [180].

and Fe^{2+}-N_x to nanoparticles based on the proportion of different valence states of Fe irons obtained from the spectroscopic analysis, as shown in Fig. 12**E** [180]. Nevertheless, Mössbauer spectroscopy typically requires extremely low temperatures and is limited to select few elements (such as Fe and Sn), which has resulted in rare reported.

4. g-C_3N_4-based SACs for emerging reactions in energy conversion

4.1. Photocatalytic water splitting

4.1.1. Photocatalytic H_2 evolution

Developing green H_2 energy is one of the efficient ways to promote the low-carbon transformation of energy system, which is expected to solve the current energy crisis [181–184]. Photocatalytic H_2 evolution reaction (HER) from water splitting has attracted a lot of interest in recent works, as it utilizes two of the most abundant, clean, renewable, and readily available natural energy resources (solar energy and water resource). Therefore, HER is considered the "Holy Grail" reaction as a sustainable solution [185]. Unfortunately, conventional semiconductors suffer from rapid recombination of photo-generated carriers, which severely limits their scale application [186–188]. Typically, loading noble metal nanoparticles accelerates photo-generated charge separation and enhances HER activity [189–191]. By comparison, atomically dispersed metal atoms could promote photogenerated carrier separation due to the atomic coordination structure caused by strong metal-support interaction (SMSI), and greatly reduce the reaction cost, providing another feasible way to improve HER performance [192,193].

In this regard, Shi's team introduced Ni-C_1N_4 coordination in g-C_3N_4 (CN-0.2Ni-HO) (Fig. 13**A-B**) [139], where unpaired d electrons in the 3d orbitals of partially oxidized single Ni atomic sites can be excited under irradiation, resulting in an increase of HER activity by more than 30 times (reaching 354.9 μmol h^{-1} g^{-1}). Notably, CN-0.2Ni-HO showed excellent chemical stability in a long-term (36 h in total) cyclic experiment (Fig. 13**C**). Moreover, Zou et al. investigated the effect of atomically dispersed Ag species with different coordination structures (Ag-C_2N_2 and Ag-N_4) on HER activity over g-C_3N_4 [96]. The results indicate that Ag-C_2N_2 is more conducive to charge redistribution (Fig. 13**D**), leading to faster charge migration from g-C_3N_4 to Ag atoms. In DFT calculations, potential barrier of H^+ reduction to H_2 is reduced and ultimately leading to efficient H_2 evolution, significantly exceeding the g-C_3N_4 loaded with Ag nanoparticles (Fig. 13**E-F**). In addition, the rare metal-based Ga-N_4 structure is integrated into g-C_3N_4 (GCN) (Fig. 13**G**) as a single photocatalyst to reduce HER efficiency loss [143]. In the absence of co-catalyst, the HER performance of the optimized GCN sample is significantly improved, which is 162 and 3.3 times than that of pristine g-C_3N_4 and 1.0 wt% Pt loaded g-C_3N_4, respectively (Fig. 13**H**). Fig. 13**I** shows in-situ transient photovoltage (TPV) measurements to further understand the photocatalytic reaction process of GCN. The maximum charge extraction efficiency of GCN (A_2, 0.0162) is larger than that of CN (A_1, 0.0143), suggesting that the electron extraction capacity of GCN is greater than CN. Therefore, Ga-N_4 sites can effectively capture electrons, accelerate electron transfer and suppress the recombination of electron-hole pairs, thus enhancing the HER activity. Fig. 13**J** demonstrated that Fu et al. have successfully synthesized tubular accordion-like carbon nitride with Cu atoms loaded (SA-Cu-TCN) by combining the layered melamine-hydrolytic supramolecular precursor with chlorophyll sodium copper salt [124]. DFT calculations showed that the in-plane Cu-N_3 and interplane Cu-N_4 structures could promote the formation of new in-plane and interlayer charge transportation channels (Fig. 13**K-L**), thus enhancing photocatalytic HER activity. These works highlight the importance of different

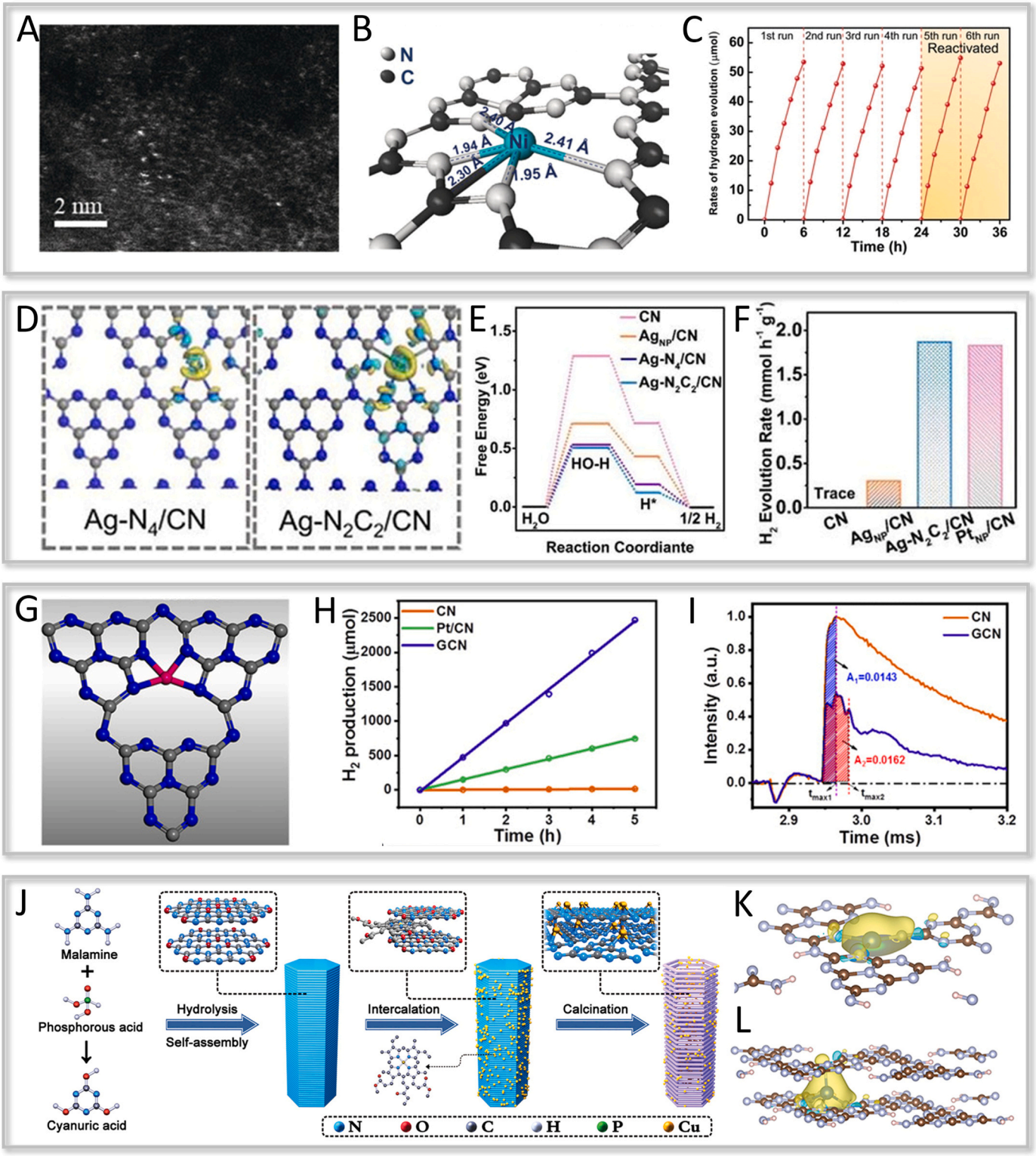

Fig. 13. (A) HAADF-STEM image, (B) structure model of Ni atoms and (C) cycling stability of H_2 evolution over CN-0.5 Ni-HO sample [139]. (D) Charge density difference maps, (E) free energy profiles for HER and (F) H_2 evolution rates over different samples [96]. (G) The GaN_4 site structure model in GCN. (H) The photocatalytic HER activity of different samples. (I) Maximum charge extraction rate of CN and GCN [143]. (J) Schematic preparation illustration of SA-Cu-TCN. (K-L) Calculated charge difference maps of the Cu-N_3 and Cu-N_4 coordination [124].

spatial atomic coordination structures on g-C_3N_4 to improve photocatalytic activity.

Based on these important advances, g-C_3N_4-based SACs have been considered as promising candidates for photocatalytic HER. Some excellent works over the recent 3 years of g-C_3N_4 based SACs with other atomic coordination to promote HER, which have been documented in detail in Table 2.

4.1.2. *Photocatalytic overall water splitting (OWS)*

Theoretically, the solar energy would be converted into chemical

Table 2
Recent works in HER of g-C_3N_4 based photocatalysts anchoring different single metal atoms.

Year	Catalyst	Coordination structure	Loading (wt%)	Performance (mmol $g_{cat.}^{-1}$ h^{-1})	Reference
2020	SA-Pt/g-C_3N_4	-	0.35	3.97	Huang et al.[194]
2020	SA-Pt/g-C_3N_4-8.7	Pt-N_4	8.7	22.65	Quan et al.[195]
2021	Cu/CN-45	Cu-N_3	-	3.77	Wang et al.[196]
2021	W_{SA}-CN-PUNS	W-N_1O_2	0.33	3.02 (With 1 wt% Pt)	Zhang et al.[144]
2022	0.16% Pd/D_N-$UCN_{0.50}$	Pd-N_3	0.16	22	Yang et al. [99]
2022	CCN-Co	Co-N_4-O	0.32	32.1 (With 1 wt% Pt)	Zhang et al.[105]
2022	Co-CCN/PTI-4	Co-N_4	0.40	3.54	Shen et al. [197]
2022	AgSA-SCN	Ag-N_3S_1	1.41	11.60	Yu et al. [153]
2022	Ag_1/CN	Ag-N_2	-	3.69	Yan et al. [191]
2022	Ir-g-CN Ru-g-CN	Ir-N_2 Ru-N_2	1.71 (Ir) 0.24 (Ru)	2.12 (Ir-g-CN) 1.18(Ru-g-CN)	Liu et al. [198]
2022	PtSAs/PCNS	Pt-N_2	1.6	8.69	Yang et al. [199]
2022	K_1Na_1/pCN	K-N_6 Na-N_6	8.84 (K) 2.32 (Na)	4.56 (With 1 wt% Pt)	Niu et al. [200]
2022	PCN-Ru	Ru-N_4	-	0.63	Dong et al. [201]
2023	Mo^1@CNNTs	Mo-N_2	0.53	4.86 (With 1 wt% Pt)	Chen et al. [202]
2023	Cu1.5-PCN	-	0.16	2.14	Xiao et al. [203]

energy when sunlight illuminates a designated photocatalyst, which split H_2O into H_2 and O_2 [204]. In terms of thermodynamics, both the proton reduction potential and the H_2O oxidation potential have to fall in the bandgap of the semiconductor, where the CB position of the semiconductor is more negative than the H_+ reduction potential (0 V, vs. NHE) and the VB position of the semiconductor is more positive than the H_2O oxidation potential (1.23 V, vs. NHE) [205–207]. Moreover, photocatalytic OWS is considered as a non-spontaneous reaction (ΔG=237 kJ mol^{-1}) that is very challenging [208]. For kinetics, oxygen evolution reaction (OER) occurs more slowly than HER because OER requires four photogenerated h^+ to proceed and O_2, which is more difficult to desorb from the semiconductor surface than H_2. As a result, it is difficult to accomplish photocatalytic OWS.

Early in 1972, the advent of the Honda-Fujishima effect opened a new era of photocatalytic OWS research [209]. The main semiconductor catalysts currently used for OWS include g-C_3N_4 [210], TiO_2 [211], CdS [212], $BiVO_4$ [213], etc., however, all of them suffer from severe carrier recombination. Atomic-level dispersion catalysts with specific coordination structures and the highest atomic utilization efficiency have become a new frontier for photocatalytic OWS in recent years [214, 215]. Surprisingly, due to the tunable electronic structure of g-C_3N_4, combined with an appropriate atomic-level coordination structure, photo-generated e^- and h^+ transfer of OWS process could be effectively promoted, thus accelerating the reaction kinetics on g-C_3N_4 surface. Therefore, g-C_3N_4-based SACs have shown great potential for photocatalytic OWS.

For example, Wei and coworkers prepared a single Co_1-P_4 site confined to g-C_3N_4 nanosheets (Co_1-phosphide/PCN) by a facile phosphorylation method [216], then XAFS and XPS measurements strongly suggested that part of the P atom may have replaced the C atom on the triazine ring of g-C_3N_4, forming a P-N bond (Fig. 14**A**). As shown in Fig. 14**B**, the Co atom was completely phosphorylated to form the Co-P_4 coordination structure. Co_1-phosphide/PCN was placed in pure water without any sacrificial agents and co-catalysts under simulated solar irradiation, and H_2 and O_2 evolution in the expected molar ratio of 2:1 was observed. Of note, there was a new midgap state in Co_1-phosphide/PCN, allowing the photoexcitation of electrons leaping from the VB to the midgap state to enhance the light trapping capacity, thus enabling the OWS reaction in visible light (Fig. 14**C**). Therefore, unsaturated Co sites could effectively suppress charge recombination and prolong the carrier lifetime to promote the adsorption and activation of oxygen in water molecules, which is conducive to facilitating the OWS reaction. Similarly, Lei et al. obtained a high density (3.0 wt%) of isolated Co-N_4 sites on the g-C_3N_4 surface (Co/CNNS) via a simple organic solvent-driven deposition method (Fig. 14**D**) [167]. The abundant exposed Co atoms not only act as active sites to promote oxidation reaction of absorbed water in surface, but also can rapidly trap holes to facilitate charge separation and transfer, achieving H_2 and O_2 evolution rates of 14 and 7.2 μmol h^{-1}, respectively, which are about 5 times higher than those of pristine CNNS (Fig. 14**E**).

To deepen the role of atomic-level coordination on g-C_3N_4-based photocatalysts for photocatalytic OWS, Fig. 14**F** separately shows a 3D sponge-like g-C_3N_4 with electron-deficient Zn-N_6 isolated structure (Zn-PCN) [117]. The results demonstrated that Zn-PCN was able to perform H_2 and O_2 evolution reactions in pure water at rates of 35.2 and 17.3 μmol h^{-1} g^{-1}, respectively (Fig. 14**G**). These were attributed to the electron deficient property of Zn-N_6 induced the intermediate state energy level, enhancing the charge polarization (Fig. 14**H**), promoting the electronic excitation, accelerating the charge separation and reducing the overall water splitting overpotential (Fig. 14**I**). The work provides insight into the conformational relationships of single-atom photocatalysts in terms of atomic coordination and electronic configuration, thereby bringing new understanding for the design and construction of effective photocatalytic OWS and other solar energy conversion systems.

As we all know, the light capture capability is considered one of the important factors limiting semiconductor OWS. Currently, most semiconductor photocatalysts could only respond to ultraviolet (UV) light, thus it is urgent to develop near-infrared (NIR) driven OWS system to fully utilize the abundant solar energy resources. Shi et al. constructed an NIR light-driven photocatalyst for OWS by selective photo-deposition of Pt single atoms/clusters on phytate nickel-sensitized polymerized carbon nitride (PA-$Ni_{1.1}$ @PCN/Pt_{5hNIR}) (Fig. 14**J**) [155], which could be realized as an electron collector at $\lambda > 800$ nm to greatly enhance the H_2 and O_2 evolution reaction in pure water (Fig. 14**K**). Experimental datas indicated that PA-Ni complex was excited under NIR light ($\lambda > 800$ nm) irradiation to produce photogenerated e^- and PA-Ni^+ complex. Subsequently, e^- were injected into the CB of PCN and participate in the H^+ reduction to H_2 with Pt-SAC co-catalyst. Meanwhile, the PA-Ni^+ would return to the original PA-Ni state by accepting electrons from water oxidation to produce O_2 (Fig. 14**L**). In summary, high-efficiency photocatalysts with wide light absorption range for OWS will be a hot topic in energy conversion.

4.1.3. *Photocatalytic H_2 evolution coupled with organics oxidation*

Sacrificial agents are often used to consume photogenerated holes and thus improve the efficiency of photocatalytic HER [217–219]. Nevertheless, this case does not seem to be the most reasonable solution. It would be intriguing, economical and controllable to replace the sacrificial agent oxidation reaction with organics selective oxidation reaction at the oxidation end [220]. In this case, simultaneous obtainment of the gas-phase product H_2 and the liquid-phase value-added chemicals can be realized, and the two are spatially separated. Importantly, efficient utilization of the photogenerated h^+ while suppressing the rapid photogenerated carriers recombination are two key challenges in photocatalytic HER coupled with organics selective oxidation reaction. For this purpose, SACs with unique coordination structures can recognize/adsorb organic molecules in a directional manner and

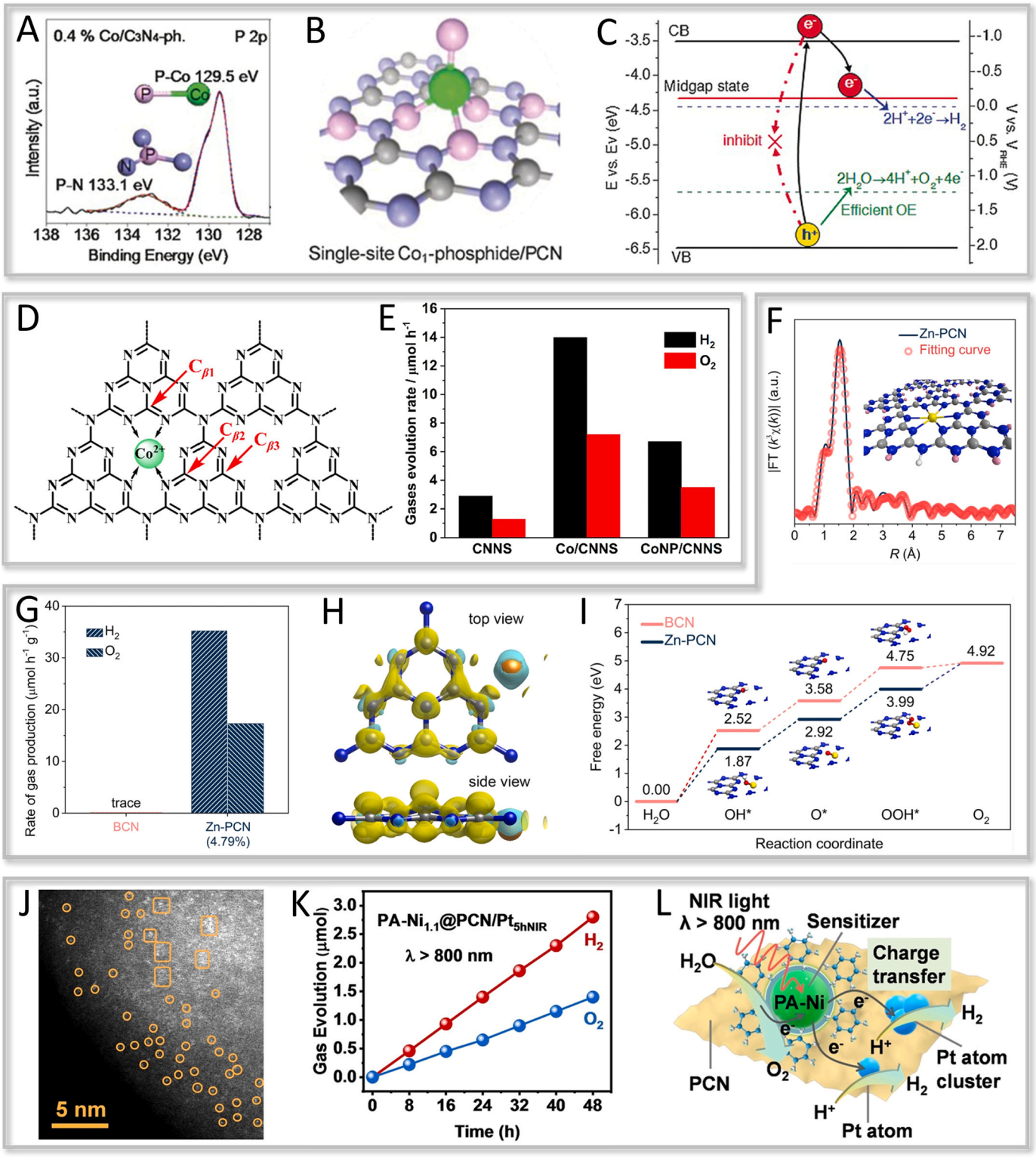

Fig. 14. (A) P 2p XPS spectra of 0.4 wt% Co/C_3N_4-phosphidation. (B) Schematic structural model and (C) electronic band structure diagram for Co_1-phosphide/PCN [216]. (D) The proposed structure of Co/CNNS. (E) Photocatalytic overall water splitting performances of different samples [167]. (F) Fitting curve of FT-EXAFS and structure model for Zn-PCN. (G) Photocatalytic overall water splitting performance, (H) differential charge density map and (I) calculated free energy diagrams of Zn-PCN [117]. (J) HAADF-STEM image, (K) time-coursed water splitting reaction and (L) possible photocatalytic overall water splitting mechanism of PA-Ni-sensitized PCN coupled with Pt-SACs system [155].

activate the reaction substrate efficiently. Furthermore, the highly dispersed isolated metal atoms suggested the abundant active sites and high atomic utilization, which provides the possibility to improve the photogenerated carrier separation.

Zhao's group reported an intercalated structure of hollow carbon nitride spheres composed of carbon nitride nanosheets loaded with Cu single atoms (Cu_1 @HCNS) (Fig. 15**A**) [141]. The results showed that isolated Cu species embedded in HCNS are indicated to form a Cu-N_3

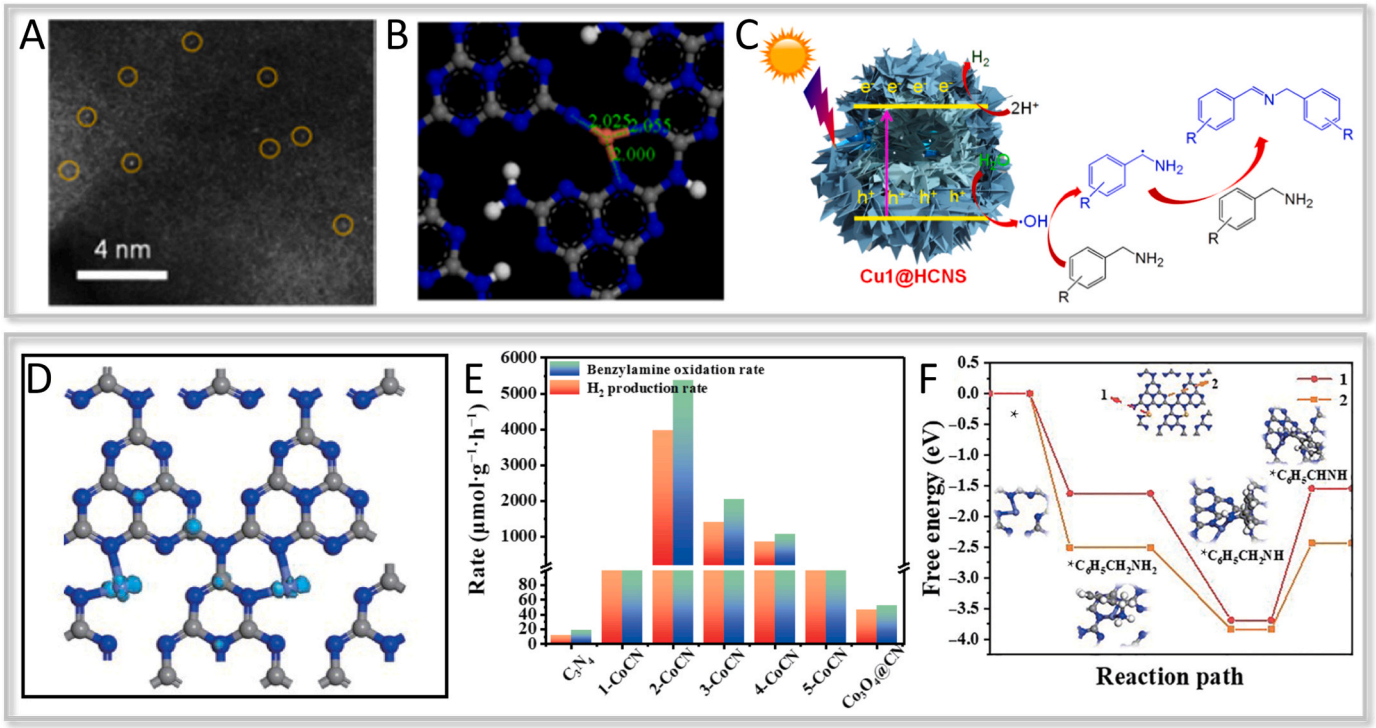

Fig. 15. (A) HAADF-STEM image and (B) Cu_1N_3 site coordination model of Cu_1 @HCNS. (C) Plausible reaction mechanism of photocatalytic synergistic reaction over Cu_1 @HCNS [141]. (D) The polarized charge distribution of 2-CoCN. (E) Photocatalytic HER coupled with benzylamine oxidation rate under the magnetic field. (F) DFT calculated Gibbs free energy for amines oxidation [126].

structure with three N atoms coordinated (Fig. 15**B**). The optimized Cu_1 @HCNS sample exhibited an H_2 evolution rate of 3261 μmol g^{-1} h^{-1} with TEOA as the sacrificial agent and 3 wt% Pt as the co-catalyst. Interestingly, in benzylamine aqueous solution, Cu_1 @HCNS was still able to perform photocatalytic HER and selectively oxidize benzylamine to the coupling product imine without oxygen participation. The mechanism of photocatalytic HER coupled with benzylamine non-oxygen coupling reaction was proposed by free radical scavenging experiments. Under light irradiation, photogenerated e^- are excited from the VB of Cu_1 @HCNS to CB, and the corresponding h^+ left in VB. Then, the e^- reduce H^+ to H_2, while the h^+ oxidize H_2O to hydroxyl radicals (·OH). Subsequently, the carbon-center cation is generated from the·OH and coupled with benzylamine to produce imine, as shown in Fig. 15**C**. Furthermore, the presence of Co-N bonds in Yin et al.'s research results in the generation of spin charge under the influence of a weak magnetic field (Fig. 15**D**) [126]. They harnessed the magnetic field to enhance the photocatalytic synergistic activity, and the optimized 2-CoCN sample exhibited remarkable HER rate and benzylamine oxidation rate of 3979.0 μmol·g^{-1}·h^{-1} and 5371.6 μmol·g^{-1}·h^{-1} respectively (Fig. 15**E**). DFT calculations revealed that the introduction of Co-N bonds not only disrupts the original overlap state of the C_3N_4 electron cloud, leading to spin charge polarization, but also effectively reduces the energy barrier of rate-determining step for the benzylamine oxidation process (Fig. 15**F**). These works provide a new strategy to construct bifunctional photoredox system based on g-C_3N_4 SACs, for improving the efficient utilization of solar energy.

4.2. *Photocatalytic H_2O_2 synthesis*

As a strong oxidizing agent, hydrogen peroxide (H_2O_2) is widely used in medical, military and industrial applications as a disinfectant, fuel and chemical raw material, and it is more easily stored and transported as a liquid energy source [221–223]. Traditionally, H_2O_2 has been produced industrially by the "anthraquinone method", but it is plagued by high-energy consumption and environmental pollution [224,225]. The efficient production of H_2O_2 from H_2O and O_2 by artificial photosynthesis using solar energy under ambient temperature and pressure is a promising green pathway [226]. Moreover, the development of efficient and stable photocatalysts has become the key to synthesize H_2O_2 using solar energy. In recent years, g-C_3N_4-based SACs have made great progress in H_2O_2 photochemical green synthesis due to the SMSI effect, and it is expected that the energy conversion efficiency of solar-chemical energy can be further improved through rational structural design.

The photosynthesis of H_2O_2 mainly consists of oxygen reduction (ORR) and water oxidation (WOR) pathways, as demonstrated in Fig. 16. As we all know, most g-C_3N_4-based SACs are reported to follow the 2-electron ORR process. The main bottlenecks currently in photocatalytic H_2O_2 production are the slow oxidation process of H_2O molecule and the difficulty in controlling the kinetic process of oxygen reduction. In order to solve the problems of low activity and low selectivity of the two-electron ORR, Ohno and coworkers developed a robust photocatalyst with Sb species atomically dispersed on g-C_3N_4 (Sb-SAPC) [96], which was used for the efficient H_2O_2 synthesis in a pure water and oxygen mixture under visible light irradiation by tuning the adsorption state of oxygen (Fig. 17**A**). Fig. 17**B** demonstrates the surface

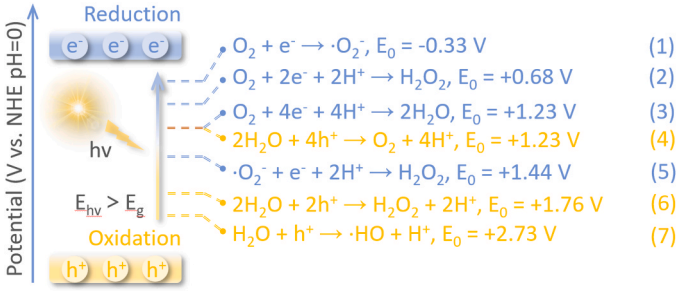

Fig. 16. H_2O_2 production pathways via photocatalysis.

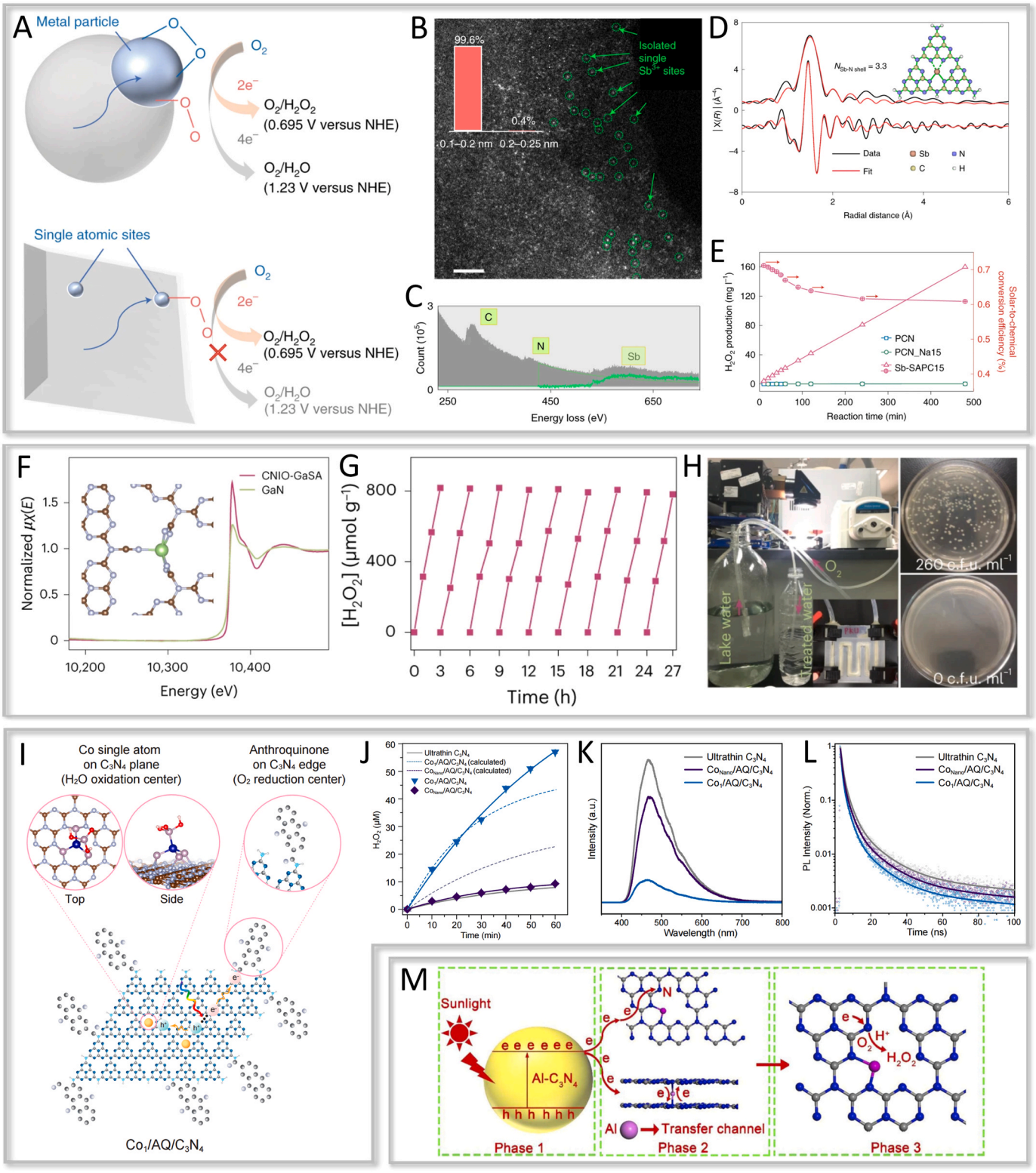

Fig. 17. (A) Photocatalytic H_2O_2 production via ORR process on a metal particle and an isolated atomic site, respectively. (B) HAADF-STEM image, (C) EELS spectrum and (D) EXAFS data fitting result of Sb-SAPC15. (E) Solar-to-chemical conversion efficiency of different samples [98]. (F) XANES at K-edge, (G) cyclic stability and (H) antibacterial properties evaluation of CNIO-GaSA [102]. (I) The structure model of $Co_1/AQ/C_3N_4$. (J) Time coursed H_2O_2 production, (K) PL spectra and (L) TR-PL spectra of prepared samples [227]. (M) Schematic diagram of the photocatalytic H_2O_2 production mechanism over Al-C_3N_4 [228].

state of Sb-SAPC, with the bright spots believed to be isolated Sb atoms, almost all of which are between 0.1 and 0.2 nm in size. Electron energy loss spectroscopy (EELS) further verified the presence of Sb and the successful preparation of Sb-SAPC photocatalyst (Fig. 17**C**), while EXAFS spectra further reveal the Sb-N_4 structure in Sb-SAPC (Fig. 17**D**). Impressively, H_2O_2 was prepared with an apparent quantum yield (AQY) of 17.6% at 420 nm and a solar chemical conversion efficiency of 0.61% (Fig. 17**E**). The photocatalytic performance of Sb-SAPC can be

attributed to the significantly enhanced kinetics of 2-electron ORR, with the formation of μ-peroxides at the Sb site and a high concentration of holes at neighboring N atoms. In addition, the in-situ generated O_2 via water oxidation reaction is rapidly consumed by the ORR, which effectively accelerates the overall reaction kinetics. Recently, Guo and co-workers designed a photocatalyst with fast charge separation of antiproteinite-structured carbon nitride-anchored Ga atoms (CNIO--GaSA) (Fig. 17**F**) [102], which could enable the metastable 2-electron WOR and 2-electron ORR pathways for H_2O_2 photosynthesis. In 2-electron WOR process, *OH, as a key intermediate, can be coordinated with Ga and N atoms in Ga-N_5 sites, respectively, which reduced the reaction formation energy and optimizes the kinetics of WOR. The photocatalysts were coated on the serpentine channels of a homemade quartz microreactor for the continuous H_2O_2 production, which was found to be able to sustain 9 cycle tests totaling 27 h (Fig. 17**G**). Interestingly, in Fig. 17**H**, the H_2O_2 produced in-situ in the microreactor could effectively kill bacteria in the lake water due to its decomposition into the strongly oxidizing·OH radical.

Meanwhile, simultaneous loading of oxidation and reduction co-catalysts is expected to improve the selectivity and efficiency of photocatalytic H_2O_2 green synthesis. Kim et al. proposed a center-edge strategy by loading single-atom cobalt co-catalysts at the center of C_3N_4 as oxidation centers [227], and anthraquinone molecule (AQ) co-catalysts at the edges of C_3N_4 as reduction centers (Co_1/AQ/C_3N_4) (Fig. 17**I**), which can spatially separate the oxidation-reduction centers of C_3N_4. The photocatalytic activity of C_3N_4 was significantly enhanced by the simultaneous loading of oxidizing and reducing co-catalysts, with the H_2O_2 generation rate reaching 62 μM/h (Fig. 17**J**). Moreover, steady-state photoluminescence (PL) (Fig. 17**K**) and transient photoluminescence (TR-PL) (Fig. 17**L**) have demonstrated that Co_1/AQ/C_3N_4 had lower fluorescence intensity with excitation lifetime, respectively, strongly suggesting that the Co single atoms and AQ lead to spatial separation of photo-excitons. Notably, the boosted multiplicity coincides with the product of the Co-loaded and AQ-loaded multiplicities due to the contribution of co-catalytic co-effect of Co single sites and AQ, implying no short-circuiting of the oxidation-reduction centers occurs.

As a general rule, monodisperse metal atoms are often used as traffic hubs for photogenerated carrier migration or adsorption sites for reaction substrates after forming coordination sites with C or N atoms of g-C_3N_4. Interestingly, a new role for monodisperse metal sites in g-C_3N_4 was redefined by Han et al. [228] They constructed a g-C_3N_4-based SAC with Al-N_2 coordination, where monodisperse Al metal sites act as bridges between the g-C_3N_4 networks to facilitate efficient carrier separation and provide efficient non-metallic N active sites for H_2O_2 photosynthesis (Fig. 17**M**). This novel work reveals the innovative role of atomically dispersed metal sites in creating non-metallic active centers for high-performance catalytic reactions.

4.3. *Photocatalytic organic synthesis*

The theme of contemporary organic synthesis reaction (OSR) focuses on the preparation of value-added compounds or substances not found in nature from simple organic/inorganic small molecules via convenient, efficient, and accurate synthetic methods [115]. Photons as a non-traceable reagent can provide energy to activate substrates or catalytic intermediates under mild conditions, thus making photocatalysis a sustainable and powerful tool in OSR, which has attracted much attention in recent years [229–231]. However, OSR is traditionally occurred accompanied by unpredictable and uncontrollable non-selective reactions, leading to significant limitations in practical industrial applications due to slow reaction rates. Numerous excellent works have demonstrated the superiority of isolated catalytic sites of SACs for selective modulation of OSR products, bringing atomic-level ideas to OSR [81,232]. Herein, we discuss the recent advances in g-C_3N_4-based SACs for photocatalytic OSR efforts, such as C-H bond activation, hydrogenation and C-C coupling.

C-H bond activation/functionalization has a positive impact on improving reaction efficiency and atom economy, and is considered a dream reaction for OSR [233,234]. New compounds could be created by directly and selectively breaking the C-H bond and replacing it by C-X bond [235]. However, due to the high bond energy, small polarity and strong inertness of C-H bond, it is extremely challenging to achieve C-H bond activation under mild conditions. Fu et al. demonstrated the formation of a low self-selecting state Fe-N_4 structure by anchoring single Fe atoms on C_3N_4 [236]. The isolated Fe sites functioned as bridges, allowing the rapid transfer of photogenerated electrons from the C_3N_4 network to adsorbed O_2 molecules (Fig. 18**A**), generating superoxide radical ($\cdot O_2^-$). As a result, the $\cdot O_2^-$-driven ethylbenzene-to-acetophenone conversion reaction has a high conversion of 99% and a high selectivity of 99%. Furthermore, comparing the influence degree of different radicals on the reaction (Fig. 18**B**), the reaction involving $\cdot O_2^-$ was found to have much lower energy barriers to overcome compared to the pathway involving·OH, suggesting that the $\cdot O_2^-$ induced reaction pathway is more accessible (Fig. 18**C**). In addition, heterogeneous atom coordination strategy modulates the separation of photogenerated electrons and holes at atomic-level, promoting efficient charge carrier separation and benefiting photocatalytic green solar energy conversion. Zhao and co-workers reported a g-C_3N_4-based SACs (Cu-N_1O_2 SA/CN) with a novel Cu_1-N_1O_2 coordination structure (Fig. 18**D**) [128]. The introduction of O atoms with strong electronegativity is beneficial to promote rapid charge transfer between C_3N_4 and Cu single atoms compared to pure Cu-N coordination. Bader charge results (Fig. 18**E**) verify that the number of electrons transferred from Cu atoms to neighboring atoms in the Cu_1-N_1O_2 site (0.966 |e|) is much higher than that in the Cu_1-N_2 (0.741 |e|) and Cu_1-N_3 (0.664 |e|) sites. In addition, the strong electrophilicity and rapid electron-transferring ability of the O atoms led to the Cu_1-N_1O_2 site possessing fewer Cu-3d electrons, implying more empty 3d orbitals were generated (Fig. 18**F**), which facilitated the reactants adsorption. As a result, the Cu_1-N_1O_2 site could provide an advantageous reaction pathway with few steps and low energy barriers for the selective oxidation of benzene to phenol reaction (Fig. 18**G**), which effectively promotes the selective oxidation of benzene to phenol (SOBP) reaction at a very low molar ratio of H_2O_2/benzene (2:1), exhibiting a high benzene conversion of 83.7% and a phenol selectivity of 98.1%. Moreover, the construction of dual active sites can expose a greater number of reactive sites, thereby providing additional reaction channels and enhancing catalytic efficiency. Additionally, the dual active sites can synergistically interact to promote the progress of OSR, thus improving the selectivity and activity. Wang et al. proposed a dual active-site g-C_3N_4-based photocatalyst (Cu SAs/p-CNS) containing Cu-N_4 and C-S-C active moieties (Fig. 18**H-I**) [168]. Under visible light irradiation, Cu SAs/p-CNS successfully oxidized 5-hydroxymethylfurfural (HMF) to 2,5-dicarbonylfuran (DFF) with 77.1% conversion and 85.6% selectivity, respectively, and the activity was significantly higher than that of other reference samples (Fig. 18**J**). In Fig. 18**K**, mechanistic studies show that Cu SAs/p-CNS has a longer carrier lifetime (4.90 ns) compared with Cu SAs/p-CN and p-CNS, which is attributed to the fact that the isolated Cu-N_4 site and the surrounding S atoms can serve as the capture units for photogenerated electrons and holes, respectively. This synergistic promotion of spatial separation of photogenerated carriers was engineered to effectively enhance the photocatalytic OSR activity. These works regulate the spatial charge transport kinetics by rationally modulating the interactions between single metal atoms and g-C_3N_4 support to obtain selectively upgraded products, which provides new research thought for the development of g-C_3N_4-based SACs in photosynthesis.

Hydrogenation reactions, which prepare new compounds by the interaction of compounds with H species, have been widely used in the synthesis of fragrances, petroleum, and other industries [237–239]. The downside is that the H source is traditionally derived from H_2 due to the large dissociation energy barrier of H_2O molecules ($\Delta G = +237$ kJ mol^{-1}). Fortunately, the photocatalytic mechanism confers the

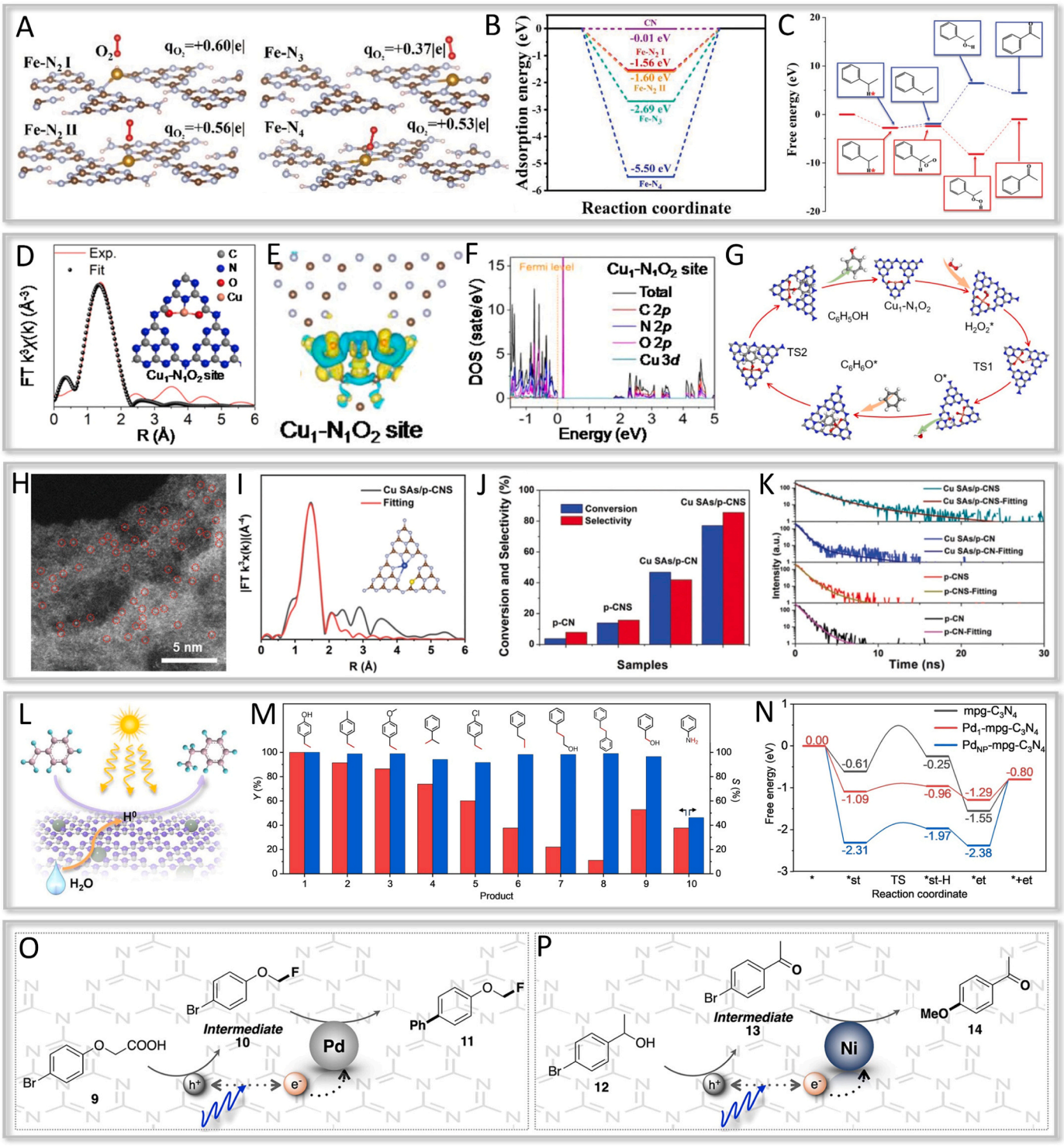

Fig. 18. (A) Calculated charge difference maps and (B) oxygen adsorption energy of different Cu coordination. (C) Energy diagram of the two different pathways of ethylbenzene oxidation by SA-Fe-TCN [236]. (D) EXAFS fitting curve in R space. (E) Differential charge density map and (F) density of states of Cu_1-N_1O_2. (G) Possible mechanism of Cu_1-N_1O_2 site for selective benzene oxidation [128]. (H) AC STEM image and (I) EXAFS fitting result at R space of Cu SAs/pCNS. (J) Photo-oxidation of HMF to DFF and (K) TR-PL spectra over different samples [168]. (L) Graphic scheme and (M) photocatalytic activity of hydrogenation over Pd_1-mpg-C_3N_4. (N) Energy profiles for the photocatalytic styrene-to-ethylbenzene conversion [76]. Schematic of relay catalysis mechanism on (O) Pd_1/C_3N_4 and (P) Ni_1/C_3N_4 under irradiation [242].

potential to achieve hydrogenation conversion under ambient pressure and temperature [240,241], making it possible to use H_2O as an ultimately desirable green H source for hydrogenation reactions. Chen et al. successfully prepared a non-homogeneous catalyst loaded with single Pd atoms on C_3N_4 (Pd_1-mpg-C_3N_4) [76], which can be used universally for the active H species produced by hydrolysis for the hydrogenation of unsaturated bonds (C═C, C═O, N = O), as shown in Fig. 18**L-M**. Compared with mpg-C_3N_4 and Pd_{NP}-mpg-C_3N_4, the energy distribution of the reaction process for the hydrogenation of styrene into ethylbenzene revealed by DFT calculations (Fig. 18**N**) shows that

Pd_1-mpg-C_3N_4 is more favorable for lowering the hydrogenation energy barriers and promoting the ethylbenzene desorption.

The photocatalytic C-C coupling, facilitated by light-activated catalysts, enables the efficient construction of intricate organic molecular structures and facilitates the formation of carbon-carbon bonds. By harnessing renewable energy sources, it streamlines synthetic pathways, thereby reducing waste generation and aligning with the imperatives of sustainability. Consequently, photocatalytic C-C coupling reactions hold significant promise for applications, particularly in the realm of pharmaceutical synthesis. For example, Yoo et al. have unraveled the relay photooxidation reaction mechanism of Pd and Ni species in single atom photocatalysis [242]. Compared with Pd nanoparticles, Pd single atom species can efficiently drive photocatalytic C-C cross coupling to achieve the decarboxylative fluorination reaction with 4-tert-butylphenoxyacetic acid (73% total yield, Fig. 18**O**). Fluorine radicals were introduced into alkyl radicals by photogenerated electron interaction and the desired products were generated by radical combination. In addition, the prepared Ni_1/C_3N_4 exhibited C-O cross coupling relay catalysis to oxidize 4-bromo-α-methylbenzyl alcohol to 4′-methoxyacetophenone (92% total yield, Fig. 18**P**). Obviously, this one-pot relay strategy was superior to the stepwise method in terms of OSR yield and efficiency. More importantly, the catalytic coupling orthogonality induced by M_1/C_3N_4 has a broad substrate range and is considered a green and sustainable synthetic process.

4.4. Photocatalytic N_2 fixation to NH_3

In the century boom of energy conservation and emission reduction, countries around the world are actively searching for next-generation energy technologies, and the efficient utilization of ammonia (NH_3) is becoming the focus of recent global attention [243–245]. Currently, NH_3 synthesis is expanding from the most traditional Haber-Bosch process to green methods. Photocatalytic N_2 fixation is considered as one of the important ways to achieve green synthesis of NH_3, yet its yield is limited by slow charge transfer kinetics and inert N≡N bonds (binding energy up to 941 kJ mol^{-1}) [246]. In general, SMSI effect between

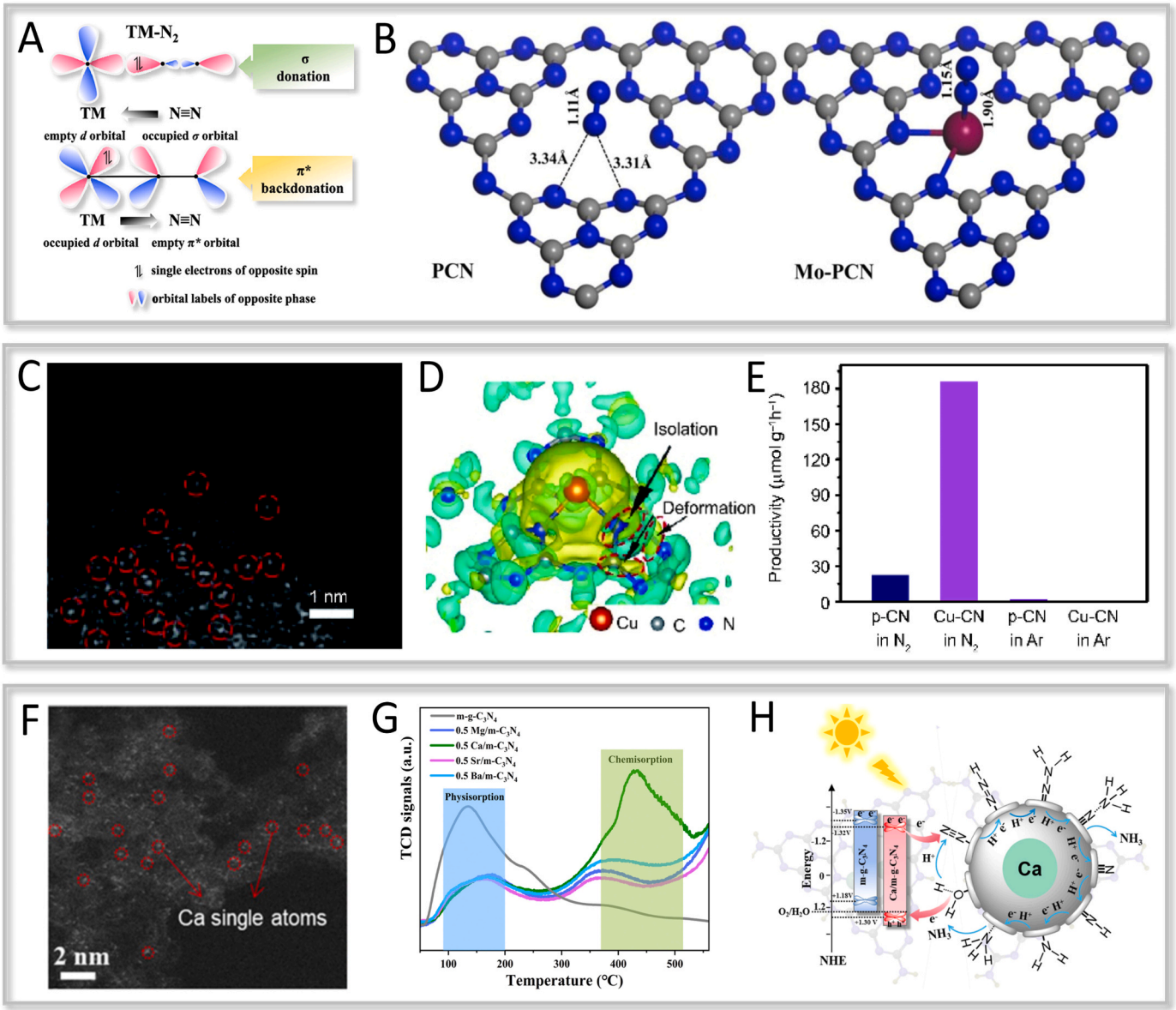

Fig. 19. (A) Simplified schematic of N_2 bonding to transition metals [247]. (B) Optimized N_2 adsorption model on pure PCN and Mo-PCN [248]. (C) HAADF-STEM image, (D) charge density distribution map and (E) photocatalytic N_2-to-NH_3 production rate of Cu-CN [93]. (F) HAADF-STEM image of 0.5 Ca/m-g-C_3N_4. (G) N_2 chemisorption spectra of different samples. (H). The energy band structure and the possible pathway of N_2 fixation to NH_3 [249].

single metal atoms and g-C_3N_4 induce charge transfer and create empty orbitals with the potential to accommodate N_2 molecules. Taking this into account, Guo et al. computationally predicted the possibility of a series of transition metal single atoms anchored to g-C_3N_4 for N_2 fixation [247]. They demonstrated that the empty d-orbitals of transition metal atoms allow accepting lone electron pairs from N_2 and sharing the discrete d-electrons to the π^*-orbitals of N_2 molecules (Fig. 19**A**). Although this work was initially intended to be used for designing N_2 fixation electrocatalysts, it has also inspired researchers that the electronic "acceptance-donation" interactions between transition metal single atoms and N_2 molecules are effective in weakening N≡N bonds. Thus, g-C_3N_4-based SACs could be served as an ideal photocatalyst for N_2 fixation. For example, in exploring the photoreduction of N_2 to NH_3, Lu et al. found that the loading of single Mo atoms effectively reduced the distance between N_2 and the g-C_3N_4 surface (from 3.34 Å to 1.90 Å) [248], indicating that the presence of the Mo-N_2 structure could enhance the N_2 adsorption. More importantly, the N≡N bond length is elongated from 1.11 Å to 1.15 Å with single Mo atom anchoring, which well explains the role of single metal atoms on the weakening of N≡N (Fig. 19**B**). In addition, Xie and coworkers introduced single Cu atoms into g-C_3N_4 for coordination with three N atoms (Cu-CN) (Fig. 19**C**) [93]. The formation of Cu-N_3 coordination changes the electron density of the neighboring N atoms, and π-electrons used in the conjugation result in off-domains or are isolated due to coordination effects (Fig. 19**D**). These valence electrons freed from the constraints of the conjugated π-electron cloud increase the number of effective electrons, which facilitates subsequent hydrogenation reactions. The single Cu atom was also able to effectively drive the photogenerated electron-hole separation, allowing electron transfer to adsorbed N_2 molecules via Cu. As a result, Cu-CN achieved a stepwise hydrogenation reaction to produce NH_3 in aqueous solution under mild conditions with a yield rate of 186 μmol g^{-1} h^{-1} (Fig. 19**E**). Typically, p-block elements often activate the N_2 photo-fixation reaction with transition metal atoms as active sites, while few reports on s-block elements are available. In 2022, Han et al. have modified Ca single atoms on g-C_3N_4 (Fig. 19**F**) to enhance the photocatalytic N_2 fixation activity [249]. Surprisingly, N_2 temperature programmed desorption experiments confirmed that isolated Ca sites were able to substantially enhance N_2 chemisorption (Fig. 19**G**), implying that Ca sites are similarly weakening for N≡N. Finally, successive hydrogenation reduction processes led to the formation of an NH_3 molecule (Fig. 19**H**).

5. g-C_3N_4-based SACs for emerging reactions in environmental remediation

5.1. Water purification

5.1.1. Photocatalytic pollutants degradation

Rapidly developing industrialization processes have uncontrolledly demanded resources from nature, leaving behind irreversible environmental damage despite the great technological advances [250–252]. The main threat comes from organic dyes (such as methyl orange [253], methylene blue [254], rhodamine B [255], carbamazepine [256], etc.) in industrial effluents, causing adverse effects on human health due to their rapid spread and persistence. Photocatalytic pollutants degradation uses solar energy to generate highly active free radicals in the reaction system [257,258], which will undergo processes such as addition, substitution, and electron transfer with organic pollutants, thus degrading or mineralizing the pollutants into inorganic substances. To date, oxide-based photocatalysts represented by TiO_2 have been widely used in wastewater purification [259–261]. However, the narrow range of light-absorbing wavelengths severely limits the practical application of TiO_2 [262]. Surprisingly, visible light-responsive g-C_3N_4-based photocatalysts show promising results in removing pollutants in aqueous phase [263,264]. g-C_3N_4-based SACs are considered as a very attractive photocatalysts due to the non-metallic nature of the support and low metal content, which can minimize the secondary pollution to the environment. Here, we discuss the recent advances of g-C_3N_4-based SACs in pollutants degradation to elucidate the microscopic mechanism of the isolated site structure design for the reactive radicals generation, charge transfer, and pollutants removal.

In this regard, Lu et al. obtained photocatalysts (W-CN) immobilizing a high loading (11.16 wt%) of W single atoms on g-C_3N_4 (Fig. 20**A**) by a conventional thermal depolymerization method [265]. As illustrated in Fig. 20**B**, the EXAFS and DFT results further verified that W is atomically dispersed on g-C_3N_4 and is co-coordinated with both one N atom and three O atoms to form a unique N-W-O_3 moiety. As expected, W-CN achieved 96% removal efficiency of carbamazepine under visible light. The enhanced photocatalytic activity of W-CN is mainly due to the synergistic effect of multiple active species, including photogenerated holes (h^+), superoxide radicals ($\bullet O_2^-$) and singlet oxygen ($^1O_2$) (Fig. 20**C**). Moreover, the catalytic performance of transition metal single atom photocatalysts is affected by the electronic configuration of the d-orbitals. Niu and coworkers introduced P atoms with lower electronegativity into the synthesis of Co and Ni double single-atom-loaded g-C_3N_4 (CCoNiP) (Fig. 20**D**) [266]. The DFT calculation results showed that the CCoNiP was capable to transfer more electrons to the target pollutant tetrachlorobisphenol A (TCBPA) (Fig. 20**E**). Under visible light irradiation, CCoNiP could effectively degrade TCBPA, achieving 100% removal and 44.1% dichlorination (Fig. 20**F**). To sum up, P atoms can be introduced to change the local coordination environment to avoid the oxidation of the metal active site and increase the d-band center position (Fig. 20**G**), which can also synergize with N atoms to improve the catalytic activity. Indeed, apart from organic dye pollutants, pharmaceuticals and personal care products (e.g., Naproxen (NPX) and tetracycline hydrochloride) are widely present in natural waters and their ecological threat is indisputable [267,268]. Liang et al. successfully prepared tubular amorphous g-C_3N_4 photocatalysts (MA-2) with anchored single Ag atoms using supramolecular melamine hydrogels as precursors [269]. The doping of single Ag atoms broke the horizontal and vertical alignment order within the g-C_3N_4 layers, contributing to homogeneous amorphization (Fig. 20**H-I**). In Fig. 20**J**, the pseudo-first-order kinetic constant (k) for the degradation of NPX by MA-2 was calculated to be 1.92×10^{-1} min^{-1} under visible light, which was 90 times higher than that of pure g-C_3N_4 (2.1×10^{-3} min^{-1}). Furthermore, both acute toxicity and bioaccumulation factor assessments (Fig. 20**K**) indicated that MA-2 could effectively attenuate the ecotoxicity of NPX to aquatic organisms.

Moreover, the Fenton system has found its place in environmental chemistry, where Fenton reagents with high capacity to remove difficult-to-degrade organic pollutants have demonstrated a wide application in wastewater purification [270,271]. Typically, Fenton reagents are mixtures of H_2O_2 and Fe^{2+}, and are highly oxidizing due to the formation of·OH during the reaction ($Fe^{2+} + H_2O_2 \rightarrow Fe^{3+} + OH^- + \cdot OH$). Then the generated Fe^{3+} is reduced back to Fe^{2+} by H_2O_2, forming a closed cycle ($Fe^{3+} + H_2O_2 \rightarrow Fe^{2+} + HO_2\cdot + H^+$) [272]. In recent years, researchers have introduced UV and visible light into Fenton reactions to achieve higher pollutants degradation and resource utilization efficiency [273]. For Fe single atom photocatalysts, more and more attention has been paid to Fe atoms due to the maximum atomic utilization. Zhan et al. proposed a defective engineering of single Fe atoms anchored to g-C_3N_4 with abundant nitrogen vacancies (N_V) (Fig. 21**A**) for activation of H_2O_2 under visible light irradiation [145]. The results showed that the optimized sample (Fe_1-N_V/CN) exhibited excellent ciprofloxacin degradation activity, which was equivalent to 18 times that of pristine CN (Fig. 21**B**). The single Fe site was considered as a highly concentrated center of photocatalytic charge, which accelerated the H_2O_2 decomposition into·OH to efficiently degrade organic pollutants (Fig. 21**C**). Of note, a later improved protocol has emerged using non-ferrous salts and H_2O_2, referred to as the Fenton-like process [274]. It mainly involves other alternative transition metals and externally added or in situ generated H_2O_2. For example, Zhang and coworkers constructed N3c vacancies on the g-C_3N_4 surface to immobilize

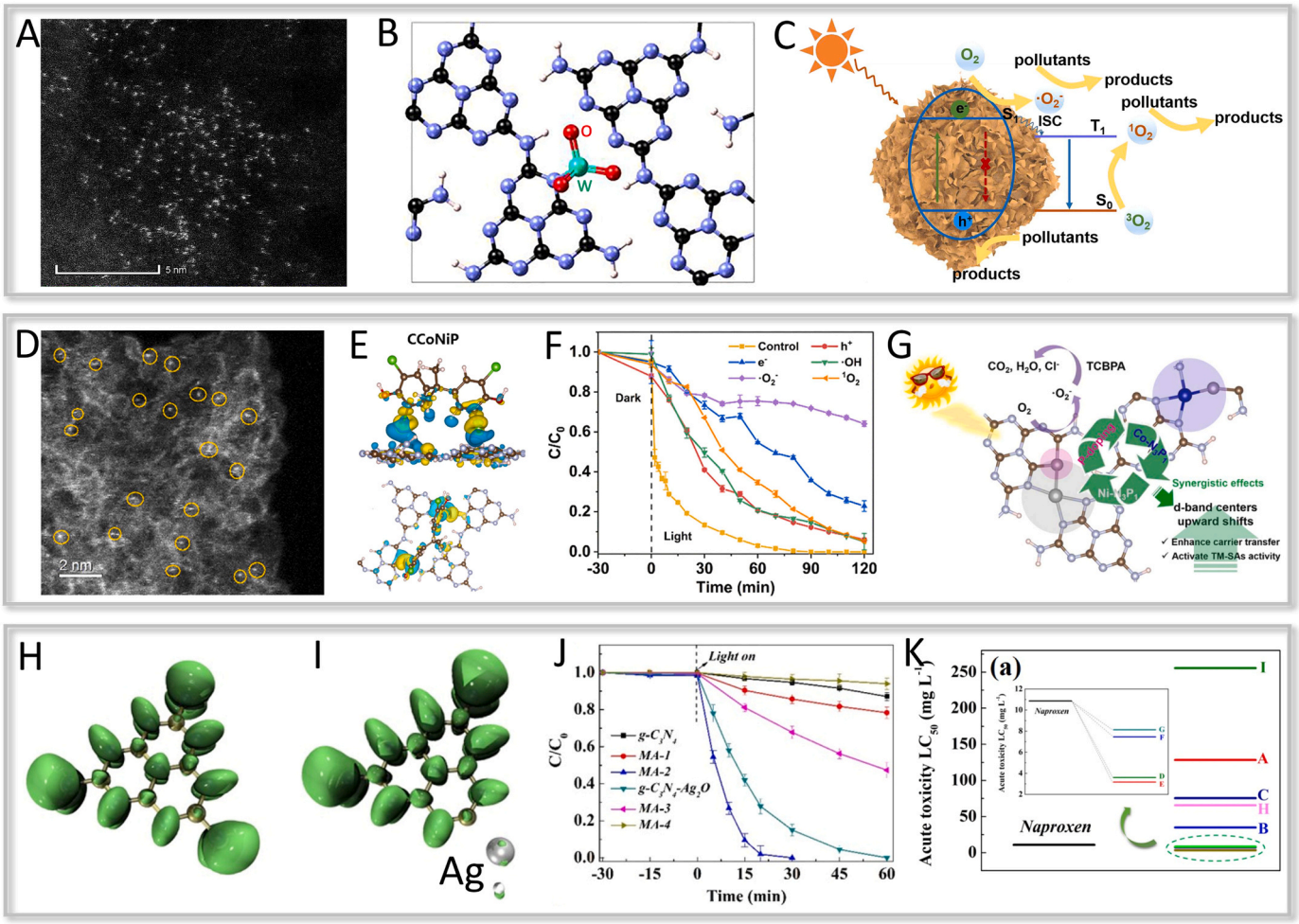

Fig. 20. (A) AC-TEM, (B) structural model of W sites and (C) photocatalytic pollutants degradation mechanism in W-CN system [265]. (D) HADDF-STEM image, (E) charge density maps, (F) quenching experiment and (G) possible mechanism of CCoNiP [266]. Isosurface of the pi-bond electron localization function of melem (H) without and (I) with Ag. (J) Photocatalytic NPX degradation activity and (K) toxicity evaluation of MA-2 [269].

isolated Cu-N_4 active sites (Cu/N_v-CN) (Fig. 21**D**) [275]. This strategy endowed Cu/N_v-CN with excellent degradation performance for multiple species of pollutants, such as phenolic compounds, endocrine disruptors, antibiotics and dyes. In particular, the phenol degradation efficiency reaches 14 times that of pure g-C_3N_4 (Fig. 21**E**). During the degradation process, the Cu(I) catalytic site follows a Fenton-like process, as shown in Fig. 21**F**. Firstly, H_2O_2 was activated to·OH for phenol degradation, and the depleted Cu(I) was regenerated by H_2O_2 reduction and continued to activate H_2O_2 to·OH. Finally, phenol is mineralized to CO_2 and H_2O. It is worth mentioning that peroxymonosulfate (PMS), as another Fenton oxidant, is capable for driving the active radical generation [276,277]. Therefore, the removal of pollutants from wastewater by activation of PMS is considered as an emerging approach. Inspired by this, Zou's group developed a supramolecular self-assembly strategy to synthesize highly loaded (11.2 wt%) Fe single atom g-C_3N_4-based photocatalyst (Fe_1/CN) (Fig. 21**G**) [125]. The isolated and uniformly dispersed Fe-N_4 centers are more inclined to adsorb the terminal O of PMS, which promotes the oxidation of PMS to generate·SO^{5-} (Fig. 21**H**), efficiently generating $^1O_2$ with 100% selectivity. As a result, Fe_1/CN efficiently and selectively degraded p-chlorophenol by activated PMS, and the apparent rate constant (K_{obs}) of the optimized samples was as high as 1.43 min^{-1}. Furthermore, Fe_1/CN exhibited a wide pH tolerance, and good cyclic stability, and strong resistance to interferences of anions and cations, organic matter, etc (Fig. 21**I**). In Table 3, we further demonstrate the recent 3 years advances on g-C_3N_4-based single atom photocatalysts for wastewater purification, to give the readers a deeper understanding of the trends in this field.

5.1.2. *Photocatalytic sterilization*

Apart from chemical contamination, biological contamination also deserves attention. Harmful bacteria are the main pathogens that enter the human body through drinking water, causing diarrhea and bacillary dysentery easily [288,289]. It has been reported that by 2050, more than 10 million people will die each year due to the misuse of wastewater containing bacterial pathogens [290]. To date, the commonly used sterilization techniques mainly include ultra-high temperature/high pressure sterilization [291], ultraviolet sterilization [292], and microwave sterilization [293], etc. The existing methods/equipment rely heavily on external energy consumption and high operating costs, while more toxic intermediates may be generated. Therefore, the development of highly efficient, low-toxicity, non-residual water disinfection biocides is still a top priority. Recently, artificial photocatalytic sterilization under ambient conditions provides a more sustainable method than conventional sterilization processes [294,295]. The g-C_3N_4-based SACs with good biocompatibility have emerged as an emerging platform for photocatalytic sterilization.

Wang et al. reported a carbon nitride semiconductor nano-enzyme (Cr-SA-CN) containing a Cr-N_4 coordination structure [296], which could produce and overcome H_2O_2 from O_2 and H_2O under visible light irradiation, resulting in the continuous production of hypobromous acid with significant bactericidal ability (Fig. 22**A**). The results showed that Cr-SA-CN had superior bacterial targeting ability for *Escherichia coli*

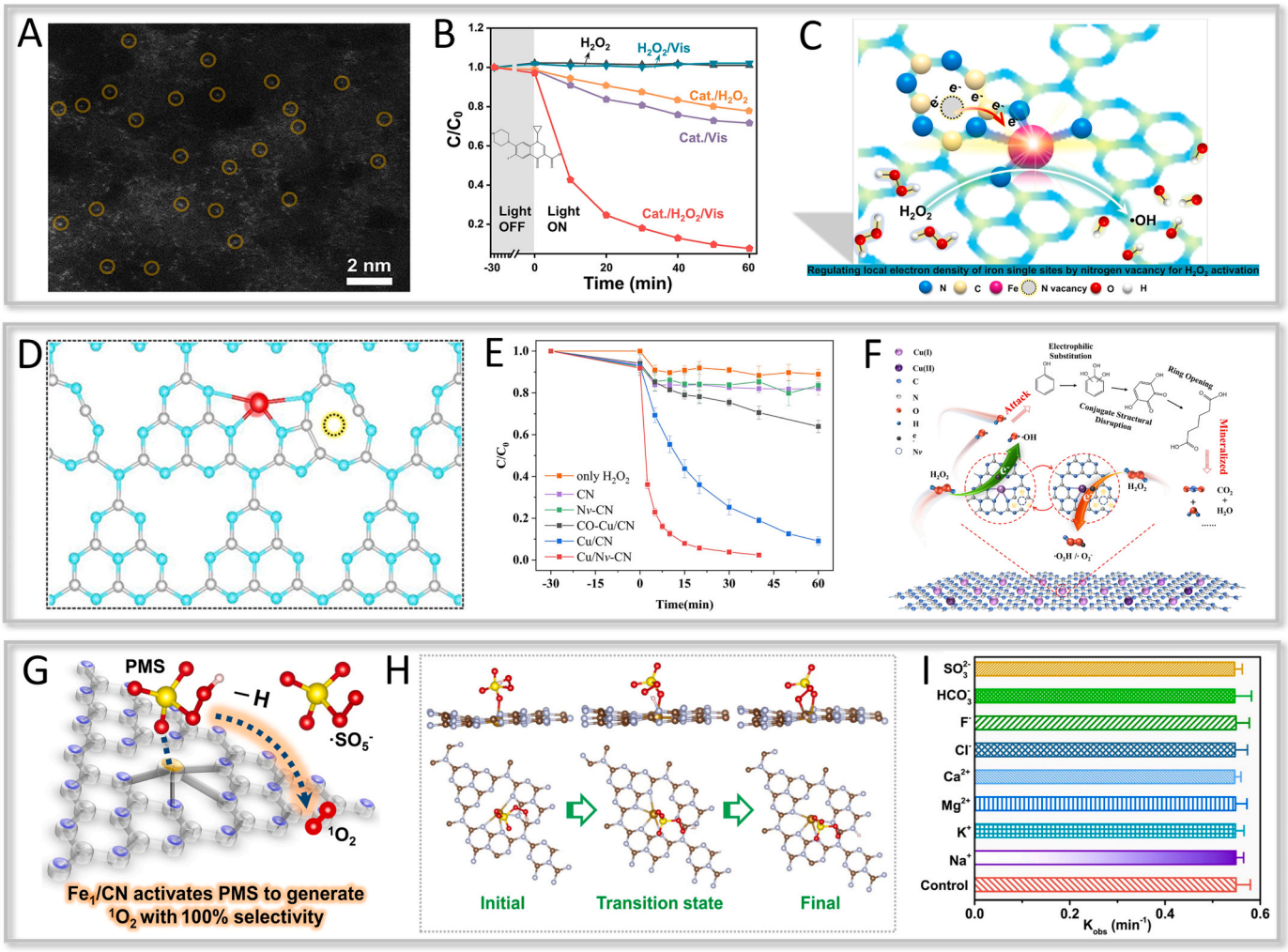

Fig. 21. (A) HAADF-STEM image of Fe_1-N_v/CN. (B) Photocatalytic degradation performance of CIP via Fenton process. (C) Schemic diagram of Fe atom structure and photocatalytic mechanism [145]. (D) Structural model of Cu-N_4 site with N3c vacancies, (E) phenol degradation and (F) mechanism over Cu/N_v-CN [275]. (G) Structural model, (H) evolution process of PMS-to-$\cdot SO_5^-$ and (I) stability test on Fe_1/CN [128].

Table 3
Recent works of g-C_3N_4-based SACs for photocatalytic wastewater purification.

Year	Catalyst	Coordination structure	Target pollutants (concentration)	Degradation efficiency		Reference
				Removal rate	k (min^{-1})	
2021	HFeNC-g-C_3N_4 +PMS	Fe-N_4	4-chlorophenol (10 μM)	99.6% (5 min)	1.663	Lv et al.[278]
2022	SA-Cu-CN+H_2O_2	-	Doxycycline hyclate (20 mg/L)	-	0.425	Kong et al.[279]
2022	FeCNs+ peracetic acid	-	Bisphenol A (10 mg/L)	100% (6 min)	0.75	Yu et al.[280]
2022	NiCN-4	Ni-N_4	Tetracycline (10 mg/L)	89.4% (120 min)	0.016	Liang et al.[281]
2022	Co-N_3O_1 +PMS	Co-N_3O_1	Ciprofloxacin (5 mg/L)	100% (20 min)	0.287	Xu et al.[282]
2022	SAFe-MCN +PMS	Fe-N_4	Sulfamethoxazole (10 mg/L)	98.7% (6 min)	0.602	Ren et al.[283]
2022	10-Mo/Nv-TCN	Mo- C_2N_2	Tetracycline (-)	94.45% (60 min)	0.049	Zeng et al.[88]
2022	FeSA-NGK+PMS	Fe-N_5	Bisphenol A (30 mg/L)	> 98% (10 min)	$k_1 = 0.545$ $k_2 = 0.288$	Sun et al.[284]
2023	Fe-SACs /g-C_3N_4	Fe-N_4	2-Mercaptobenzothiazole (20 mg/L)	99% (35 min)	0.078	Hu et al.[285]
2023	Co-MCN+PMS	Co-N_{1+3}	Bisphenol A (10 mg/L)	~100% (60 min)	> 0.07	Wang et al.[286]
2023	CoCN-2 +PMS	Co-N_4	Carbamazepine (10 mg/L)	99.6%	0.355	Li et al.[156]
2023	SA Fe-g-C_3N_4 +PMS	Fe-N_4	Tetracycline (10 mg/L)	93.29% (40 min)	~0.045	Hu et al.[287]

(*E. coli*) and *Staphylococcus aureus* (*S. aureus*). After light irradiation, the number of Cr-SA-CN+Br^- group bacterial colonies was significantly reduced, and the inhibition efficiencies reached 97% and 96%, respectively (Fig. 22**B**). Surprisingly, the applying of Cr-SA-CN to actual seawater (where Br^- is naturally present) demonstrated significant anti-fouling effects, resulting in a significant reduction of marine microbial attachment (Fig. 22**C**). In addition, Li and coworkers prepared a novel photocatalyst with switchable single Ti-Nx sites anchored on g-C_3N_4 surface (Fig. 22**D**) [297]. As shown in Fig. 22**E**, the covalent interaction between single Ti atom and six nitrogen atoms enriches the off-domain electrons around the single Ti atom. Notably, the coordination number of the flexible Ti-Nx sites could be significantly in-situ tuned from Ti-N_6 to Ti-N_4 upon light-driven interaction with adsorbed O_2, resulting in the production of clean active species ($\cdot O_2^-$ and·OH) in

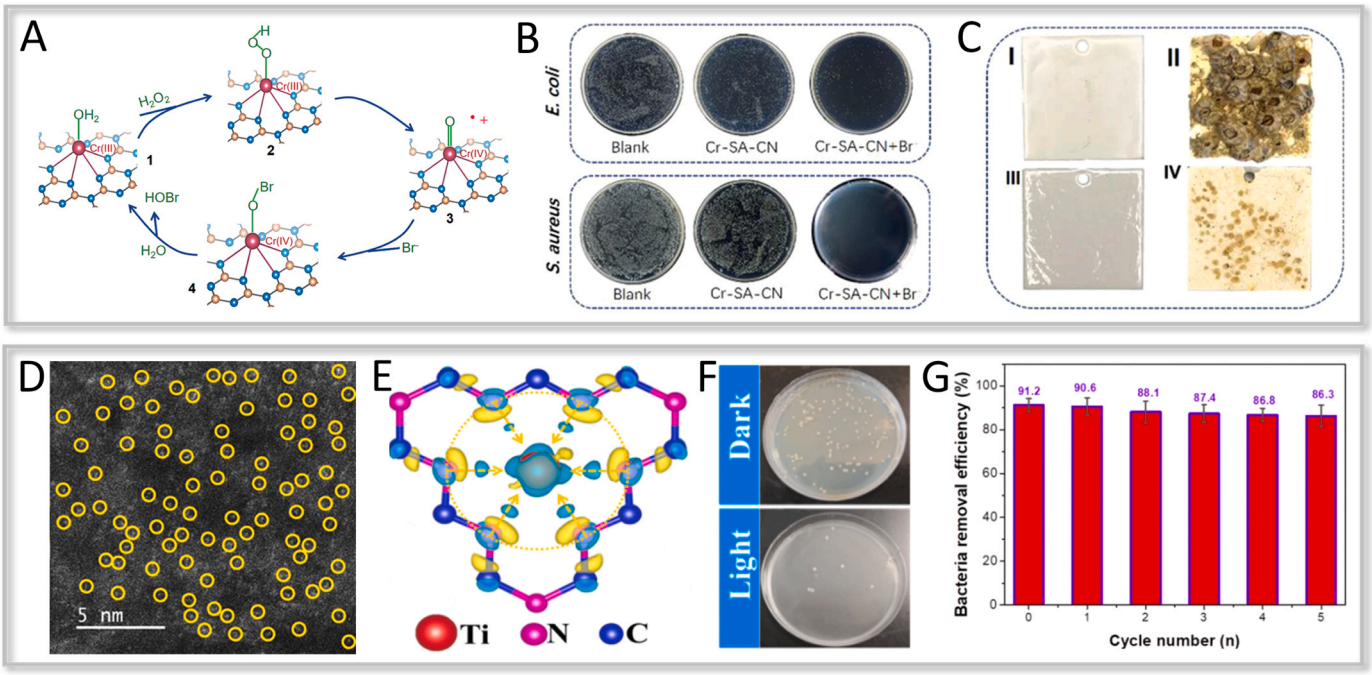

Fig. 22. (A) The catalytic process of Cr-SA-CN. (B) Digital images of *E. coli* and *S. aureus* sterilized under visible light irradiation and (C) stainless-steel plates painted in seawater by different samples [296]. (D) HAADFSTEM image, (E) charge difference map, (F) photocatalytic antibacterial activity and (G) recycling test of CN-Ti_{50} [297].

the disinfection reaction. The optimized sample (CN-Ti_{50}) exhibited excellent sterilization activity and recoverability, and the inactivation efficiency of *E. coli* achieved 91.2% after 30 min irradiation (Fig. 22**F**). Furthermore, CN-Ti_{50} performed stably in the cyclic tests (Fig. 22**G**), indicating that it holds promise for efficient sterilization via solar energy. Furthermore, in addition to the significantly enhanced reactivity and potential applications in antibacterial activities, these catalysts also exhibit excellent recyclability, rendering g-C_3N_4-based SACs promising candidates for sustainable photocatalytic purification processes.

5.2. Atmospheric protection

5.2.1. Photocatalytic CO_2 reduction

The booming industrial development leads to the over-consumption of fossil energy, and the greenhouse gases, mainly CO_2, are increasing and being emitted into the atmosphere progressively, which causes a series of problems that have aroused widespread concern [4,298–300]. Nowadays, various promising photocatalysts have been developed, including TiO_2 [301], WO_3 [302], CdS [303], UIO-66 [304] and g-C_3N_4 [305], etc. To date, g-C_3N_4 appears to be the best metal-free semiconductor for triggering photoactivated CO_2 due to the visible light response and matching reduction potential [306,307]. Unfortunately, the in-plane charge migration is severely suppressed by the π-conjugation planes [308]. To address this issue, Xiong and co-workers rationalized a synthetic method for controlling the local environment of single Pt atoms [179], so that the unsaturated Pt atoms could be simultaneously coordinated to the two N atoms of defective g-C_3N_4 (Fig. 23**A**). The authors verified the strong interaction of isolated Pt atoms with g-C_3N_4 support to enrich photogenerated electrons by light-assisted Kelvin probe force microscopy (KPFM) (Fig. 23**B**). Interestingly, the Pt atoms do not participate in the generation of H_2 in aqueous solution, which is inconsistent with most reports. This is mainly because H_2O reduction is revealed to occur preferentially at the hydroxyl (-OH) group of the defect (Fig. 23**C**). As a result, H atoms preferentially participate in the formation of C-H bonds, highly selectively (99%) evolved CH_4. In addition, with the deeper study of the mechanism of the liquid phase CO_2RR process, scientists have gained new insights into the role of H_2O. Fu's group found that CO_2RR could be accelerated by effectively inducing a H_2O activation process instead of activating CO_2 [97]. They successfully anchored a hexacoordinated single Ni site to the g-C_3N_4 surface (0.7Ni-5OB-CN) (Fig. 23**D**) by a facile ion exchange method using boron oxygen species. Fig. 23**E** exhibits a detectable positive response of the transient surface photovoltage spectrum (TS-SPV), indicating that the introduction of Ni sites could effectively promote the charge carriers separation. As a result, H_2O is preferentially activated and produces reactive H atoms impinging on CO_2 (Fig. 23**F**), leading to CO and CH_4. Due to the lower multi-electron transfer efficiency of the CO_2RR process and slow C-C coupling reaction kinetics, there are still serious challenges to realize the synthesis of C2 + alkanes and alcohol products such as C_2H_4, C_2H_6, and C_2H_5OH via CO_2 photoreduction [298]. In view of this, a photocatalyst modified with P and Cu double sites on C_3N_4 (P/Cu SAs@CN) was reported by Mao et al. [309] The results indicated that the matched energy levels of P/Cu SAs@CN provided an opportunity for photocatalytic CO_2RR to CO, CH_4 and C_2H_6 (Fig. 23**G**). Notably, P/Cu SAs@CN demonstrated an excellent generation rate (616.6 μmol g^{-1} h^{-1}) to evolve the C-C coupling product C_2H_6, which was nearly 26 times higher than that of the reference sample Cu SAs@CN (Fig. 23**H**). Subsequently, DFT calculations (Fig. 23**I**) explained how the dual active site facilitates the photoconversion of CO_2 into C2 + products on the basis of experimental results. The introduction of the P species is able to spatially transfer the photogenerated holes, which results in the photogenerated electrons enrichment on the Cu site. Then, the adsorbed *CO species on Cu carries out the subsequent electron transfer and hydrogenation process, which readily generates the key C-C coupling intermediate species *OC-COH, with the dominant product being C_2H_6. These excellent works provide new insights into the relationship between single-atom configurations and reaction pathways on g-C_3N_4. In addition, some recent works on g-C_3N_4-based SACs for photo-driven CO_2RR is selected in Table 4. Their atomic local coordination has been shown to be a key factor in modulating the product selectivity, some of them are even close to 100%.

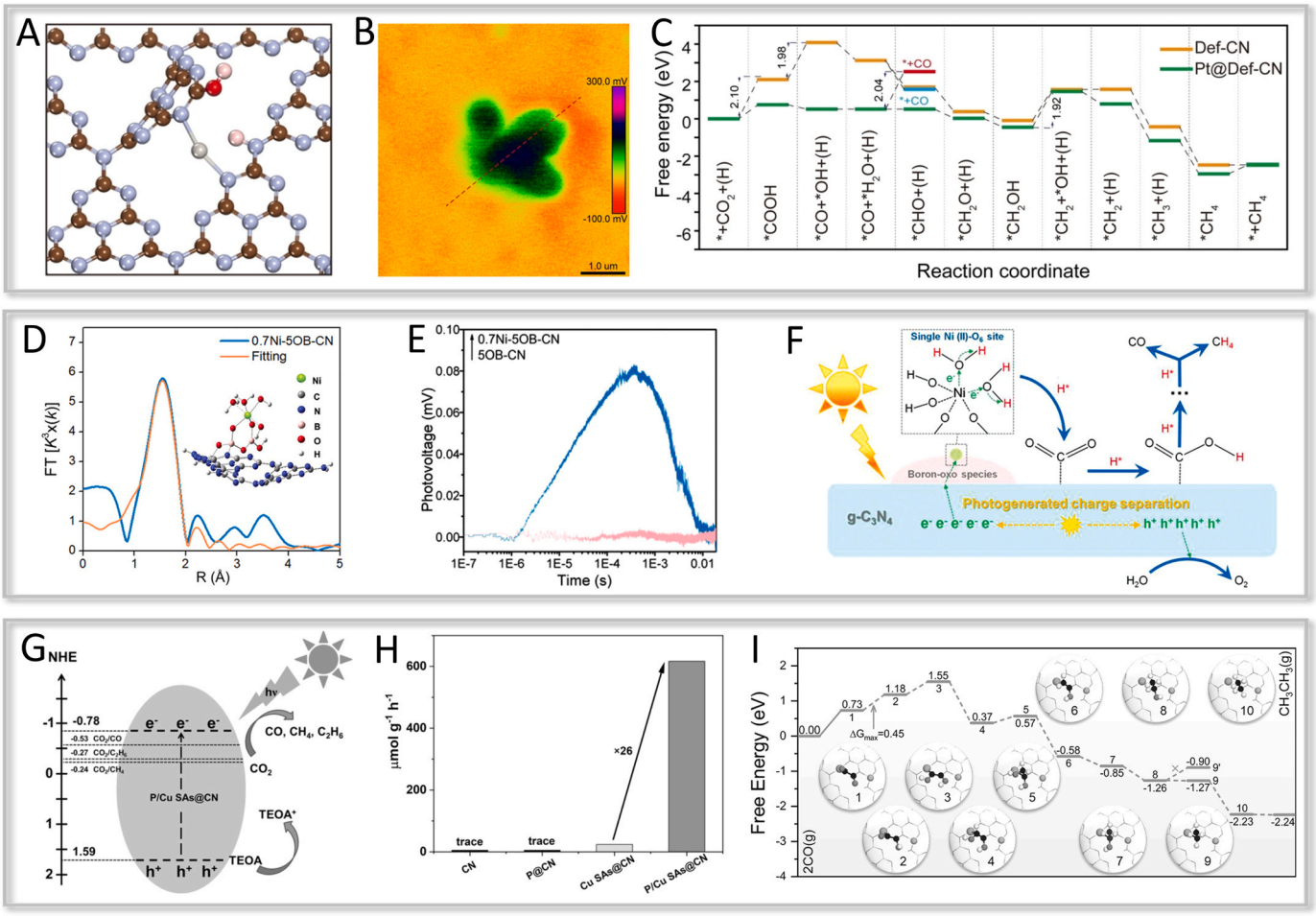

Fig. 23. (A) Local atomic structure of single Pt atom. (B) KPFM topography image of Pt@Def-CN under light irradiation. (C) Calculated free-energy diagram for photo-reduced CO_2-to-CH_4 [179]. (D) The EXAFS fitting curve and simulated structure model, (E) TS-SPV spectra and (F) possible hydrogen-assisted CO_2 reduction mechanism over Ni-OB-CN [97]. (G) Schematic energy structure, (H) photocatalytic CO_2RR activity and (I) calculated free energy diagram of CO coupling and reduction to C2 products of P/Cu SAs@CN [309].

5.2.2. *Photocatalytic CH_4 conversion*

The natural world is rich in natural gas resources, the main component is methane (CH_4), one of the shortest and lightest hydrocarbon molecules [317]. Nowadays, CH_4 is considered as one of the greenhouse gas, but it has a great potential to replace petroleum as a major energy source and chemical raw material, and the development of CH_4 utilization technology is one of the current hot topics in the international arena [318,319]. Among the many CH_4 direct conversion technologies, the partial oxidation of CH_4 to make C1 oxygenated compounds (COCs) is considered to be the route with the most potential for industrialization. Conventional thermocatalytic processes often require high temperatures due to the stable orthotetrahedral structure and inert C-H bonds of CH_4, resulting in lower reaction rates. Emerging and sustainable photocatalysis could generate highly reactive oxidizing radicals by clean solar energy to realize CH_4-to-upgraded COCs conversion under mild conditions [320]. Moreover, dry reforming of CH_4 has attracted much attention as a means of converting CH_4 and CO_2 into syngas (H_2 and CO) [321,322]. When we investigated the literatures, we found that single atoms could be employed as the center of active species generation, and g-C_3N_4 can be used to support the active center effectively. Nevertheless, how the design of fine structures modulates CH_4 oxidation pathway selectivity has rarely been investigated exhaustively. In this section, we provide a brief overview of frontier studies of g-C_3N_4-based SACs for CH_4 photoconversion to elucidate the reaction mechanisms.

The key step in the CH_4-to-C1 COCs conversion is the dehydrogenation to produce·CH_3, while excessive oxidation would lead to CO_2 evolution. As shown in Fig. 24**A**, Zhang et al. used g-C_3N_4 to support the $W^{\delta+}$ center (W-SA-PCN-7.5) to promote the photo-oxidation of CH_4 in water vapor with a W-N_4 coordination mode [323]. Impressively, the $W^{\delta+}$ center could serve as the active site for both CH_4 activation and·OH generation. The synthesized W-SA-PCN-7.5 is multifunctional, integrating the decomposition of H_2O_2, generation of·OH, and CH_4 photo-oxidation to achieve a total yield of C1 COCS of 4956 μmol $g_{cat.}^{-1}$, with nearly 100% selectivity (Fig. 24**B**). DFT calculations have shown that the coordination environment of the W active centers has a significant effect on the catalytic performance. Firstly, the W active center can absorb·OH to form the HO-W-N_4 structure. Meanwhile, the W-N_4 structure could effectively reduce the C-H cleavage energy of CH_4 (only 0.80 eV needs to be overcome). Eventually, the·CH_3 produced after being attacked by·OH takes the place of·OH on the HO-W-N_4 structure and can be successively attacked by the free·OH, thus generating a series of C1 COCS, including CH_3OH, HCOOH, etc (Fig. 24**C**). Similarly, Zhai et al. reported a photocatalyst with structurally asymmetric single-atom Co species modified on g-C_3N_4 substrate [101]. By breaking the structural symmetry of single Co atoms on g-C_3N_4 to regulate the coordination structure (Fig. 24**D**), a high selectivity (87.22%) oxidation of CH_4 to CH_3OH was achieved under room temperature (Fig. 24**E**). As shown in Fig. 24**F**, H_2O was photo-oxidized to·OH as an oxidant during the photocatalytic process. Xie and coworkers reported the assembly of Cu_2 atom pairs (Cu_2 @C_3N_4) on C_3N_4 [324], and the characterization revealed that the Cu sites were bonded via Cu-N bonding mode and bridged by O atoms (Fig. 24**G**). As expected, Cu_2 @C_3N_4 exhibited

Table 4
Summary of photocatalytic CO_2RR to selective products of g-C_3N_4-based SACs.

Year	Catalyst	Coordination structure	Products (Sel. %)	Yield (μmol $g_{cat.}^{-1}$ h^{-1})	Reference
2020	O/La-CN	La-N_6	CO (80.3%)	92	Dong et al. [169]
2020	HD-Er_1/CN-NT	Er-N_6	CO (-) CH_4 (-)	47.1 2.5	Wang et al. [157]
2020	Cu-CCN	Cu-N_6	CO (~100%)	3.086	Xiang et al. [95]
2020	Cu/CN-0.25	Cu-C_1N_2	CO (-) CH_4 (-) CH_3OH (-)	11.21 0.61 1.75	Cao et al. [310]
2021	RuSA-mC_3N_4	Ru-X_4 (X = C/N/O)	CH_3OH (-)	250	Zbořil et al.[161]
2021	CoRu-HCNp	Co-N_4 and Ru-N_4	CO (-) CH_4 (-)	27.3 0.6	Xiang et al. [311]
2022	CoSAC@PCN	Co-N_4	Formate (-)	420	Li et al. [312]
2022	InCu/PCN	Cu-N_3 and In-N_4	C_2H_5OH (92.4%)	28.5	Guo et al. [313]
2022	CuACs/PCNs	Cu-N_4	C_2H_4 (53.2%)	10.17	Huang et al.[149]
2022	PCN-RuCu	Ru-N_4 and Cu-N_3	CH_4 (95.1%)	19.25	Xue et al. [314]
2022	Pd_{1+NPs}/C_3N_4	Pd-N_2	CH_4 (97.8%)	20.3	Zheng et al.[166]
2022	Mn_1Co_1/CN	Mn-N_4O_1 and diverse Co	CO (~100%)	47	Li et al. [315]
2023	Ag_1 @PCN	Ag-N_3	CO (>94%)	160	Wang et al. [130]
2023	$Cu_1/N_2{}_C$V-CN	Cu-N_3	CO (98.5%)	11.12	Zhou et al. [316]
2023	IL/Co-bCN	Co-O_5	CO (-) CH_4 (-)	40.5 6.3	Jing et al. [131]
2023	ICN-20	$In^{\delta+}$-N_4	CO (~100%)	398.87	Zou et al. [138]

excellent CH_4 photo-oxidation activity. CH_4 and O_2 were used as reaction feedstocks to achieve > 10% CH_4 conversion and > 98% COCS product selectivity with a mass activity of 1399.3 mmol g_{Cu}^{-1} h^{-1}. Mechanistic studies (Fig. 24**H**) showed that the bridging O atom possessed the ability to adsorb H, which led to the decomposition of the first H_2O_2 into ·OOH and *H, and the ·OOH was trapped by the Cu_α site to be *OOH. Then, the second H_2O_2 molecule was cleaved at the Cu_β site to ·OH and *OH, and ·OH would recombine with *H on the bridging O site to form a H_2O molecule. Furthermore, CH_4 was attacked after introduction, the C-H bond was broken to produce the -CH_3 group. The transfer of the -CH_3 group allows for two possibilities of product, combining with *OOH and *OH on the Cu_α and Cu_β sites, respectively, to produce CH_3OOH and CH_3OH.

5.2.3. *Photocatalytic NO_x removal*

In the face of the urgent need to prevent and control atmospheric pollution, scientists have given continuous attention and research. Both the quantity and duration of atmospheric pollutants can adversely jeopardize the natural environment and human health. In recent years, frequent industrial production activities breed large amounts of nitrogen oxides (NO_x) [6,325]. It is estimated that the combustion of 1000 kg of coal produces 8–9 kg of NO_x pollutants. On the other hand, NO_x-induced photochemical smog seriously affects our daily life, involving irritates the respiratory tract and headache [326]. Conventional processes mainly use selective catalytic reduction (SCR) [327] and selective non-catalytic reduction (SNCR) [328] for NO_x treatment to reduce emissions. Photocatalysis, as an emerging method with low cost, wide applicability, and high removal rate, gives us experience in removing NO_x pollutants [329–331]. Remarkably, Wang et al. created C defects on the g-C_3N_4 surface by thermal etching [132], which were used to confine the noble metal Pd single atoms (Pd-C_v-CN) (Fig. 25**A**). They declared that Pd atoms occupied the C defects and led to the reduction of the band gap, which was favorable for charge transport. Subsequently, Pd-C_v-CN achieved rapid conversion of NO and high selectivity for the product NO_3^-, with a conversion rate of 56.3% after 30 min under light irradiation (Fig. 25**B**). As illustrated in Fig. 25**C**, a large amount of photogenerated charge was allowed to participate in·O_2^- production, which further oxidized NO to NO_3^-.

6. Concluding remarks and perspectives

Currently, g-C_3N_4-based SACs have made significant progress, demonstrating promising applications in energy conversion and environmental remediation. The single atom coordination structure provides ample active sites for g-C_3N_4, accelerating charge transfer, and optimizing reaction energy barriers and pathways. Furthermore, the surface structure of g-C_3N_4-based SACs is precisely controlled to enhance the interaction with reactants, thereby improving the reaction rate and product selectivity in photocatalytic applications. In summary, g-C_3N_4-based SACs hold great potential for various applications. However, there are still some challenges that need to be addressed in practical applications and further explorations. These challenges include achieving precise design of single metal site coordination structures and increasing the loading capacity. The following aspects propose future research directions and deployable solutions that require greater efforts to overcome multifaceted challenges:

1) The coordination structure of metal atoms can directly affect the activity and selectivity of catalytic reactions. In terms of single metal atom structure, in addition to selectively participating in catalytic reactions as surface active sites, it can also provide a deeper understanding of the reaction mechanism of catalytic processes. On the other hand, the application expansion depends on the unique design of the coordination environment of metal atoms. The coordination structure of metal atoms in g-C_3N_4-based SACs should be precisely controlled during the preparation process to achieve controllable synthesis. For the selection of synthesis methods, it is necessary to develop more environmentally friendly and sustainable synthesis methods in the future. Based on this, the stability and activity of the catalyst should be optimized to achieve the goal of green production.
2) Currently, a large of research works focused on increasing the metal loading amount in SACs. However, it is inevitable that excessive loading leads to the formation of metal aggregates. Notably, g-C_3N_4 has a high degree of intrinsic structural designability, which can be fully utilized to anchor single metal sites. For example, introducing auxiliary coordinating groups or constructing defects on g-C_3N_4 support could enhance the binding between metal atoms and g-C_3N_4, thereby increasing the metal loading. These auxiliary coordinating groups can be introduced through chemical modifications, functionalization, etc., to enhance the interaction between metal atoms and support, thereby weakening metal-metal bonds.
3) Nowadays, many reported works of g-C_3N_4-based SACs have demonstrated excellent stability through cycling tests of several tens of hours. However, they still do not meet the requirements for actual production. Surface modification or encapsulation of metal atoms may be considered as a significant mean to enhance the stability. By forming a protective layer, the aggregation and migration of metal atoms could be prevented. In addition, attention should be paid to catalyst poisoning effects during catalytic reactions, with the aim of achieving regeneration of single metal atoms. It is important to timely improve the methods for assessing catalyst lifespan and evaluate the stability mechanisms of catalysts, in order to better meet the requirements of actual applications.
4) To date, multiple advanced characterization techniques (such as AC-HAADF-STEM with EELS, XAFS, in-situ Raman, in-situ XPS,

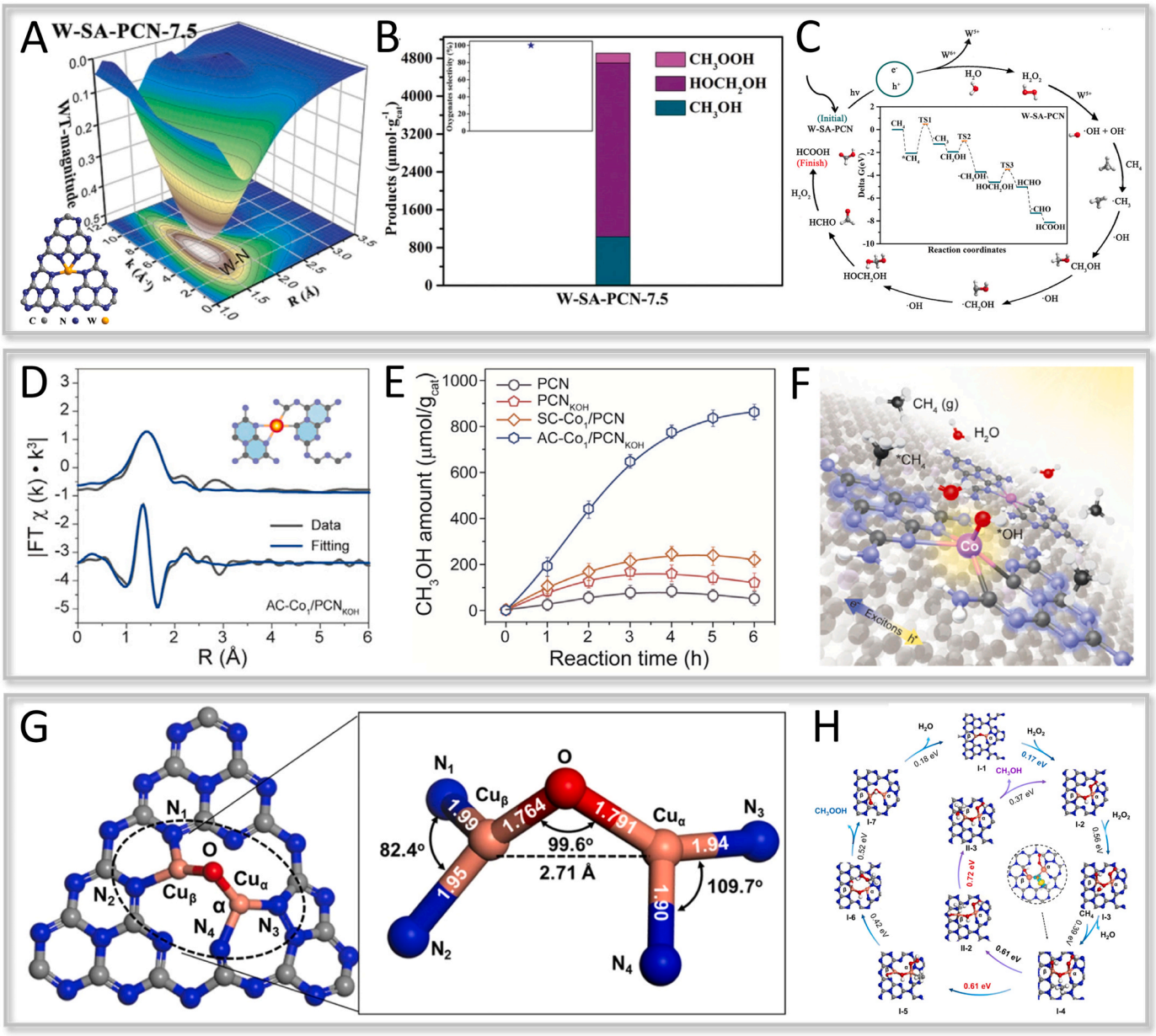

Fig. 24. (A) WT-EXAFS of W-SA-PCN-7.5. (B) The total amounts of C1 COCs via photocatalytic CH_4 conversion. (C) Proposed reaction pathway and DFT calculated results for CH_4 conversion process [323]. (D) EXAFS spectra and structural model for AC-Co_1/PCN_{KOH}. (E) Time-coursed amounts of CH_3OH photo-evolution. (F) Schematic diagram of mechanism for CH_4 conversion [101]. (G) The simulated structure model of the dicopper-oxo center in Cu_2 @C_3N_4. (H) The simulated pathways for CH_4 conversion [324].

etc) can be effectively integrated to provide rich data from different aspects, which facilitate the accuracy of distinguishing the coordination structure and intrinsic properties of g-C_3N_4-based SACs. In this regard, XAFS is often used to investigate the valence state and coordination structure of metal atoms. However, XAFS results are based on the average properties of the bulk phase and cannot fully reflect the real situation of catalysts. That is, different configurations of the same metal atom may exist simultaneously but might be attributed to a single structural model, thereby rendering the coordination structure heavily reliant on DFT simulations of structural formation energy. Therefore, characterization techniques that allow for intuitive observation of the precise coordination structures of single metal atoms are urgently needed.

5) Obviously, g-C_3N_4-based SACs have broad application prospects in the aforementioned fields. However, they still face some challenges in other photocatalytic applications expansion. For example, the oxygen evolution reaction is severely limited for g-C_3N_4-based SACs due to the complex multi-electron steps and difficult thermodynamic barriers ($\Delta E^{\circ}=-1.23$ V). Moreover, photocatalytic cascade reactions that synergistically treat various pollutants and produce high value-added products are also worth exploring. Therefore, it is necessary to further broaden the field of basic research to lead the true commercialization of g-C_3N_4-based SACs.
6) Understanding the changes in transient active sites of g-C_3N_4-based SACs under real reaction conditions is crucial for a comprehensive understanding of catalytic mechanisms. This necessitates the development of novel in-situ/atomic-scale dynamic observation techniques, such as in-situ X-ray absorption fine structure (in-situ XAFS) and in-situ diffuse reflectance infrared Fourier transform spectroscopy (in-situ DRIFTS), etc., to monitor

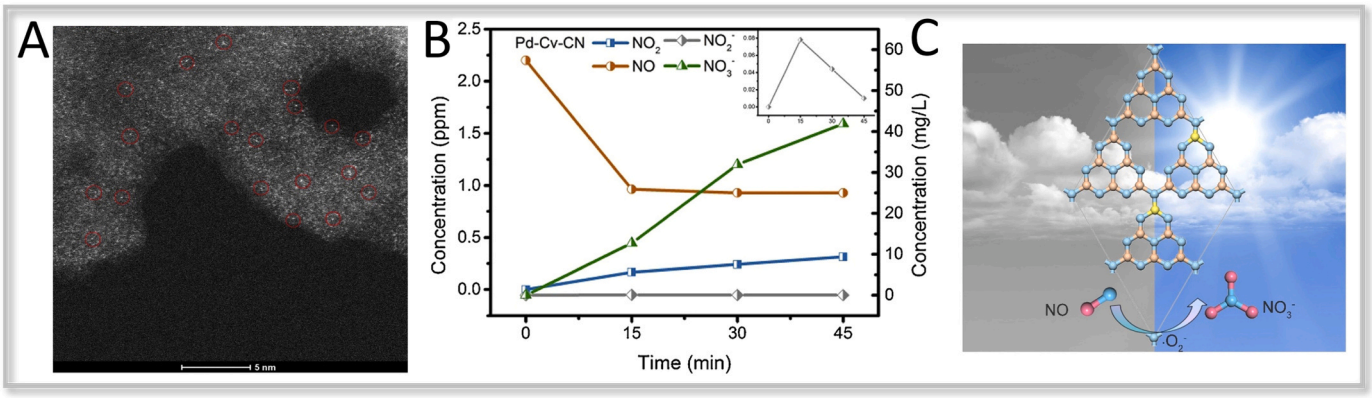

Fig. 25. (A) AC-HAADF-STEM, (B) photocatalytic NOx removal performance and (C) reaction mechanism of Pd-C_v-CN [132].

in real-time the structural changes and intermediates generated during the reaction process. According to previously reported work, transient Cu clusters restructuring has been observed in the H-adhesion state of Cu single atom catalyst, which would play a leading role in the oxidation process [332]. Moreover, the phenomenon of metal species reversible transformation has already been observed in TiO_2-based SACs for photocatalytic applications [333,334]. Nevertheless, the phenomenon of restructuring atomically dispersed metal species in g-C_3N_4-based SACs has not yet received sufficient attention, which warrants further investigation through DFT calculations and molecular dynamics simulations.

7) Higher light absorption leads to more light energy being utilized to generate active intermediates, thus increasing the reaction efficiency. Although g-C_3N_4 is a visible light-responsive semiconductor, there is still room for improvement in terms of light absorption and utilization. Atomic-level dispersed metal species can effectively modulate the density of states and localized electronic structure of g-C_3N_4. Building upon this foundation, the hybridization of g-C_3N_4-based SACs with photosensitizers or heterogeneous semiconductors provides additional channels for light absorption, even extending into the near-infrared (NIR) region, thereby further enhancing solar energy utilization. However, a challenge that needs to be overcome is the potential coverage of individual metal active sites. Therefore, the light absorption and electron transfer capabilities need to be balanced to achieve the best catalytic effect according to the specific application scenario and requirements.
8) g-C_3N_4, as a non-metallic semiconductor, possesses adjustable conjugated repetitive units, porous structures and abundant lone pair electrons, making it a promising candidate for constructing SACs. When designing metal atom coordination structures, the focus is typically on the binding of the single atoms with C/N, with little consideration given to the coordination outcomes with heteroatoms. Furthermore, research on non-metallic SACs in this regard is limited. Due to the strong electronegativity of non-metal atoms, they can form polar bonds with the surface metal sites of g-C_3N_4-based SACs, thereby modulating the catalytic performance. Therefore, doping with non-metal atoms of different electronegativities may lead to surprised results in terms of the diverse metal atom coordination and selective reaction pathways, thereby providing a new direction for future research on g-C_3N_4-based SACs.
9) The numerous advantages of g-C_3N_4-based SACs make them one of the current research hotspots, and many research works have been reported based on the modulation of atomic-level coordination structures. With the development of characterization and mechanism probing techniques, the amount of data obtained is increasing. Through artificial intelligence and machine learning, gene sequence lists can be formed based on the relationship between performance and atomic coordination structure, mainly to enable the design and optimization of g-C_3N_4-based SACs. Modeling the relationship between performance and the coordination structure of different metal atoms using machine learning algorithms can be used to discover patterns and trends hidden behind the data through large-scale experimental datasets. In addition, a large number of candidate metal atoms can be rapidly predicted and screened. Machine learning models can be combined with high-throughput calculations and experiments to form a closed-loop catalyst design loop. The development of novel g-C_3N_4-based SACs is guided by continuous iterative optimization of models and experimental protocols.
10) g-C_3N_4-based SACs is regarded as a promising new catalyst with high efficiency, low cost and multifunctionality. Apart from photocatalytic applications, g-C_3N_4-based SACs show great potential in electrocatalysis, sensors, and solar cells, etc. Future research on g-C_3N_4-based SACs will focus on the exploration of scale-up and industrialization, with consideration of subsequent entry into practical applications.

Author statement

H. Su: writing original draft; writing-review & editing; managing graphics and figures. H. Yin: performed conceptualization. R. Wang, Y. Wang, W. Orbell, and Y. Peng: writing-review & editing. J. Li: supervision.

CRediT authorship contribution statement

Li Junhua: Supervision, Funding acquisition. **Peng Yue:** Writing – review & editing, Visualization. **Su Haiwei:** Resources, Methodology, Investigation, Formal analysis, Data curation, Conceptualization, Writing - review & editing. **Yin Haibo:** Methodology, Funding acquisition, Conceptualization. **Wang Rong:** Writing – review & editing, Methodology. **Orbell William:** Software. **Wang Yunlong:** Formal analysis.

Declaration of Competing Interest

The authors declare that they have no known competing financial interests or personal relationships that could have appeared to influence the work reported in this paper.

Data Availability

Data will be made available on request.

Acknowledgments

The authors acknowledge the financial support provided by the National Natural Science Foundation of China (22206096 and 21936005) and China Postdoctoral Science Foundation (2020TQ0166 and 2021M691771).

Appendix A. Supporting information

Supplementary data associated with this article can be found in the online version at doi:10.1016/j.apcatb.2023.123683.

References

[1] Y. Shiraishi, M. Hashimoto, K. Chishiro, K. Moriyama, S. Tanaka, T. Hirai, Photocatalytic dinitrogen fixation with water on bismuth oxychloride in chloride solutions for solar-to-chemical energy conversion, J. Am. Chem. Soc. 142 (2020) 7574–7583.
[2] Z.-H. Xue, D. Luan, H. Zhang, X.W. Lou, Single-atom catalysts for photocatalytic energy conversion, Joule 6 (2022) 92–133.
[3] X. Lin, S.-F. Ng, W.-J. Ong, Coordinating single-atom catalysts on two-dimensional nanomaterials: a paradigm towards bolstered photocatalytic energy conversion, Coord. Chem. Rev. 471 (2022) 214743.
[4] S. Fang, M. Rahaman, J. Bharti, E. Reisner, M. Robert, G.A. Ozin, Y.H. Hu, Photocatalytic CO_2 reduction, Nat. Rev. Methods Prim. 3 (2023) 61.
[5] Y. Zhao, Y. Wang, H. Chi, Y. Zhang, C. Sun, H. Wei, R. Li, Coupling photocatalytic water oxidation on decahedron $BiVO_4$ crystals with catalytic wet peroxide oxidation for removing organic pollutions in wastewater, Appl. Catal. B-Environ. 318 (2022) 121858.
[6] N. Li, C. Wang, K. Zhang, H. Lv, M. Yuan, D.W. Bahnemann, Progress and prospects of photocatalytic conversion of low-concentration NO, Chin. J. Catal. 43 (2022) 2363–2387.
[7] Y. Zhang, H. Liu, F. Gao, X. Tan, Y. Cai, B. Hu, Q. Huang, M. Fang, X. Wang, Application of MOFs and COFs for photocatalysis in CO_2 reduction, H_2 generation, and environmental treatment, EnergyChem 4 (2022) 100078.
[8] Y. Ni, M. Wang, L. Liu, M. Li, S. Hu, J. Lin, J. Sun, T. Yue, M.-Q. Zhu, J. Wang, Efficient and reusable photocatalytic river water disinfection by addictive graphitic carbon nitride/magnesium oxide nano-onions with particular "nano-magnifying glass effect, J. Hazard. Mater. 439 (2022) 129533.
[9] D. Zu, Y. Ying, Z. Xu, G. Chen, L. Bai, S. Ahmed, Z. Lin, Y. Zhu, A.M. Saleque, S. She, M.M. Li, M.N.A.S. Ivan, H. Wu, Y.H. Tsang, H. Huang, Molten salt-lithium process induced controllable surface defects in titanium oxide for efficient photocatalysis, Appl. Catal. B-Environ. 328 (2023) 122494.
[10] Y. Wan, J. Li, J. Ni, C. Wang, C. Ni, H. Chen, Crystal-facet and microstructure engineering in ZnO for photocatalytic NO oxidation, J. Hazard. Mater. 435 (2022) 129073.
[11] M. Ma, J. Liu, H. Zhao, S. Yue, L. Zhong, Y. Huang, X. Jia, K. Liu, X. Li, Z. Wang, S. Qu, Y. Lei, Broadened photocatalytic capability to near-infrared for CdS hybrids and positioning hydrogen evolution sites, Appl. Catal. B-Environ. 325 (2023) 122327.
[12] X. Cao, Y. Gu, Y. Fang, D. Johnson, C. Chen, J. Chen, H. Tian, Y. Huang, Self-assembled $BiVO_4$ mesocrystals for efficient photocatalytic decontamination of microcystin-LR, Environ. Chem. Lett. 20 (2022) 1595–1601.
[13] J. Liang, H. Yu, J. Shi, B. Li, L. Wu, M. Wang, Dislocated bilayer MOF enables high-selectivity photocatalytic reduction of CO_2 to CO, Adv. Mater. 35 (2023) 2209814.
[14] H. Piao, G. Choi, X. Jin, S.-J. Hwang, Y.J. Song, S.-P. Cho, J.-H. Choy, Monolayer graphitic carbon nitride as metal-free catalyst with enhanced performance in photo- and electro-catalysis, Nano-Micro Lett. 14 (2022).
[15] J. Yang, S. He, H. Liu, E. Jaatinen, E. Waclawik, J. Quan, S. Sarina, C. He, S. Huang, H. Zhu, M. Wu, Enhancing visible-light photocatalytic performance of Au/TiO_2 catalysts through light reflection-promoted optical absorption with oriented anatase mesocrystals, J. Mater. Chem. A 11 (2023) 4751–4757.
[16] S. Mao, J.-W. Shi, G. Sun, D. Ma, C. He, Z. Pu, K. Song, Y. Cheng, Au nanodots@thiol-UiO66@$ZnIn_2S_4$ nanosheets with significantly enhanced visible-light photocatalytic H_2 evolution: the effect of different Au positions on the transfer of electron-hole pairs, Appl. Catal. B-Environ. 282 (2021) 119550.
[17] M. Fumanal, A. Ortega-Guerrero, K.M. Jablonka, B. Smit, I. Tavernelli, Charge separation and charge carrier mobility in photocatalytic metal-organic frameworks, Adv. Funct. Mater. 30 (2020) 2003792.
[18] H. Su, W. Wang, R. Shi, H. Tang, L. Sun, L. Wang, Q. Liu, T. Zhang, Recent advances in quantum dot catalysts for hydrogen evolution: synthesis, characterization, and photocatalytic application, Carbon Energy (2023) e280.
[19] L. Liu, S. Wang, H. Huang, Y. Zhang, T. Ma, Surface sites engineering on semiconductors to boost photocatalytic CO_2 reduction, Nano Energy 75 (2020) 104959.
[20] W. Gao, J. Lu, S. Zhang, X. Zhang, Z. Wang, W. Qin, J. Wang, W. Zhou, H. Liu, Y. Sang, Suppressing photoinduced charge recombination via the Lorentz force in a photocatalytic system, Adv. Sci. 6 (2019) 1901244.
[21] F. Li, L. Cheng, J. Fan, Q. Xiang, Steering the behavior of photogenerated carriers in semiconductor photocatalysts: a new insight and perspective, J. Mater. Chem. A 9 (2021) 23765–23782.
[22] Y. Wang, J. Wang, M. Zhang, S. Zheng, J. Wu, T. Zheng, G. Jiang, Z. Li, In situ constructed perovskite-chalcogenide heterojunction for photocatalytic CO_2 reduction, Small (2023) 2300841.
[23] H. Mai, X. Li, J. Lu, X. Wen, T.C. Le, S.P. Russo, D. Chen, R.A. Caruso, Synthesis of layered lead-free perovskite nanocrystals with precise size and shape control and their photocatalytic activity, J. Am. Chem. Soc. 145 (2023) 17337–17350.
[24] K. Huang, J. Bai, R. Shen, X. Li, C. Qin, P. Zhang, X. Li, Boosting photocatalytic hydrogen evolution through local charge polarization in chemically bonded single-molecule junctions between ketone molecules and covalent organic frameworks, Adv. Funct. Mater. (2023) 2307300.
[25] Y. Xue, P. Shao, M. Lin, Y. Yuan, W. Shi, F. Cui, Tailoring S-vacancy concentration changes the type of the defect and photocatalytic activity in ZFS, J. Hazard. Mater. 428 (2022) 128215.
[26] R. Peng, X. Ma, Z.D. Hood, A. Boulesbaa, A.A. Puretzky, J. Tong, Z. Wu, Synergizing plasmonic Au nanocages with 2D MoS_2 nanosheets for significant enhancement in photocatalytic hydrogen evolution, J. Mater. Chem. A 11 (2023) 16714–16723.
[27] X. Xu, Y. Wang, D. Zhang, J. Wang, Z. Yang, In situ growth of photocatalytic Ag-decorated β-Bi_2O_3/$Bi_2O_{2.7}$ heterostructure film on PVC polymer matrices with self-cleaning and antibacterial properties, Chem. Eng. J. 429 (2022) 131058.
[28] J. Ma, X. Tan, Q. Zhang, Y. Wang, J. Zhang, L. Wang, Exploring the size effect of Pt nanoparticles on the photocatalytic nonoxidative coupling of methane, ACS Catal. 11 (2021) 3352–3360.
[29] P. Zhang, S. Wang, B.Y. Guan, X.W. Lou, Fabrication of CdS hierarchical multi-cavity hollow particles for efficient visible light CO_2 reduction, Energy Environ. Sci. 12 (2019) 164–168.
[30] X. Hao, Z. Jin, H. Yang, G. Lu, Y. Bi, Peculiar synergetic effect of MoS_2 quantum dots and graphene on metal-organic frameworks for photocatalytic hydrogen evolution, Appl. Catal. B-Environ. 210 (2017) 45–56.
[31] Q. Chen, M. Zhang, J. Li, G. Zhang, Y. Xin, C. Chai, Construction of immobilized 0D/1D heterostructure photocatalyst Au/CuS/CdS/TiO_2 NBs with enhanced photocatalytic activity towards moxifloxacin degradation, Chem. Eng. J. 389 (2020) 124476.
[32] A. Mahmood, G. Shi, Z. Wang, Z. Rao, W. Xiao, X. Xie, J. Sun, Carbon quantum dots-TiO_2 nanocomposite as an efficient photocatalyst for the photodegradation of aromatic ring-containing mixed VOCs: an experimental and DFT studies of adsorption and electronic structure of the interface, J. Hazard. Mater. 401 (2021) 123402.
[33] Q. Zhang, J. Guan, Recent progress in single-atom catalysts for photocatalytic water splitting, Sol. RRL 4 (2020) 2000283.
[34] Y. Chen, S. Ji, W. Sun, Y. Lei, Q. Wang, A. Li, W. Chen, G. Zhou, Z. Zhang, Y. Wang, L. Zheng, Q. Zhang, L. Gu, X. Han, D. Wang, Y. Li, Engineering the atomic interface with single platinum atoms for enhanced photocatalytic hydrogen production, Angew. Chem. Int. Ed. 59 (2019) 1295–1301.
[35] X. Xiong, C. Mao, Z. Yang, Q. Zhang, G.I.N. Waterhouse, L. Gu, T. Zhang, Photocatalytic CO_2 reduction to CO over Ni single atoms supported on defect-rich zirconia, Adv. Energy Mater. 10 (2020) 2002928.
[36] X. Xiao, L. Zhang, H. Meng, B. Jiang, H. Fu, Single metal atom decorated carbon nitride for efficient photocatalysis: synthesis, structure, and applications, Sol. RRL 5 (2021) 2000609.
[37] T. Yang, X. Mao, Y. Zhang, X. Wu, L. Wang, M. Chu, C.-W. Pao, S. Yang, Y. Xu, X. Huang, Coordination tailoring of Cu single sites on C_3N_4 realizes selective CO_2 hydrogenation at low temperature, Nat. Commun. 12 (2021) 6022.
[38] W.-J. Ong, L.-L. Tan, Y.H. Ng, S.-T. Yong, S.-P. Chai, Graphitic carbon nitride (g-C_3N_4)-based photocatalysts for artificial photosynthesis and environmental remediation: are we a step closer to achieving sustainability? Chem. Rev. 116 (2016) 7159–7329.
[39] S. Wang, L. Wang, H. Cong, R. Wang, J. Yang, X. Li, Y. Zhao, H. Wang, A review: g-C_3N_4 as a new membrane material, J. Environ. Chem. Eng. 10 (2022) 108189.
[40] Y. Li, M. Gu, X. Zhang, J. Fan, K. Lv, S.A.C. Carabineiro, F. Dong, 2D g-C_3N_4 for advancement of photo-generated carrier dynamics: status and challenges, Mater. Today 41 (2020) 270–303.
[41] Q. Li, Y. Jiao, Y. Tang, J. Zhou, B. Wu, B. Jiang, H. Fu, Shear stress triggers ultrathin-nanosheet carbon nitride assembly for photocatalytic H_2O_2 production coupled with selective alcohol oxidation, J. Am. Chem. Soc. (2023) 20837–20848.
[42] Y. Wang, X. Liu, J. Liu, B. Han, X. Hu, F. Yang, Z. Xu, Y. Li, S. Jia, Z. Li, Y. Zhao, Carbon quantum dot implanted graphite carbon nitride nanotubes: excellent charge separation and enhanced photocatalytic hydrogen evolution, Angew. Chem. Int. Ed. 57 (2018) 5765–5771.
[43] H. Yu, R. Shi, Y. Zhao, T. Bian, Y. Zhao, C. Zhou, G.I.N. Waterhouse, L.-Z. Wu, C.-H. Tung, T. Zhang, Alkali-assisted synthesis of nitrogen deficient graphitic carbon nitride with tunable band structures for efficient visible-light-driven hydrogen evolution, Adv. Mater. 29 (2017) 1605148.
[44] X. Wang, K. Maeda, A. Thomas, K. Takanabe, G. Xin, J.M. Carlsson, K. Domen, M. Antonietti, A metal-free polymeric photocatalyst for hydrogen production from water under visible light, Nat. Mater. 8 (2008) 76–80.
[45] Q. Han, B. Wang, J. Gao, Z. Cheng, Y. Zhao, Z. Zhang, L. Qu, Atomically thin mesoporous nanomesh of graphitic C_3N_4 for high-efficiency photocatalytic hydrogen evolution, ACS Nano 10 (2016) 2745–2751.
[46] S. Yang, H. Li, H. Li, H. Li, W. Qi, Q. Zhang, J. Zhu, P. Zhao, L. Chen, Rational design of 3D carbon nitrides assemblies with tunable nano-building blocks for efficient visible-light photocatalytic CO_2 conversion, Appl. Catal. B-Environ. 316 (2022) 121612.

[47] M. Yang, R. Lian, X. Zhang, C. Wang, J. Cheng, X. Wang, Photocatalytic cyclization of nitrogen-centered radicals with carbon nitride through promoting substrate/catalyst interaction, Nat. Commun. 13 (2022) 4900.

[48] M. Chen, R. Bai, P. Jin, J. Li, Y. Yan, A. Peng, J. He, A facile hydrothermal synthesis of few-layer oxygen-doped g-C_3N_4 with enhanced visible light-responsive photocatalytic activity, J. Alloy. Compd. 869 (2021) 159292.

[49] N. Urakami, K. Takashima, M. Shimizu, Y. Hashimoto, Thermal chemical vapor deposition of layered carbon nitride films under a hydrogen gas atmosphere, CrystEngComm 25 (2023) 877–883.

[50] L. Du, Q. Tian, X. Zheng, W. Guo, W. Liu, Y. Zhou, F. Shi, Q. Xu, Supercritical CO_2-tailored 2D oxygen-doped amorphous carbon nitride for enhanced photocatalytic activity, Energy Environ. Mater. 5 (2021) 912–917.

[51] W. Niu, K. Marcus, L. Zhou, Z. Li, L. Shi, K. Liang, Y. Yang, Enhancing electron transfer and electrocatalytic activity on crystalline carbon-conjugated g-C_3N_4, ACS Catal. 8 (2018) 1926–1931.

[52] X. Liang, F. Dong, Z. Tang, Q. Wang, The significant promotion of g-C_3N_4 on Pt/CNS catalyst for the electrocatalytic oxidation of methanol, Int. J. Hydrog. Energy 46 (2021) 39645–39657.

[53] H. Jin, X. Liu, Y. Jiao, A. Vasileff, Y. Zheng, S.-Z. Qiao, Constructing tunable dual active sites on two-dimensional C_3N_4@MoN hybrid for electrocatalytic hydrogen evolution, Nano Energy 53 (2018) 690–697.

[54] Y. Zheng, Y. Jiao, Y. Zhu, Q. Cai, A. Vasileff, L.H. Li, Y. Han, Y. Chen, S.-Z. Qiao, Molecule-level g-C_3N_4 coordinated transition metals as a new class of electrocatalysts for oxygen electrode reactions, J. Am. Chem. Soc. 139 (2017) 3336–3339.

[55] K.S. Pasupuleti, M. Reddeppa, S.S. Chougule, N.-h Bak, D.-J. Nam, N. Jung, H. D. Cho, S.-G. Kim, M.-D. Kim, High performance langasite based SAW NO_2 gas sensor using 2D g-C_3N_4@TiO_2 hybrid nanocomposite, J. Hazard. Mater. 427 (2022) 128174.

[56] K.C. Devarayapalli, K. Lee, H.B. Do, N.N. Dang, K. Yoo, J. Shim, S.V. Prabhakar Vattikuti, Mesostructured g-C_3N_4 nanosheets interconnected with V_2O_5 nanobelts as electrode for coin-cell-type-asymmetric supercapacitor device, Mater. Today Energy 21 (2021) 100669.

[57] Y. Lou, Y. Cai, W. Hu, L. Wang, Q. Dai, W. Zhan, Y. Guo, P. Hu, X.-M. Cao, J. Liu, Y. Guo, Identification of active area as active center for CO oxidation over single Au atom catalyst, ACS Catal. 10 (2020) 6094–6101.

[58] Y. Wang, Y. Liu, W. Liu, J. Wu, Q. Li, Q. Feng, Z. Chen, X. Xiong, D. Wang, Y. Lei, Regulating the coordination structure of metal single atoms for efficient electrocatalytic CO_2 reduction, Energy Environ. Sci. 13 (2020) 4609–4624.

[59] Y. Chen, J. Lin, B. Jia, X. Wang, S. Jiang, T. Ma, Isolating single and few atoms for enhanced catalysis, Adv. Mater. 34 (2022) 2201796.

[60] L. Zhang, K. Doyle-Davis, X. Sun, Pt-Based electrocatalysts with high atom utilization efficiency: from nanostructures to single atoms, Energy Environ. Sci. 12 (2019) 492–517.

[61] W.H. Lai, Z. Miao, Y.X. Wang, J.Z. Wang, S.L. Chou, Atomic-local environments of single-atom catalysts: Synthesis, electronic structure, and activity, Adv. Energy Mater. (9 () (2019).

[62] T. Sun, S. Mitchell, J. Li, P. Lyu, X. Wu, J. Pérez-Ramírez, J. Lu, Design of local atomic environments in single-atom electrocatalysts for renewable energy conversions, Adv. Mater. 33 (2020) 2003075.

[63] W. Ru, Y. Liu, B. Fu, F. Fu, J. Feng, D. Li, Control of local electronic structure of Pd single atom catalyst by adsorbate induction, Small 18 (2021) 2103852.

[64] B. Qiao, A. Wang, X. Yang, L.F. Allard, Z. Jiang, Y. Cui, J. Liu, J. Li, T. Zhang, Single-atom catalysis of CO oxidation using Pt_1/FeO_x, Nat. Chem. 3 (2011) 634–641.

[65] F. Li, D.H. Kweon, G.-F. Han, H.-J. Noh, W. Che, I. Ahmad, H.Y. Jeong, Z. Fu, Y. Lu, J.-B. Baek, Merging platinum single atoms to achieve ultrahigh mass activity and low hydrogen production cost, ACS Nano 17 (2023) 2923–2931.

[66] Z. Fu, C. Ling, J. Wang, A $Ti_3C_2O_2$ supported single atom, trifunctional catalyst for electrochemical reactions, J. Mater. Chem. A 8 (2020) 7801–7807.

[67] J. Zheng, K. Lebedev, S. Wu, C. Huang, T. Ayvalı, T.-S. Wu, Y. Li, P.-L. Ho, Y.-L. Soo, A. Kirkland, S.C.E. Tsang, High loading of transition metal single atoms on chalcogenide catalysts, J. Am. Chem. Soc. 143 (2021) 7979–7990.

[68] H. Yin, F. Dong, D. Wang, J. Li, Coupling Cu single atoms and phase junction for photocatalytic CO_2 reduction with 100% CO selectivity, ACS Catal. 12 (2022) 14096–14105.

[69] C.B. Thompson, L. Liu, D.S. Leshchev, A.S. Hoffman, J. Hong, S.R. Bare, R. R. Unocic, E. Stavitski, H. Xin, A.M. Karim, CO oxidation on Ir_1/TiO_2: Resolving ligand dynamics and elementary reaction steps, ACS Catal. 13 (2023) 7802–7811.

[70] Y. Zheng, Q. Wang, Q. Yang, S. Wang, M.J. Hülsey, S. Ding, S. Furukawa, M. Li, N. Yan, X. Ma, Boosting the hydroformylation activity of a Rh/CeO_2 single-atom catalyst by tuning surface deficiencies, ACS Catal. 13 (2023) 7243–7255.

[71] P. Zhou, Q. Zhang, Y. Chao, L. Wang, Y. Li, H. Chen, L. Gu, S. Guo, Partially reduced Pd single atoms on CdS nanorods enable photocatalytic reforming of ethanol into high value-added multicarbon compound, Chem 7 (2021) 1033–1049.

[72] E. Tiburcio, R. Greco, M. Mon, J. Ballesteros-Soberanas, J. Ferrando-Soria, M. López-Haro, J.C. Hernández-Garrido, J. Oliver-Meseguer, C. Marini, M. Boronat, D. Armentano, A. Leyva-Pérez, E. Pardo, Soluble/MOF-supported palladium single atoms catalyze the ligand-, additive-, and solvent-free aerobic oxidation of benzyl alcohols to benzoic acids, J. Am. Chem. Soc. 143 (2021) 2581–2592.

[73] H. Yin, Y. Peng, J. Li, Electrocatalytic reduction of nitrate to ammonia via a Au/Cu single atom alloy catalyst, Environ. Sci. Technol. 57 (2023) 3134–3144.

[74] J. Deng, C. Zhou, Y. Yang, B. Nan, L. Dong, L. Cai, L. Li, Z.-J. Wang, X. Yang, Z. Chen, Visible-light-driven selective cleavage of C-C bonds in lignin model substrates using carbon nitride-supported ruthenium single-atom catalyst, Chem. Eng. J. 462 (2023) 142282.

[75] Z. Xue, M. Yan, Y. Zhang, J. Xu, X. Gao, Y. Wu, Understanding the injection process of hydrogen on Pt_1-TiO_2 surface for photocatalytic hydrogen evolution, Appl. Catal. B-Environ. 325 (2023) 122303.

[76] E. Zhao, M. Li, B. Xu, X.L. Wang, Y. Jing, D. Ma, S. Mitchell, J. Pérez-Ramírez, Z. Chen, Transfer hydrogenation with a carbon-nitride-supported palladium single-atom photocatalyst and water as a proton source, Angew. Chem. Int. Ed. 61 (2022) e202207410.

[77] F. Xie, C. Bie, J. Sun, Z. Zhang, B. Zhu, A. DFT, study on Pt single atom loaded COF for efficient photocatalytic CO_2 reduction, J. Mater. Sci. Technol. 170 (2024) 87–94.

[78] Q. Zuo, R. Cui, L. Wang, Y. Wang, C. Yu, L. Wu, Y. Mai, Y. Zhou, High-loading single cobalt atoms on ultrathin MOF nanosheets for efficient photocatalytic CO_2 reduction, Sci. China Chem. 66 (2023) 570–577.

[79] G. Wang, C.-T. He, R. Huang, J. Mao, D. Wang, Y. Li, Photoinduction of Cu single atoms decorated on UiO-66-NH_2 for enhanced photocatalytic reduction of CO_2 to liquid fuels, J. Am. Chem. Soc. 142 (2020) 19339–19345.

[80] J. Wang, G. Yu, Y. Wang, S. Liu, J. Qiu, Y. Xu, Z. Wang, Y. Wang, Y. Xie, H. Cao, Surface density of cobalt single atoms manipulating hydroxyl radical generation via dual pathways: electrons supply and active sites, Adv. Funct. Mater. 33 (2023) 2215245.

[81] P. Zhou, M. Luo, S. Guo, Optimizing the semiconductor-metal-single-atom interaction for photocatalytic reactivity, Nat. Rev. Chem. 6 (2022) 823–838.

[82] T. He, Z. Zhao, R. Liu, X. Liu, B. Ni, Y. Wei, Y. Wu, W. Yuan, H. Peng, Z. Jiang, Y. Zhao, Porphyrin-based covalent organic frameworks anchoring Au single atoms for photocatalytic nitrogen fixation, J. Am. Chem. Soc. 145 (2023) 6057–6066.

[83] B. Hu, B.-H. Wang, L. Chen, Z.-J. Bai, W. Zhou, J.-K. Guo, S. Shen, T.-L. Xie, C.-T. Au, L.-L. Jiang, S.-F. Yin, Electronic modulation of the interaction between Fe single atoms and $WO_{2.72-x}$ for photocatalytic N_2 reduction, ACS Catal. 12 (2022) 11860–11869.

[84] J. Chen, L. Chen, X. Wang, Z. Rao, J. Sun, A. Chen, X. Xie, Rare-earth single atoms decorated 2D-TiO_2 nanosheets for the photodegradation of gaseous O-xylene, J. Colloid Interface Sci. 605 (2022) 674–684.

[85] Z. Zeng, F. Ye, S. Deng, D. Fang, X. Wang, Y. Bai, H. Xiao, Accelerated organic pollutants mineralization in interlayer confined single Pt atom photocatalyst for hydrogen recovery, Chem. Eng. J. 444 (2022) 136561.

[86] J. Chen, G. Li, N. Lu, H. Lin, S. Zhou, F. Liu, Anchoring cobalt single atoms on 2D covalent triazine framework with charge nanospatial separation for enhanced photocatalytic pollution degradation, Mater. Today Chem. 24 (2022) 100832.

[87] H. Niu, X. Wang, C. Shao, Y. Liu, Z. Zhang, Y. Guo, Revealing the oxygen reduction reaction activity origin of single atoms supported on g-C_3N_4 monolayers: a first-principles study, J. Mater. Chem. A 8 (2020) 6555–6563.

[88] C. Zhang, D. Qin, Y. Zhou, F. Qin, H. Wang, W. Wang, Y. Yang, G. Zeng, Dual optimization approach to Mo single atom dispersed g-C_3N_4 photocatalyst: morphology and defect evolution, Appl. Catal. B-Environ. 303 (2022) 120904.

[89] K. Eid, M.H. Sliem, M. Al-Ejji, A.M. Abdullah, M. Harfouche, R.S. Varma, Hierarchical porous carbon nitride-crumpled nanosheet-embedded copper single atoms: an efficient catalyst for carbon monoxide oxidation, ACS Appl. Mater. Interfaces 14 (2022) 40749–40760.

[90] E. Yuan, M. Zhou, G. Shi, P. Jian, X. Hou, Ultralow-loading single-atom cobalt on graphitic carbon nitrogen with robust Co-N pairs for aerobic cyclohexane oxidation, Nano Res. 15 (2022) 8791–8803.

[91] X. Li, W. Bi, L. Zhang, S. Tao, W. Chu, Q. Zhang, Y. Luo, C. Wu, Y. Xie, Single-atom Pt as co-catalyst for enhanced photocatalytic H_2 evolution, Adv. Mater. 28 (2016) 2427–2431.

[92] M. Ou, S. Wan, Q. Zhong, S. Zhang, Y. Wang, Single Pt atoms deposition on g-C_3N_4 nanosheets for photocatalytic H_2 evolution or NO oxidation under visible light, Int. J. Hydrog. Energy 42 (2017) 27043–27054.

[93] P. Huang, W. Liu, Z. He, C. Xiao, T. Yao, Y. Zou, C. Wang, Z. Qi, W. Tong, B. Pan, S. Wei, Y. Xie, Single atom accelerates ammonia photosynthesis, Sci. China Chem. 61 (2018) 1187–1196.

[94] P. Zhou, X. Hou, Y. Chao, W. Yang, W. Zhang, Z. Mu, J. Lai, F. Lv, K. Yang, Y. Liu, J. Li, J. Ma, J. Luo, S. Guo, Synergetic interaction between neighboring platinum and ruthenium monomers boosts CO oxidation, Chem. Sci. 10 (2019) 5898–5905.

[95] Y. Li, B. Li, D. Zhang, L. Cheng, Q. Xiang, Crystalline carbon nitride supported copper single atoms for photocatalytic CO_2 reduction with nearly 100% CO selectivity, ACS Nano 14 (2020) 10552–10561.

[96] X.H. Jiang, L.S. Zhang, H.Y. Liu, D.S. Wu, F.Y. Wu, L. Tian, L.L. Liu, J.P. Zou, S. L. Luo, B.B. Chen, Silver single atom in carbon nitride catalyst for highly efficient photocatalytic hydrogen evolution, Angew. Chem. Int. Ed. 59 (2020) 23112–23116.

[97] Y. Wang, Y. Qu, B. Qu, L. Bai, Y. Liu, Z.D. Yang, W. Zhang, L. Jing, H. Fu, Construction of six-oxygen-coordinated single Ni sites on g-C_3N_4 with boron-oxo species for photocatalytic water-activation-induced CO_2 reduction, Adv. Mater. 33 (2021) 2105482.

[98] Z. Teng, Q. Zhang, H. Yang, K. Kato, W. Yang, Y.-R. Lu, S. Liu, C. Wang, A. Yamakata, C. Su, B. Liu, T. Ohno, Atomically dispersed antimony on carbon nitride for the artificial photosynthesis of hydrogen peroxide, Nat. Catal. 4 (2021) 374–384.

[99] M. Ren, X. Zhang, Y. Liu, G. Yang, L. Qin, J. Meng, Y. Guo, Y. Yang, Interlayer palladium-single-atom-coordinated cyano-group-rich graphitic carbon nitride for enhanced photocatalytic hydrogen production performance, ACS Catal. 12 (2022) 5077–5093.

[100] Y. Zhang, X. Chen, C. Liang, L. Yin, Y. Yang, Reconstructing the coordination environment of single atomic Fe-catalysts for boosting the Fenton-like degradation activities, Appl. Catal. B-Environ. 315 (2022) 121536.
[101] J. Ding, Z. Teng, X. Su, K. Kato, Y. Liu, T. Xiao, W. Liu, L. Liu, Q. Zhang, X. Ren, J. Zhang, Z. Chen, O. Teruhisa, A. Yamakata, H. Yang, Y. Huang, B. Liu, Y. Zhai, Asymmetrically coordinated cobalt single atom on carbon nitride for highly selective photocatalytic oxidation of CH_4 to CH_3OH, Chem 9 (2023) 1017–1035.
[102] H. Tan, P. Zhou, M. Liu, Q. Zhang, F. Liu, H. Guo, Y. Zhou, Y. Chen, L. Zeng, L. Gu, Z. Zheng, M. Tong, S. Guo, Photocatalysis of water into hydrogen peroxide over an atomic Ga-N_5 site, Nat. Synth. 2 (2023) 557–563.
[103] G.F.R. Rocha, M.A.R. da Silva, A. Rogolino, G.A.A. Diab, L.F.G. Noleto, M. Antonietti, I.F. Teixeira, Carbon nitride based materials: more than just a support for single-atom catalysis, Chem. Soc. Rev. 52 (2023) 4878–4932.
[104] S. Posada-Pérez, A. Vidal-López, M. Solà, A. Poater, 2D carbon nitride as a support with single Cu, Ag, and Au atoms for carbon dioxide reduction reaction, Phys. Chem. Chem. Phys. 25 (2023) 8574–8582.
[105] Y. Wang, D. Xie, G. Wang, Y. Wu, R. Shi, C. Zhou, X. Meng, T. Zhang, Single-atomic Co-N_4-O site boosting exciton dissociation and hole extraction for improved photocatalytic hydrogen evolution in crystalline carbon nitride, Nano Energy 104 (2022) 107938.
[106] M. Ma, Z. Huang, D.E. Doronkin, W. Fa, Z. Rao, Y. Zou, R. Wang, Y. Zhong, Y. Cao, R. Zhang, Y. Zhou, Ultrahigh surface density of Co-N_2C single-atom-sites for boosting photocatalytic CO_2 reduction to methanol, Appl. Catal. B-Environ. 300 (2022) 120695.
[107] Z. Fang, Y. Li, J. Li, C. Shu, L. Zhong, S. Lu, C. Mo, M. Yang, D. Yu, Capturing visible light in low-band-gap C_4N-derived responsive bifunctional air electrodes for solar energy conversion and storage, Angew. Chem. Int. Ed. 60 (2021) 17615–17621.
[108] Z. Zhang, R. Ji, Q. Sun, J. He, D. Chen, N. Li, H. Li, A. Marcomini, Q. Xu, J. Lu, Enhanced photocatalytic degradation of 2-chlorophenol over Z-scheme heterojunction of CdS-decorated oxygen-doped g-C_3N_4 under visible-light, Appl. Catal. B-Environ. 324 (2023) 122276.
[109] X. Zhang, T. Peng, L. Yu, R. Li, Q. Li, Z. Li, Visible/near-infrared-light-induced H_2 production over g-C_3N_4 co-sensitized by organic dye and zinc phthalocyanine derivative, ACS Catal. 5 (2014) 504–510.
[110] O. Iqbal, H. Ali, N. Li, A.I. Al-Sulami, K.F. Alshammari, H.S.M. Abd-Rabboh, Y. Al-Hadeethi, I.U. Din, A.I. Alharthi, R. Altamimi, A. Zada, Z. Wang, A. Hayat, M. Zahid, Ansari, A review on the synthesis, properties, and characterizations of graphitic carbon nitride (g-C_3N_4) for energy conversion and storage applications, Mater. Today Phys. 34 (2023) 101080.
[111] F. Yu, Q. Deng, H. Li, Y. Xia, W. Hou, A general strategy to synthesize single-atom metal-oxygen doped polymeric carbon nitride with highly enhanced photocatalytic water splitting activity, Appl. Catal. B-Environ. 323 (2023) 122180.
[112] C. Yang, Z. Zhao, Q. Liu, Regulating effect on photocatalytic water splitting performance of g-C_3N_4 via confinement of single atom Pt based on energy band engineering: A first principles investigation, Appl. Surf. Sci. 577 (2022) 151916.
[113] L.H. Xu, W. Liu, K. Liu, Single atom environmental catalysis: Influence of supports and coordination environments, Adv. Funct. Mater. (2023) 2304468.
[114] M. Chu, Y. Li, X. Chen, G. Hou, Y. Zhou, H. Kang, W. Qin, X. Wu, Constructing a built-in electric field by anchoring highly dispersed Zn single atoms on UiO-66-NH_2 for efficient CO_2 photoreduction, J. Mater. Chem. A 10 (2022) 23666–23674.
[115] W.-H. Li, J. Yang, D. Wang, Y. Li, Striding the threshold of an atom era of organic synthesis by single-atom catalysis, Chem 8 (2022) 119–140.
[116] P. Ren, T. Zhang, N. Jain, H.Y.V. Ching, A. Jaworski, G. Barcaro, S. Monti, J. Silvestre-Albero, V. Celorrio, L. Chouhan, A. Rokicińska, E. Debroye, P. Kuśtrowski, S. Van Doorslaer, S. Van Aert, S. Bals, S. Das, An atomically dispersed Mn-photocatalyst for generating hydrogen peroxide from seawater via the water oxidation reaction (WOR), J. Am. Chem. Soc. 145 (2023) 16584–16596.
[117] D. Zhao, Y. Wang, C.-L. Dong, F. Meng, Y.-C. Huang, Q. Zhang, L. Gu, L. Liu, S. Shen, Electron-deficient Zn-N_6 configuration enabling polymeric carbon nitride for visible-light photocatalytic overall water splitting, Nano-Micro Lett. 14 (2022) 223.
[118] Z. Han, Y. Zhao, G. Gao, W. Zhang, Y. Qu, H. Zhu, P. Zhu, G. Wang, Erbium single atom composite photocatalysts for reduction of CO_2 under visible light: CO_2 molecular activation and 4f levels as an electron transport bridge, Small 17 (2021) 2102089.
[119] Z. Teng, W. Cai, W. Sim, Q. Zhang, C. Wang, C. Su, T. Ohno, Photoexcited single metal atom catalysts for heterogeneous photocatalytic H_2O_2 production: Pragmatic guidelines for predicting charge separation, Appl. Catal. B-Environ. 282 (2021) 119589.
[120] Y. Zhao, Z. Han, G. Gao, W. Zhang, Y. Qu, H. Zhu, P. Zhu, G. Wang, Dual functions of CO_2 molecular activation and 4f levels as electron transport bridge in dysprosium single atom composite photocatalysts with enhanced visible-light photoactivities, Adv. Funct. Mater. 31 (2021) 2104976.
[121] H. Zhang, Y. Zhao, Y. Sun, Q. Xu, R. Yang, H. Zhang, C. Lin, K. Kato, X. Li, M. Yamauchi, Z. Jiang, A novel self-assembly approach for synthesizing nanofiber aerogel supported platinum single atoms, J. Mater. Chem. A 8 (2020) 15094–15102.
[122] H. Li, Q. Wan, C. Du, Q. Liu, J. Qi, X. Ding, S. Wang, S. Wan, J. Lin, C. Tian, L. Li, T. Peng, W. Zhao, K.H.L. Zhang, J. Huang, X. Zhang, J. Gu, B. Yang, H. Guo, S. Lin, A.K. Datye, Y. Wang, H. Xiong, Vapor-phase self-assembly for generating thermally stable single-atom catalysts, Chem 8 (2022) 731–748.
[123] J. Zhou, D. Xu, G. Tian, Q. He, X. Zhang, J. Liao, L. Mei, L. Chen, L. Gao, L. Zhao, G. Yang, W. Yin, G. Nie, Y. Zhao, Coordination-driven self-assembly strategy-activated Cu single-atom nanozymes for catalytic tumor-specific therapy, J. Am. Chem. Soc. 145 (2023) 4279–4293.
[124] X. Xiao, Y. Gao, L. Zhang, J. Zhang, Q. Zhang, Q. Li, H. Bao, J. Zhou, S. Miao, N. Chen, J. Wang, B. Jiang, C. Tian, H. Fu, A promoted charge separation/transfer system from Cu single atoms and C_3N_4 layers for efficient photocatalysis, Adv. Mater. 32 (2020).
[125] L.S. Zhang, X.H. Jiang, Z.A. Zhong, L. Tian, Q. Sun, Y.T. Cui, X. Lu, J.P. Zou, S. L. Luo, Carbon nitride supported high-loading Fe single-atom catalyst for activation of peroxymonosulfate to generate $^1O_2$ with 100% selectivity, Angew. Chem. Int. Ed. 60 (2021) 21751–21755.
[126] G. Li, X. Sun, P. Chen, M. Song, T. Zhao, F. Liu, S.-F. Yin, Insights into spin polarization regulated exciton dissociation and charge separation of C_3N_4 for efficient hydrogen evolution and simultaneous benzylamine oxidation, Nano Res 16 (2023) 8845–8852.
[127] P. Colonna, S. Bezzenine, R. Gil, J. Hannedouche, Alkene hydroamination via earth-abundant transition metal (iron, cobalt, copper and zinc) catalysis: a mechanistic overview, Adv. Synth. Catal. 362 (2020) 1550–1563.
[128] T. Zhang, Z. Sun, S. Li, B. Wang, Y. Liu, R. Zhang, Z. Zhao, Regulating electron configuration of single Cu sites via unsaturated N,O-coordination for selective oxidation of benzene, Nat. Commun. 13 (2022) 6996.
[129] J. Shen, C. Luo, S. Qiao, Y. Chen, Y. Tang, J. Xu, K. Fu, D. Yuan, H. Tang, H. Zhang, C. Liu, Single-atom Cu channel and N-vacancy engineering enables efficient charge separation and transfer between C_3N_4 interlayers for boosting photocatalytic hydrogen production, ACS Catal. 13 (2023) 6280–6288.
[130] S. Hu, P. Qiao, X. Yi, Y. Lei, H. Hu, J. Ye, D. Wang, Selective photocatalytic reduction of CO_2 to CO mediated by silver single atoms anchored on tubular carbon nitride, Angew. Chem. Int. Ed. 62 (2023) e202304585.
[131] Y. Liu, J. Sun, H. Huang, L. Bai, X. Zhao, B. Qu, L. Xiong, F. Bai, J. Tang, L. Jing, Improving CO_2 photoconversion with ionic liquid and Co single atoms, Nat. Commun. 14 (2023) 1457.
[132] C. Yang, Y. Zhu, J. Liu, Y. Qin, H. Wang, H. Liu, Y. Chen, Z. Zhang, W. Hu, Defect engineering for electrochemical nitrogen reduction reaction to ammonia, Nano Energy 77 (2020) 105126.
[133] G. Liu, Y. Huang, H. Lv, H. Wang, Y. Zeng, M. Yuan, Q. Meng, C. Wang, Confining single-atom Pd on g-C_3N_4 with carbon vacancies towards enhanced photocatalytic NO conversion, Appl. Catal. B-Environ. 284 (2021) 119683.
[134] Q. He, J. Ding, H.-J. Tsai, Y. Liu, M. Wei, Q. Zhang, Z. Wei, Z. Chen, J. Huang, S.-F. Hung, H. Yang, Y. Zhai, Boosting photocatalytic hydrogen peroxide production by regulating electronic configuration of single Sb atoms via carbon vacancies in carbon nitrides, J. Colloid Interface Sci. 651 (2023) 18–26.
[135] Y. Yang, F. Li, J. Chen, J. Fan, Q. Xiang, Single Au atoms anchored on amino-group-enriched graphitic carbon nitride for photocatalytic CO_2 reduction, ChemSusChem 13 (2020) 1979–1985.
[136] C. Yang, Z. Cheng, G. Divitini, C. Qian, B. Hou, Y. Liao, A Ni or Co single atom anchored conjugated microporous polymer for high-performance photocatalytic hydrogen evolution, J. Mater. Chem. A 9 (2021) 19894–19900.
[137] E. Vorobyeva, V.C. Gerken, S. Mitchell, A. Sabadell-Rendón, R. Hauert, S. Xi, A. Borgna, D. Klose, S.M. Collins, P.A. Midgley, D.M. Kepaptsoglou, Q. M. Ramasse, A. Ruiz-Ferrando, E. Fako, M.A. Ortuño, N. López, E.M. Carreira, J. Pérez-Ramírez, Activation of copper species on carbon nitride for enhanced activity in the arylation of amines, ACS Catal. 10 (2020) 11069–11080.
[138] C. Ding, X. Lu, B. Tao, L. Yang, X. Xu, L. Tang, H. Chi, Y. Yang, D.M. Meira, L. Wang, X. Zhu, S. Li, Y. Zhou, Z. Zou, Interlayer spacing regulation by single-atom indium$^{\delta+}$-N_4 on carbon nitride for boosting CO_2/CO photo-conversion, Adv. Funct. Mater. 33 (2023) 2302824.
[139] X. Jin, R. Wang, L. Zhang, R. Si, M. Shen, M. Wang, J. Tian, J. Shi, Electron configuration modulation of nickel single atoms for elevated photocatalytic hydrogen evolution, Angew. Chem. Int. Ed. 59 (2020) 6827–6831.
[140] J. Feng, H. Gao, L. Zheng, Z. Chen, S. Zeng, C. Jiang, H. Dong, L. Liu, S. Zhang, X. Zhang, A. Mn-N_3, Single-atom catalyst embedded in graphitic carbon nitride for efficient CO_2 electroreduction, Nat. Commun. 11 (2020) 4341.
[141] G. Wang, T. Zhang, W. Yu, R. Si, Y. Liu, Z. Zhao, Modulating location of single copper atoms in polymeric carbon nitride for enhanced photoredox catalysis, ACS Catal. 10 (2020) 5715–5722.
[142] Y. Yang, G. Zeng, D. Huang, C. Zhang, D. He, C. Zhou, W. Wang, W. Xiong, B. Song, H. Yi, S. Ye, X. Ren, In situ grown single-atom cobalt on polymeric carbon nitride with bidentate ligand for efficient photocatalytic degradation of refractory antibiotics, Small 16 (2020) 2001634.
[143] W. Jiang, Y. Zhao, X. Zong, H. Nie, L. Niu, L. An, D. Qu, X. Wang, Z. Kang, Z. Sun, Photocatalyst for high-performance H_2 production: Ga-doped polymeric carbon nitride, Angew. Chem. Int. Ed. 60 (2021) 6124–6129.
[144] F. Zhang, J. Zhang, H. Wang, J. Li, H. Liu, X. Jin, X. Wang, G. Zhang, Single tungsten atom steered band-gap engineering for graphitic carbon nitride ultrathin nanosheets boosts visible-light photocatalytic H_2 evolution, Chem. Eng. J. 424 (2021) 130004.
[145] L. Su, P. Wang, X. Ma, J. Wang, S. Zhan, Regulating local electron density of iron single sites by introducing nitrogen vacancies for efficient photo-fenton process, Angew. Chem. Int. Ed. 60 (2021) 21261–21266.
[146] J. Bian, Y. Liao, R. Liu, X. An, C. Hu, H. Liu, J. Qu, Synergy of cyano groups and cobalt single atoms in graphitic carbon nitride for enhanced bio-denitrification, Water Res 218 (2022) 118465.
[147] C. Zhu, Y. Nie, F. Cun, Y. Wang, Z. Tian, F. Liu, Two-step pyrolysis to anchor ultrahigh-density single-atom FeN_5 sites on carbon nitride for efficient Fenton-like catalysis near 0 °C, Appl. Catal. B-Environ. 319 (2022) 121900.

[148] X. Liu, Y. Deng, L. Zheng, M.R. Kesama, C. Tang, Y. Zhu, Engineering low-coordination single-atom cobalt on graphitic carbon nitride catalyst for hydrogen evolution, ACS Catal. 12 (2022) 5517–5526.
[149] W. Xie, K. Li, X.H. Liu, X. Zhang, H. Huang, P-mediated Cu-N_4 sites in carbon nitride realizing CO_2 photoreduction to C_2H_4 with selectivity modulation, Adv. Mater. 35 (2022) 2208132.
[150] M. Zhang, C. Lai, F. Xu, D. Huang, T. Hu, B. Li, D. Ma, S. Liu, Y. Fu, L. Li, L. Tang, L. Chen, Ultrahigh performance H_2O_2 generation by single-atom Fe catalysts with N/O bidentate ligand via oxalic acid and oxygen molecules activation, Small 19 (2023) 2301817.
[151] H. Yang, N. Lu, J. Zhang, R. Wang, S. Tian, M. Wang, Z. Wang, K. Tao, F. Ma, S. Peng, Ultra-low single-atom Pt on g-C_3N_4 for electrochemical hydrogen peroxide production, Carbon Energy (2023) e337.
[152] Y. Cao, D. Wang, Y. Lin, W. Liu, L. Cao, X. Liu, W. Zhang, X. Mou, S. Fang, X. Shen, T. Yao, Single Pt atom with highly vacant d-orbital for accelerating photocatalytic H_2 evolution, ACS Appl. Energy Mater. 1 (2018) 6082–6088.
[153] M. Liu, X. Liu, D. Fu, Z. Xie, X. Zou, W. Liu, Y. Yu, J. Wang, H. Wang, C. Tong, Z. Cheng, S. Wu, K. Ding, Y. Yu, A facile complexing agent-assistant single atom Ag-N_3S_1 site photodeposition strategy, Appl. Catal. B-Environ. 318 (2022) 121896.
[154] L. Zhang, R. Long, Y. Zhang, D. Duan, Y. Xiong, Y. Zhang, Y. Bi, Direct observation of dynamic bond evolution in single-atom Pt/C_3N_4, Catal., Angew. Chem. Int. Ed. 59 (2020) 6224–6229.
[155] Y. Huang, D. Li, S. Feng, Y. Jia, S. Guo, X. Wu, M. Chen, W. Shi, Pt atoms/clusters on Ni-phytate-sensitized carbon nitride for enhanced NIR-light-driven overall water splitting beyond 800 nm, Angew. Chem. Int. Ed. 61 (2022) e202212234.
[156] Y. Zou, J. Li, J. Tan, L. Lyu, S. Li, Y. Wang, Y. Lu, X. Zhu, T. Zhang, High-valent cobalt-oxo species triggers singlet oxygen for rapid contaminants degradation along with mild peroxymonosulfate decomposition in single Co atom-doped g-C_3N_4, Chem. Eng. J. 471 (2023) 144531.
[157] S. Ji, Y. Qu, T. Wang, Y. Chen, G. Wang, X. Li, J. Dong, Q. Chen, W. Zhang, Z. Zhang, S. Liang, R. Yu, Y. Wang, D. Wang, Y. Li, Rare-earth single erbium atoms for enhanced photocatalytic CO_2 reduction, Angew. Chem. Int. Ed. 59 (2020) 10651–10657.
[158] J. Gu, M. Jian, L. Huang, Z. Sun, A. Li, Y. Pan, J. Yang, W. Wen, W. Zhou, Y. Lin, H.-J. Wang, X. Liu, L. Wang, X. Shi, X. Huang, L. Cao, S. Chen, X. Zheng, H. Pan, J. Zhu, S. Wei, W.-X. Li, J. Lu, Synergizing metal-support interactions and spatial confinement boosts dynamics of atomic nickel for hydrogenations, Nat. Nanotechnol. 16 (2021) 1141–1149.
[159] H. Yang, F. Ma, N. Lu, S. Tian, G. Liu, Y. Wang, Z. Wang, D. Wang, K. Tao, H. Zhang, S. Peng, Transition metal single atom-optimized g-C_3N_4 for the highly selective electrosynthesis of H_2O_2 under neutral electrolytes, Nanoscale Horiz. 8 (2023) 695–704.
[160] Z. Shixuan, L. Donghao, J. Jiwei, F. Li, T. Hua, Oxygen reduction activity of a Pt-N_4 single-atom catalyst prepared by electrochemical deposition and its bioelectrochemical application, Electrochim. Acta 437 (2023) 141543.
[161] P. Sharma, S. Kumar, O. Tomanec, M. Petr, J. Zhu Chen, J.T. Miller, R.S. Varma, M.B. Gawande, R. Zboril, Carbon nitride-based ruthenium single atom photocatalyst for CO_2 reduction to methanol, Small 17 (2021) 2006478.
[162] T. Jia, D. Meng, R. Duan, H. Ji, H. Sheng, C. Chen, J. Li, W. Song, J. Zhao, Single-atom nickel on carbon nitride photocatalyst achieves semihydrogenation of alkynes with water protons via monovalent nickel, Angew. Chem. Int. Ed. 62 (2023) e202216511.
[163] X. Liu, Y. Luo, C. Ling, Y. Shi, G. Zhan, H. Li, H. Gu, K. Wei, F. Guo, Z. Ai, L. Zhang, Rare earth La single atoms supported MoO_{3-x} for efficient photocatalytic nitrogen fixation, Appl. Catal. B-Environ. 301 (2022) 120766.
[164] J. Zhuang, S. Ren, B. Zhu, C. Han, Y. Li, X. Zhang, H. Gao, M. Fan, Q. Tian, Lignin-based carbon dots as high-performance support of Pt single atoms for photocatalytic H_2 evolution, Chem. Eng. J. 446 (2022) 136873.
[165] P. Qi, J. Wang, X. Djitcheu, D. He, H. Liu, Q. Zhang, Techniques for the characterization of single atom catalysts, RSC Adv. 12 (2022) 1216–1227.
[166] P. Liu, Z. Huang, X. Gao, X. Hong, J. Zhu, G. Wang, Y. Wu, J. Zeng, X. Zheng, Synergy between palladium single atoms and nanoparticles via hydrogen spillover for enhancing CO_2 photoreduction to CH_4, Adv. Mater. 34 (2022) 2200057.
[167] H. Zhang, Y. Cao, S. Qin, Z. Yang, L. Shangguan, J. He, J. Sun, W. Lei, Surface modification of carbon nitride with single Co sites via a solvent-driven strategy promoting high-efficiency photocatalytic overall water splitting, Appl. Surf. Sci. 581 (2022) 152328.
[168] G. Wang, R. Huang, J. Zhang, J. Mao, D. Wang, Y. Li, Synergistic modulation of the separation of photo-generated carriers via engineering of dual atomic sites for promoting photocatalytic performance, Adv. Mater. 33 (2021) 2105904.
[169] P. Chen, B. Lei, Xa Dong, H. Wang, J. Sheng, W. Cui, J. Li, Y. Sun, Z. Wang, F. Dong, Rare-earth single-atom La-N charge-transfer bridge on carbon nitride for highly efficient and selective photocatalytic CO_2 reduction, ACS Nano 14 (2020) 15841–15852.
[170] Z. Wang, J. Yang, J. Cao, W. Chen, G. Wang, F. Liao, X. Zhou, F. Zhou, R. Li, Z.-Q. Yu, G. Zhang, X. Duan, Y. Wu, Room-temperature synthesis of single iron site by electrofiltration for photoreduction of CO_2 into tunable syngas, ACS Nano 14 (2020) 6164–6172.
[171] Y. Tian, M. Li, Z. Wu, Q. Sun, D. Yuan, B. Johannessen, L. Xu, Y. Wang, Y. Dou, H. Zhao, S. Zhang, Edge-hosted atomic Co-N_4 sites on hierarchical porous carbon for highly selective two-electron oxygen reduction reaction, Angew. Chem. Int. Ed. 61 (2022) e202213296.
[172] A.J. Therrien, A.J.R. Hensley, M.D. Marcinkowski, R. Zhang, F.R. Lucci, B. Coughlin, A.C. Schilling, J.-S. McEwen, E.C.H. Sykes, An atomic-scale view of single-site Pt catalysis for low-temperature CO oxidation, Nat. Catal. 1 (2018) 192–198.
[173] L. Zhang, J. Liao, Y. Li, W. Sun, C. Ge, Cu single atoms embedded on hollow g-C_3N_4 nanospheres with enhanced charge transfer and separation for efficient photocatalysis, Chin. Chem. Lett. (2023) 108568.
[174] S. P, J. John, T.P.D. Rajan, G.M. Anilkumar, T. Yamaguchi, S.C. Pillai, U. S. Hareesh, Graphitic carbon nitride (g-C_3N_4) based heterogeneous single atom catalysts: synthesis, characterisation and catalytic applications, J. Mater. Chem. A 11 (2023) 8599–8646.
[175] R. Xu, B. Xu, X. You, D. Shao, G. Gao, F. Li, X.-L. Wang, Y.-F. Yao, Preparation of single-atom palladium catalysts with high photocatalytic hydrogen production performance by means of photochemical reactions conducted with frozen precursor solutions, J. Mater. Chem. A 11 (2023) 11202–11209.
[176] L. Liu, Z. Du, J. Sun, S. He, K. Wang, M. Li, L. Xie, W. Ai, Engineering the first coordination shell of single Zn atoms via molecular design strategy toward high-performance sodium-ion hybrid capacitors, Small 19 (2023) 2300556.
[177] T. Wang, X. Tao, X. Li, K. Zhang, S. Liu, B. Li, Synergistic Pd single atoms, clusters, and oxygen vacancies on TiO_2 for photocatalytic hydrogen evolution coupled with selective organic oxidation, Small 17 (2020) 2006255.
[178] H. Peng, T. Yang, H. Lin, Y. Xu, Z. Wang, Q. Zhang, S. Liu, H. Geng, L. Gu, C. Wang, X. Fan, W. Chen, X. Huang, Ru/In dual-single atoms modulated charge separation for significantly accelerated photocatalytic H_2 evolution in pure water, Adv. Energy Mater. 12 (2022) 2201688.
[179] X. Shi, Y. Huang, Y. Bo, D. Duan, Z. Wang, J. Cao, G. Zhu, W. Ho, L. Wang, T. Huang, Y. Xiong, Highly selective photocatalytic CO_2 methanation with water vapor on single-atom platinum-decorated defective carbon nitride, Angew. Chem. Int. Ed. 61 (2022) e202203063.
[180] H. Cao, J. Wang, J.-H. Kim, Z. Guo, J. Xiao, J. Yang, J. Chang, Y. Shi, Y. Xie, Different roles of Fe atoms and nanoparticles on g-C_3N_4 in regulating the reductive activation of ozone under visible light, Appl. Catal. B-Environ. 296 (2021) 120362.
[181] Q. Zhu, Z. Xu, B. Qiu, M. Xing, J. Zhang, Emerging cocatalysts on g-C_3N_4 for photocatalytic hydrogen evolution, Small 17 (2021) 2101070.
[182] Y. Zhang, Y. Li, X. Xin, Y. Wang, P. Guo, R. Wang, B. Wang, W. Huang, A. J. Sobrido, X. Li, Internal quantum efficiency higher than 100% achieved by combining doping and quantum effects for photocatalytic overall water splitting, Nat. Energy 8 (2023) 504–514.
[183] Y. Zhang, C. Pan, G. Bian, J. Xu, Y. Dong, Y. Zhang, Y. Lou, W. Liu, Y. Zhu, H_2O_2 generation from O_2 and H_2O on a near-infrared absorbing porphyrin supramolecular photocatalyst, Nat. Energy 8 (2023) 361–371.
[184] J. Kosco, M. Bidwell, H. Cha, T. Martin, C.T. Howells, M. Sachs, D.H. Anjum, S. Gonzalez Lopez, L. Zou, A. Wadsworth, W. Zhang, L. Zhang, J. Tellam, R. Sougrat, F. Laquai, D.M. DeLongchamp, J.R. Durrant, I. McCulloch, Enhanced photocatalytic hydrogen evolution from organic semiconductor heterojunction nanoparticles, Nat. Mater. 19 (2020) 559–565.
[185] G. Liao, Y. Gong, L. Zhang, H. Gao, G.-J. Yang, B. Fang, Semiconductor polymeric graphitic carbon nitride photocatalysts: the "holy grail" for the photocatalytic hydrogen evolution reaction under visible light, Energy Environ. Sci. 12 (2019) 2080–2147.
[186] Z. Li, F. Huang, Y. Xu, A. Yan, H. Dong, X. Xiong, X. Zhao, Electron-extracting system with enhanced photocatalytic hydrogen production performance: Synergistic utilization of Z-scheme and Ohmic heterojunctions, Chem. Eng. J. 429 (2022) 132476.
[187] Z. Li, T. Deng, S. Ma, Z. Zhang, G. Wu, J. Wang, Q. Li, H. Xia, S.-W. Yang, X. Liu, Three-component donor-π-acceptor covalent-organic frameworks for boosting photocatalytic hydrogen evolution, J. Am. Chem. Soc. (2023) 8364–8374.
[188] W. Dong, Y. Xiao, Z. Qin, B. Qiao, L. Li, Partially H-bonded covalent organic frameworks for photocatalytic hydrogen evolution, J. Mater. Chem. A 11 (2023) 14760–14767.
[189] I. Vamvasakis, B. Liu, G.S. Armatas, Size effects of platinum nanoparticles in the photocatalytic hydrogen production over 3D mesoporous networks of CdS and Pt nanojunctions, Adv. Funct. Mater. 26 (2016) 8062–8071.
[190] M. Eder, C. Courtois, P. Petzoldt, S. Mackewicz, M. Tschurl, U. Heiz, Size and coverage effects of Ni and Pt co-catalysts in the photocatalytic hydrogen evolution from methanol on TiO_2(110), ACS Catal. 12 (2022) 9579–9588.
[191] B. Yan, Y. He, G. Yang, Nanoscale self-wetting driven monatomization of Ag nanoparticle for excellent photocatalytic hydrogen evolution, Small 18 (2022) 2107840.
[192] X. Xiang, L. Zhang, C. Luo, J. Zhang, B. Cheng, G. Liang, Z. Zhang, J. Yu, Ultrafast electron transfer from CdS quantum dots to atomically-dispersed Pt for enhanced H_2 evolution and value-added chemical synthesis, Appl. Catal. B-Environ. 340 (2024).
[193] Z. Luo, G. Zhao, H. Pan, W. Sun, Strong metal-support interaction in heterogeneous catalysts, Adv. Energy Mater. 12 (2022) 123196.
[194] L. Wang, R. Tang, A. Kheradmand, Y. Jiang, H. Wang, W. Yang, Z. Chen, X. Zhong, S.P. Ringer, X. Liao, W. Liang, J. Huang, Enhanced solar-driven benzaldehyde oxidation with simultaneous hydrogen production on Pt single-atom catalyst, Appl. Catal. B-Environ. 284 (2021) 119759.
[195] Z. Zeng, Y. Su, X. Quan, W. Choi, G. Zhang, N. Liu, B. Kim, S. Chen, H. Yu, S. Zhang, Single-atom platinum confined by the interlayer nanospace of carbon nitride for efficient photocatalytic hydrogen evolution, Nano Energy 69 (2020) 104409.
[196] C. Wang, J. Xie, N. Chen, W. Chen, P. Bai, H. Wang, Non-noble-metal catalyst of Cu/g-C_3N_4 for efficient photocatalytic hydrogen evolution, ACS Appl. Energy Mater. 4 (2021) 13796–13802.

[197] S. Shen, J. Chen, Y. Wang, C.-L. Dong, F. Meng, Q. Zhang, Y. Huangfu, Z. Lin, Y.-C. Huang, Y. Li, M. Li, L. Gu, Boosting photocatalytic hydrogen production by creating isotype heterojunctions and single-atom active sites in highly-crystallized carbon nitride, Sci. Bull. 67 (2022) 520–528.
[198] Z. Yu, Y. Li, A. Torres-Pinto, A.P. LaGrow, V.M. Diaconescu, L. Simonelli, M. J. Sampaio, O. Bondarchuk, I. Amorim, A. Araujo, A.M.T. Silva, C.G. Silva, J. L. Faria, L. Liu, Single-atom Ir and Ru anchored on graphitic carbon nitride for efficient and stable electrocatalytic/photocatalytic hydrogen evolution, Appl. Catal. B-Environ. 310 (2022) 121318.
[199] M. Gao, F. Tian, Z. Guo, X. Zhang, Z. Li, J. Zhou, X. Zhou, Y. Yu, W. Yang, Mutual-modification effect in adjacent Pt nanoparticles and single atoms with sub-nanometer inter-site distances to boost photocatalytic hydrogen evolution, Chem. Eng. J. 446 (2022) 137127.
[200] M. Yu, H. Liang, R. Zhan, C. Liu, J. Guo, Y. Sun, L. Xu, J. Niu, Bimetal single atom on defect-tailoring carbon nitride that boosts photocatalytic hydrogen evolution and superfast contaminant degradation, Sep. Purif. Technol. 287 (2022) 120556.
[201] C. Li, N. Su, H. Wu, C. Liu, G. Che, H. Dong, Synergies of adjacent sites in atomically dispersed ruthenium toward achieving stable hydrogen evolution, Inorg. Chem. 61 (2022) 13453–13461.
[202] M. Mateen, W.-C. Cheong, C. Zheng, S.H. Talib, J. Zhang, X. Zhang, S. Liu, C. Chen, Y. Li, Molybdenum atomic sites embedded 1D carbon nitride nanotubes as highly efficient bifunctional photocatalyst for tetracycline degradation and hydrogen evolution, Chem. Eng. J. 451 (2023) 138305.
[203] T. Zhou, H. Wei, B. Xiao, T. Lv, L. Duan, Q. Lu, J. Zhang, Y. Zhang, Q. Liu, Anchored Cu single atoms on porous g-C_3N_4 for superior photocatalytic H_2 evolution from water splitting, RSC Adv. 13 (2023) 8915–8922.
[204] L. Hu, J. Huang, J. Wang, S. Jiang, C. Sun, S. Song, Efficiently photocatalytic H_2O overall splitting within the strengthened polarized field by reassembling surface single atoms, Appl. Catal. B-Environ. 320 (2023) 121945.
[205] L. Wang, Y. Zhang, L. Chen, H. Xu, Y. Xiong, 2D polymers as emerging materials for photocatalytic overall water splitting, Adv. Mater. 30 (2018) 1801955.
[206] P. Niu, L. Li, Photocatalytic overall water splitting of carbon nitride by band-structure modulation, Matter 4 (2021) 1765–1767.
[207] G. Zhang, X. Wang, Oxysulfide semiconductors for photocatalytic overall water splitting with visible light, Angew. Chem. Int. Ed. 58 (2019) 15580–15582.
[208] C. Bie, L. Wang, J. Yu, Challenges for photocatalytic overall water splitting, Chem 8 (2022) 1567–1574.
[209] A. Fujishima, K. Honda, Electrochemical photolysis of water at a semiconductor electrode, Nature 238 (1972) 37–38.
[210] D. Zhao, Y. Wang, C.-L. Dong, Y.-C. Huang, J. Chen, F. Xue, S. Shen, L. Guo, Boron-doped nitrogen-deficient carbon nitride-based Z-scheme heterostructures for photocatalytic overall water splitting, Nat. Energy 6 (2021) 388–397.
[211] L. Ding, S. Yang, Z. Liang, X. Qian, X. Chen, H. Cui, J. Tian, TiO_2 nanobelts with anatase/rutile heterophase junctions for highly efficient photocatalytic overall water splitting, J. Colloid Interface Sci. 567 (2020) 181–189.
[212] T. Chen, C. Yang, S. Rajendran, Y. Lei, X. Zhang, J. Qin, Boosting visible-light hydrogen evolution on CdS hollow nanospheres with CoN as cocatalyst, Fuel 316 (2022) 123307.
[213] D. Dai, X. Liang, B. Zhang, Y. Wang, Q. Wu, X. Bao, Z. Wang, Z. Zheng, H. Cheng, Y. Dai, B. Huang, P. Wang, Strain adjustment realizes the photocatalytic overall water splitting on tetragonal zircon $BiVO_4$, Adv. Sci. 9 (2022) 2105299.
[214] Y. Liu, X. Xu, S. Zheng, S. Lv, H. Li, Z. Si, X. Wu, R. Ran, D. Weng, F. Kang, Ni single atoms anchored on nitrogen-doped graphene as H_2-Evolution cocatalyst of $SrTiO_3$(Al)/CoO for photocatalytic overall water splitting, Carbon 183 (2021) 763–773.
[215] L. Zhang, Q. Luo, S. Hu, Z. Hu, W. Zhang, J. Yang, Enhanced electron-hole separation in phosphorus-coordinated Co atom on g-C_3N_4 toward photocatalytic overall water splitting, J. Phys. Chem. Lett. 13 (2022) 11961–11967.
[216] W. Liu, L. Cao, W. Cheng, Y. Cao, X. Liu, W. Zhang, X. Mou, L. Jin, X. Zheng, W. Che, Q. Liu, T. Yao, S. Wei, Single-site active cobalt-based photocatalyst with a long carrier lifetime for spontaneous overall water splitting, Angew. Chem. Int. Ed. 56 (2017) 9312–9317.
[217] B. Dai, J. Fang, Y. Yu, M. Sun, H. Huang, C. Lu, J. Kou, Y. Zhao, Z. Xu, Construction of infrared-light-responsive photoinduced carriers driver for enhanced photocatalytic hydrogen evolution, Adv. Mater. 32 (2020) 2070087.
[218] X. Liu, Y. Zhao, Y. Ni, F. Shi, X. Guo, C. Li, Hydroxylated organic semiconductors for efficient photovoltaics and photocatalytic hydrogen evolution, Energy Environ. Sci. 16 (2023) 4065–4072.
[219] B. Xia, B. He, J. Zhang, L. Li, Y. Zhang, J. Yu, J. Ran, S.Z. Qiao, TiO_2/$FePS_3$ S-scheme heterojunction for greatly raised photocatalytic hydrogen evolution, Adv. Energy Mater. 12 (2022) 2201449.
[220] Y.F. Wang, M.Y. Qi, M. Conte, Z.R. Tang, Y.J. Xu, New radical route and insight for the highly efficient synthesis of benzimidazoles integrated with hydrogen evolution, Angew. Chem. Int. Ed. 62 (2023) e202304306.
[221] B.C. Moon, B. Bayarkhuu, K.A.I. Zhang, D.K. Lee, J. Byun, Solar-driven H_2O_2 production via cooperative auto- and photocatalytic oxidation in fine-tuned reaction media, Energy Environ. Sci. 15 (2022) 5082–5092.
[222] X. Zhang, P. Ma, C. Wang, L. Gan, X. Chen, P. Zhang, Y. Wang, H. Li, L. Wang, X. Zhou, K. Zheng, Unraveling the dual defect sites in graphite carbon nitride for ultra-high photocatalytic H_2O_2 evolution, Energy Environ. Sci. 15 (2022) 830–842.
[223] Y. Zhao, X. Li, X. Fan, H. Wang, Y. Liu, Y. Chen, T. Yang, J. Ye, H. Huang, H. Li, X. Zhang, Y. Liu, H. Lin, Y. Zhao, Z. Kang, Small-molecule catalyzed H_2O_2 production via a phase-transfer photocatalytic process, Appl. Catal. B-Environ. 314 (2022) 121499.
[224] K. Li, Q. Ge, Y. Liu, L. Wang, K. Gong, J. Liu, L. Xie, W. Wang, X. Ruan, L. Zhang, Highly efficient photocatalytic H_2O_2 production in microdroplets: accelerated charge separation and transfer at interfaces, Energy Environ. Sci. 16 (2023) 1135–1145.
[225] S. Li, G. Dong, R. Hailili, L. Yang, Y. Li, F. Wang, Y. Zeng, C. Wang, Effective photocatalytic H_2O_2 production under visible light irradiation at g-C_3N_4 modulated by carbon vacancies, Appl. Catal. B-Environ. 190 (2016) 26–35.
[226] X. Xu, Y. Sui, W. Chen, G. Zhou, Y. Li, H. Zhong, H.-R. Wen, Anthraquinone-based conjugated organic polymers containing dual oxidation centers for photocatalytic H_2O_2 production from H_2O and O_2 under visible-light irradiation, ACS Appl. Polym. Mater. 5 (2023) 7571–7580.
[227] C. Chu, Q. Zhu, Z. Pan, S. Gupta, D. Huang, Y. Du, S. Weon, Y. Wu, C. Muhich, E. Stavitski, K. Domen, J.-H. Kim, Spatially separating redox centers on 2D carbon nitride with cobalt single atom for photocatalytic H_2O_2 production, Proc. Natl. Acad. Sci. U. S. A. 117 (2020) 6376–6382.
[228] C. Zhuang, W. Li, T. Zhang, J. Li, Y. Zhang, G. Chen, H. Li, Z. Kang, J. Zou, X. Han, Monodispersed aluminum in carbon nitride creates highly efficient nitrogen active sites for ultra-high hydrogen peroxide photoproduction, Nano Energy 108 (2023) 108225.
[229] X. Huang, K. Zhang, B. Peng, G. Wang, M. Muhler, F. Wang, Ceria-based materials for thermocatalytic and photocatalytic organic synthesis, ACS Catal. 11 (2021) 9618–9678.
[230] L.-L. Liao, L. Song, S.-S. Yan, J.-H. Ye, D.-G. Yu, Highly reductive photocatalytic systems in organic synthesis, Trends Chem. 4 (2022) 512–527.
[231] S. Reischauer, B. Pieber, Emerging concepts in photocatalytic organic synthesis, iScience 24 (2021).
[232] Y. Xia, M. Sayed, L. Zhang, B. Cheng, J. Yu, Single-atom heterogeneous photocatalysts, Chem. Catal. 1 (2021) 1173–1214.
[233] Y. Jiang, Y. Fan, S. Li, Z. Tang, Photocatalytic methane conversion: insight into the mechanism of C(sp^3)-H bond activation, CCS Chem. 5 (2023) 30–54.
[234] L. Zhao, W. Cai, G. Ji, J. Wei, Z. Du, C. He, C. Duan, Anthraquinone-based metal-organic frameworks as a bifunctional photocatalyst for C-H activation, Inorg. Chem. 61 (2022) 9493–9503.
[235] F. Li, B. Wang, X. Chen, W. Zeng, R. Sun, X. Liu, Z. Ren, X. Yang, H. Fan, Q. Guo, Photocatalytic C-H bond activation of toluene on rutile TiO_2(110), J. Phys. Chem. C. 126 (2022) 11963–11970.
[236] X. Xiao, Z. Ruan, Q. Li, L. Zhang, H. Meng, Q. Zhang, H. Bao, B. Jiang, J. Zhou, C. Guo, X. Wang, H. Fu, A unique Fe-N_4 coordination system enabling transformation of oxygen into superoxide for photocatalytic C-H activation with high efficiency and selectivity, Adv. Mater. 34 (2022) 2200612.
[237] Z. Chen, J. Chen, Y. Li, Metal-organic-framework-based catalysts for hydrogenation reactions, Chin. J. Catal. 38 (2017) 1108–1126.
[238] H. Liu, L. Shi, Q. Zhang, P. Qi, Y. Zhao, Q. Meng, X. Feng, H. Wang, J. Ye, Photothermal catalysts for hydrogenation reactions, Chem. Commun. 57 (2021) 1279–1294.
[239] S. Mao, Z. Wang, Q. Luo, B. Lu, Y. Wang, Geometric and electronic effects in hydrogenation reactions, ACS Catal. 13 (2022) 974–1019.
[240] C.-H. Hao, X.-N. Guo, Y.-T. Pan, S. Chen, Z.-F. Jiao, H. Yang, X.-Y. Guo, Visible-light-driven selective photocatalytic hydrogenation of cinnamaldehyde over Au/SiC catalysts, J. Am. Chem. Soc. 138 (2016) 9361–9364.
[241] M. Guo, M. Zhang, R. Liu, X. Zhang, G. Li, State-of-the-art advancements in photocatalytic hydrogenation: Reaction mechanism and recent progress in metal-organic framework (MOF)-based catalysts, Adv. Sci. 9 (2021) 2103361.
[242] S. Kim, J. Bok, B.-H. Lee, H. Choi, Y. Seo, J. Kim, J. Kim, W. Ko, K.-S. Lee, S.-P. Cho, T. Hyeon, D. Yoo, Orthogonal dual photocatalysis of single atoms on carbon nitrides for one-pot relay organic transformation, ACS Nano 17 (2023) 21470–21479.
[243] J. Ran, B. Xia, Y. Zhang, S.-Z. Qiao, Two-dimensional building blocks for photocatalytic ammonia production, J. Mater. Chem. A 9 (2021) 18733–18745.
[244] Y. Peng, J. Albero, A. Franconetti, P. Concepción, H. García, Visible and NIR light assistance of the N_2 reduction to NH_3 catalyzed by Cs-promoted Ru nanoparticles supported on strontium titanate, ACS Catal. 12 (2022) 4938–4946.
[245] Z.-K. Shen, M. Cheng, Y.-J. Yuan, L. Pei, J. Zhong, J. Guan, X. Li, Z.-J. Li, L. Bao, X. Zhang, Z.-T. Yu, Z. Zou, Identifying the role of interface chemical bonds in activating charge transfer for enhanced photocatalytic nitrogen fixation of Ni_2P-black phosphorus photocatalysts, Appl. Catal. B-Environ. 295 (2021) 120274.
[246] D.L.T. Nguyen, M.A. Tekalgne, T.H.C. Nguyen, M.T.N. Dinh, S.S. Sana, A. N. Grace, M. Shokouhimehr, D.-V.N. Vo, C.K. Cheng, C.C. Nguyen, S.Y. Kim, Q. V. Le, Recent development of high-performance photocatalysts for N_2 fixation: a review, J. Environ. Chem. Eng. 9 (2021) 104997.
[247] H. Niu, X. Wang, C. Shao, Z. Zhang, Y. Guo, Computational screening single-atom catalysts supported on g-CN for N_2 reduction: high activity and selectivity, ACS Sustain. Chem. Eng. 8 (2020) 13749–13758.
[248] X.-W. Guo, S.-M. Chen, H.-J. Wang, Z.-M. Zhang, H. Lin, L. Song, T.-B. Lu, Single-atom molybdenum immobilized on photoactive carbon nitride as efficient photocatalysts for ambient nitrogen fixation in pure water, J. Mater. Chem. A 7 (2019) 19831–19837.
[249] G. Pan, W. Zhang, T. Liu, Q. Tan, B. Wei, K. Ye, Y. Yang, D. Han, Z. Liu, L. Niu, Atomically dispersed s-block metal calcium site modified mesoporous g-C_3N_4 for boosting photocatalytic N_2 reduction, Catal. Sci. Technol. 13 (2023) 111–118.
[250] L. Huang, X. Huang, J. Yan, Y. Liu, H. Jiang, H. Zhang, J. Tang, Q. Liu, Research progresses on the application of perovskite in adsorption and photocatalytic removal of water pollutants, J. Hazard. Mater. 442 (2023) 130024.
[251] M. Ran, H. Xu, Y. Bao, Y. Zhang, J. Zhang, M. Xing, Selective production of CO from organic pollutants by coupling piezocatalysis and advanced oxidation processes, Angew. Chem. Int. Ed. 62 (2023) e202303728.

[252] L. Xu, P.K. Wong, Z. Jiang, J.C. Yu, Iodide-mediated selective photocatalytic treatment of phenolic pollutants, Appl. Catal. B-Environ. 338 (2023) 123080.
[253] L. Gnanasekaran, D. Shanmugapriya, V. Sasikala, S. Vadivel, W.-H. Chen, M. Arthi, M. Soto-Moscoso, Nanocubic copper cobaltite for methyl orange degradation through photocatalytic process, Chemosphere 312 (2023) 137311.
[254] A.K. Yontar, S. Avcioğlu, S. Çevik, Nature-based nanocomposites for adsorption and visible light photocatalytic degradation of methylene blue dye, J. Clean. Prod. 380 (2022) 135070.
[255] L. Wang, H. Yin, S. Wang, J. Wang, S. Ai, Ni^{2+}-assisted catalytic one-step synthesis of Bi/BiOCl/$Bi_2O_2CO_3$ heterojunction with enhanced photocatalytic activity under visible light, Appl. Catal. B-Environ. 305 (2022) 121039.
[256] H. Mohan, V. Ramalingam, A. Adithan, K. Natesan, K.-K. Seralathan, T. Shin, Highly efficient visible light driven photocatalytic activity of zinc/ferrite: Carbamazepine degradation, mechanism and toxicity assessment, J. Hazard. Mater. 416 (2021) 126209.
[257] J.-W. Hsu, L.-W. Wei, C. Chen, H.P. Wang, Photocatalytic H_2O-to-H_2O_2 synchronized oxidation of an organic pollutant by carbon dot/g-C_3N_4 composites, J. Clean. Prod. 380 (2022) 134918.
[258] Z. Zhou, K. Li, W. Deng, J. Li, Y. Yan, Y. Li, X. Quan, T. Wang, Nitrogen vacancy mediated exciton dissociation in carbon nitride nanosheets: enhanced hydroxyl radicals generation for efficient photocatalytic degradation of organic pollutants, J. Hazard. Mater. 387 (2020) 122023.
[259] H. Ji, W. Liu, F. Sun, T. Huang, L. Chen, Y. Liu, J. Qi, C. Xie, D. Zhao, Experimental evidences and theoretical calculations on phenanthrene degradation in a solar-light-driven photocatalysis system using silica aerogel supported TiO_2 nanoparticles: insights into reactive sites and energy evolution, Chem. Eng. J. 419 (2021) 129605.
[260] Y. Zhang, M. Xiong, A. Sun, Z. Shi, B. Zhu, D.K. Macharia, F. Li, Z. Chen, J. Liu, L. Zhang, MIL-101(Fe) nanodot-induced improvement of adsorption and photocatalytic activity of carbon fiber/TiO_2-based weavable photocatalyst for removing pharmaceutical pollutants, J. Clean. Prod. 290 (2021) 125782.
[261] H. Zhu, N. Goswami, Q. Yao, T. Chen, Y. Liu, Q. Xu, D. Chen, J. Lu, J. Xie, Cyclodextrin-gold nanocluster decorated TiO_2 enhances photocatalytic decomposition of organic pollutants, J. Mater. Chem. A 6 (2018) 1102–1108.
[262] W. Liu, Y. Wang, K. Qi, F. Wen, J. Wang, Broad spectral response Z-scheme three-dimensional ordered macroporous carbon quantum dots/TiO_2/g-C_3N_4 composite for boosting photocatalysis, Langmuir 38 (2022) 4839–4847.
[263] B. He, S. Chen, Y. Cui, X. Chen, Y. Lei, J. Sun, Hollow polymeric ionic liquid spheres with hierarchical electron distribution: a novel composite of g-C3N4 for visible light photocatalytic water splitting enhancement, Chem. Eng. J. 440 (2022) 135625.
[264] C.-Q. Xu, W.-D. Zhang, K. Deguchi, S. Ohki, T. Shimizu, R. Ma, T. Sasaki, Construction of a push-pull system in g-C_3N_4 for efficient photocatalytic hydrogen evolution under visible light, J. Mater. Chem. A 8 (2020) 13299–13310.
[265] Y. Gu, T. Xu, X. Chen, W. Chen, W. Lu, High-loading single-atom tungsten anchored on graphitic carbon nitride (melon) for efficient oxidation of emerging contaminants, Chem. Eng. J. 427 (2022) 131973.
[266] Y. Zhou, W. Qin, X. Sun, Y. Zhu, J. Niu, Synergistic effects on d-band center via coordination sites of M-N_3P_1 (M = Co and Ni) in dual single atoms that enhances photocatalytic dechlorination from tetrachlorobispheonl A, J. Hazard. Mater. 430 (2022) 128419.
[267] N. Ahmadpour, M.H. Sayadi, S. Sobhani, M. Hajiani, A potential natural solar light active photocatalyst using magnetic $ZnFe_2O_4$@TiO_2/Cu nanocomposite as a high performance and recyclable platform for degradation of naproxen from aqueous solution, J. Clean. Prod. 268 (2020) 122023.
[268] Z. Cao, Y. Zhao, J. Li, Q. Wang, Q. Mei, H. Cheng, Rapid electron transfer-promoted tetracycline hydrochloride degradation: Enhanced activity in visible light-coupled peroxymonosulfate with PdO/g-C_3N_4/kaolinite catalyst, Chem. Eng. J. 457 (2023) 141191.
[269] Z. Zhao, W. Zhang, W. Liu, Y. Li, J. Ye, J. Liang, M. Tong, Single-atom silver induced amorphization of hollow tubular g-C3N4 for enhanced visible light-driven photocatalytic degradation of naproxen, Sci. Total Environ. 742 (2020) 140642.
[270] Y. Chu, X. Zheng, J. Fan, Preparation of sodium and boron co-doped graphitic carbon nitride for the enhanced production of H_2O_2 via two-electron oxygen reduction and the degradation of 2,4-DCP via photocatalytic oxidation coupled with Fenton oxidation, Chem. Eng. J. 431 (2022) 134020.
[271] X. Huang, Y. Chen, E. Walter, M. Zong, Y. Wang, X. Zhang, O. Qafoku, Z. Wang, K. M. Rosso, Facet-specific photocatalytic degradation of organics by heterogeneous fenton chemistry on hematite nanoparticles, Environ. Sci. Technol. 53 (2019) 10197–10207.
[272] Z. Tang, P. Zhao, H. Wang, Y. Liu, W. Bu, Biomedicine meets fenton chemistry, Chem. Rev. 121 (2021) 1981–2019.
[273] Q. Wang, Y. Cui, R. Huang, L. Zhong, P. Yan, S. Zhang, Q. Zhao, D. Jiang, A. Tang, H. Yang, A heterogeneous Fenton reaction system of N-doped TiO_2 anchored on sepiolite activates peroxymonosulfate under visible light irradiation, Chem. Eng. J. 383 (2020) 123142.
[274] J. Lin, W. Tian, Z. Guan, H. Zhang, X. Duan, H. Wang, H. Sun, Y. Fang, Y. Huang, S. Wang, Functional carbon nitride materials in photo-fenton-like catalysis for environmental remediation, Adv. Funct. Mater. 32 (2022) 2201743.
[275] A. Chen, J. Xiao, X. Kong, L. Chen, C. Li, Y. Wei, Q. Du, W. Sun, J. Zhang, Regulating the charge density of Cu(I) single sites enriched on the surface of N3c Vacancies-engineered g-C_3N_4 for efficient Fenton-like reactions, Sep. Purif. Technol. 314 (2023) 123525.
[276] X. Dou, Y. Chen, H. Shi, $CuBi_2O_4$/BiOBr composites promoted PMS activation for the degradation of tetracycline: S-scheme mechanism boosted Cu^{2+}/Cu^{+} cycle, Chem. Eng. J. 431 (2022) 134054.
[277] J. Lee, B.K. Singh, M.A. Hafeez, K. Oh, W. Um, Comparative study of PMS oxidation with Fenton oxidation as an advanced oxidation process for Co-EDTA decomplexation, Chemosphere 300 (2022) 134494.
[278] L. Chen, K. Xing, Q. Shentu, Y. Huang, W. Lv, Y. Yao, Well-dispersed iron and nitrogen co-doped hollow carbon microsphere anchoring by g-C_3N_4 for efficient peroxymonosulfate activation, Chemosphere 280 (2021) 130911.
[279] D. Yang, Y. Hu, P. Hong, G. Shen, Y. Li, J. He, K. Zhang, Z. Wu, C. Xie, J. Liu, L. Kong, Preassembly strategy to anchor single atoms on carbon nitride layers achieving versatile Fenton-like catalysis, Sep. Purif. Technol. 308 (2023) 122955.
[280] F. Chen, L.L. Liu, J.H. Wu, X.H. Rui, J.J. Chen, Y. Yu, Single-atom iron anchored tubular g-C_3N_4 catalysts for ultrafast fenton-like reaction: roles of high-calency iron-oxo species and organic radicals, Adv. Mater. 34 (2022) 2202891.
[281] Y.-Z. Zhang, C. Liang, H.-P. Feng, W. Liu, Nickel single atoms anchored on ultrathin carbon nitride for selective hydrogen peroxide generation with enhanced photocatalytic activity, Chem. Eng. J. 446 (2022) 137379.
[282] Z. Wang, E. Almatrafi, H. Wang, H. Qin, W. Wang, L. Du, S. Chen, G. Zeng, P. Xu, Cobalt single atoms anchored on oxygen-doped tubular carbon nitride for efficient peroxymonosulfate activation: simultaneous coordination structure and morphology modulation, Angew. Chem. Int. Ed. 61 (2022) e202202338.
[283] G. Zhao, W. Li, H. Zhang, W. Wang, Y. Ren, Single atom Fe-dispersed graphitic carbon nitride (g-C_3N_4) as a highly efficient peroxymonosulfate photocatalytic activator for sulfamethoxazole degradation, Chem. Eng. J. 430 (2022) 132937.
[284] X. Zhang, C. Li, X. Wang, S. Yang, Y. Tan, F. Yuan, S. Zheng, D.D. Dionysiou, Z. Sun, Defect engineering modulated iron single atoms with assist of layered clay for enhanced advanced oxidation processes, Small 18 (2022) 2204793.
[285] C. Yang, X. Hu, Y. Bai, B. Cai, Y. Li, Fe single atoms reduced by $NaBH_4$ mediate g-C_3N_4 electron transfer and effectively remove 2-mercaptobenzothiazole, Catalysts 13 (2023) 619.
[286] J. Lin, L. Jiang, W. Tian, Y. Yang, X. Duan, Y. Jiao, H. Zhang, S. Wang, The structure-dependent mechanism of single-atom cobalt on macroporous carbon nitride in (photo-)Fenton-like reactions, J. Mater. Chem. A 11 (2023) 13653–13664.
[287] X. Peng, J. Wu, Z. Zhao, X. Wang, H. Dai, L. Xu, G. Xu, Y. Jian, F. Hu, Activation of peroxymonosulfate by single-atom Fe-g-C_3N_4 catalysts for high efficiency degradation of tetracycline via nonradical pathways: role of high-valent iron-oxo species and Fe-N_x sites, Chem. Eng. J. 427 (2022) 130803.
[288] Z. Liu, W. Gao, L. Liu, S. Luo, C. Zhang, T. Yue, J. Sun, M. Zhu, J. Wang, Work function mediated interface charge kinetics for boosting photocatalytic water sterilization, J. Hazard. Mater. 442 (2023) 130036.
[289] Y.-L. Li, J.-F. Ai, Z.-C. Chen, H.-L. Wang, Z.-H. Zhu, F.-P. Liang, H.-H. Zou, Multiple strategies enhance the ROS of metal-organic frameworks for energy-efficient photocatalytic water purification and sterilization, ACS Mater. Lett. 5 (2023) 1317–1331.
[290] Y. Zhang, H. Li, X. Zhang, H. Zhang, W. Zhang, H. Huang, H. Ou, Y. Zhang, Enhanced adsorption and photocatalytic Cr(VI) reduction and sterilization of defective MoS_2/PVP, J. Colloid Interface Sci. 630 (2023) 742–753.
[291] B. Song, P. Zhu, Y. Zhang, N. Ju, X. Si, X. Pang, J. Lv, S. Zhang, Preparation and quality assessment of processed cream cheese by high hydrostatic pressure combined thermal processing and spore-induced germination, J. Food Eng. 341 (2023) 111319.
[292] J. Chen, P. Wang, J. Li, C. Wang, J. Wang, D. Zhang, Y. Peng, B. Wang, Z. Wu, Self-powered antifouling UVC pipeline sterilizer driven by the discharge stimuli based on the modified freestanding rotary triboelectric nanogenerator, Nano Energy 95 (2022) 106969.
[293] Y. Lv, G. Hu, J. Liang, X. Chen, B. Chen, T. Zhao, X. Lu, B. Wang, W. Yuan, Y. Li, Study on microwave sterilization technology of humidifier in central air conditioning system, Build. Environ. 160 (2019) 106220.
[294] X. Zhang, F. Tian, X. Lan, Y. Liu, W. Yang, J. Zhang, Y. Yu, Building P-doped MoS_2/g-C_3N_4 layered heterojunction with a dual-internal electric field for efficient photocatalytic sterilization, Chem. Eng. J. 429 (2022) 132588.
[295] B. Wu, Y. Li, K. Su, L. Tan, X. Liu, Z. Cui, X. Yang, Y. Liang, Z. Li, S. Zhu, K.W. K. Yeung, S. Wu, The enhanced photocatalytic properties of MnO_2/g-C_3N_4 heterostructure for rapid sterilization under visible light, J. Hazard. Mater. 377 (2019) 227–236.
[296] Q. Luo, Y. Li, X. Huo, L. Li, Y. Song, S. Chen, H. Lin, N. Wang, Atomic chromium coordinated graphitic carbon nitride for bioinspired antibiofouling in seawater, Adv. Sci. 9 (2022) 2105346.
[297] Z. Hu, Y. Zhang, L. Pu, B. Wang, S. Yang, H. Li, Atomic Ti-Nx sites with switchable coordination number for enhanced visible-light photocatalytic water disinfection, J. Clean. Prod. 377 (2022) 134423.
[298] J. Albero, Y. Peng, H. García, Photocatalytic CO_2 reduction to C2+ products, ACS Catal. 10 (2020) 5734–5749.
[299] J. Fu, K. Jiang, X. Qiu, J. Yu, M. Liu, Product selectivity of photocatalytic CO_2 reduction reactions, Mater. Today 32 (2020) 222–243.
[300] J. You, M. Xiao, Z. Wang, L. Wang, Non-noble metal-based cocatalysts for photocatalytic CO_2 reduction, J. CO_2 Util. 55 (2022) 101817.
[301] H. Zhang, Y. Li, J. Wang, N. Wu, H. Sheng, C. Chen, J. Zhao, An unprecedent hydride transfer pathway for selective photocatalytic reduction of CO_2 to formic acid on TiO_2, Appl. Catal. B-Environ. 284 (2021) 119692.
[302] X. Jiang, Y. Ding, S. Zheng, Y. Ye, Z. Li, L. Xu, J. Wang, Z. Li, X.J. Loh, E. Ye, L. Sun, In-situ generated $CsPbBr_3$ nanocrystals on O-defective WO_3 for photocatalytic CO_2 reduction, ChemSusChem 15 (2022) e202102295.

[303] Y.-X. Feng, H.-J. Wang, J.-W. Wang, W. Zhang, M. Zhang, T.-B. Lu, Stand-alone CdS nanocrystals for photocatalytic CO_2 reduction with high efficiency and selectivity, ACS Appl. Mater. Interfaces 13 (2021) 26573–26580.
[304] W.C. Chung, S.Y. Hsu, C.W. Pao, Y.C. Chuang, K.T. Lu, J.M. Chen, Correlation of photocatalytic CO_2 conversion and electronic structure of UiO-66 and Cu-UiO-66-NH_2 under irradiation studied by in-situ X-ray absorption spectroscopy, J. CO_2 Util. 60 (2022) 101961.
[305] Z. Sun, W. Fang, L. Zhao, H. Chen, X. He, W. Li, P. Tian, Z. Huang, g-C_3N_4 foam/Cu_2O QDs with excellent CO_2 adsorption and synergistic catalytic effect for photocatalytic CO_2 reduction, Environ. Int. 130 (2019) 104898.
[306] W.-F. Wang, Y.-K. Zhang, L.-F. Feng, H.-R. Li, L.-N. He, In-plane benzene incorporated g-C_3N_4 microtubes: enhanced visible light harvesting and carrier transportation for photocatalytic CO_2 reduction, Fuel 326 (2022) 125073.
[307] L. Wang, L. Zang, F. Shen, J. Wang, Z. Yang, Y. Zhang, L. Sun, Preparation of Cu modified g-C_3N_4 nanorod bundles for efficiently photocatalytic CO_2 reduction, J. Colloid Interface Sci. 622 (2022) 336–346.
[308] J. Fu, K. Liu, K. Jiang, H. Li, P. An, W. Li, N. Zhang, H. Li, X. Xu, H. Zhou, D. Tang, X. Wang, X. Qiu, M. Liu, Graphitic carbon nitride with dopant induced charge localization for enhanced photoreduction of CO_2 to CH_4, Adv. Sci. 6 (2019) 1900796.
[309] G. Wang, Z. Chen, T. Wang, D. Wang, J. Mao, P and Cu dual sites on graphitic carbon nitride for photocatalytic CO_2 reduction to hydrocarbon fuels with high C_2H_6 evolution, Angew. Chem. Int. Ed. 61 (2022) e202210789.
[310] J. Wang, T. Heil, B. Zhu, C.-W. Tung, J. Yu, H.M. Chen, M. Antonietti, S. Cao, A single Cu-center containing enzyme-mimic enabling full photosynthesis under CO_2 reduction, ACS Nano 14 (2020) 8584–8593.
[311] L. Cheng, X. Yue, L. Wang, D. Zhang, P. Zhang, J. Fan, Q. Xiang, Dual-single-atom tailoring with bifunctional integration for high-performance CO_2 photoreduction, Adv. Mater. 33 (2021) 2105135.
[312] Y. Tan, J. Ma, F. Zhang, S. Wang, F. Lan, H. Liu, R. Li, Polymer photocatalyst-enzyme coupled artificial photosynthesis system for CO_2 reduction into formate using water as the electron donor, ACS Sustain. Chem. Eng. 10 (2022) 12065–12071.
[313] H. Shi, H. Wang, Y. Zhou, J. Li, P. Zhai, X. Li, G.G. Gurzadyan, J. Hou, H. Yang, X. Guo, Atomically dispersed indium-copper dual-metal active sites promoting C-C coupling for CO_2 photoreduction to ethanol, Angew. Chem. Int. Ed. 61 (2022) e202208904.
[314] L. Zeng, J.-W. Chen, L. Zhong, W. Zhen, Y.Y. Tay, S. Li, Y.-G. Wang, L. Huang, C. Xue, Synergistic effect of Ru-N_4 sites and Cu-N_3 sites in carbon nitride for highly selective photocatalytic reduction of CO_2 to methane, Appl. Catal. B-Environ. 307 (2022) 121154.
[315] H. Ou, S. Ning, P. Zhu, S. Chen, A. Han, Q. Kang, Z. Hu, J. Ye, D. Wang, Y. Li, Carbon nitride photocatalysts with integrated oxidation and reduction atomic active centers for improved CO_2 conversion, Angew. Chem. Int. Ed. 61 (2022) e202206579.
[316] Y. Duan, Y. Wang, W. Zhang, J. Zhang, C. Ban, D. Yu, K. Zhou, J. Tang, X. Zhang, X. Han, L. Gan, X. Tao, X. Zhou, Simultaneous CO_2 and H_2O activation via integrated Cu single atom and N vacancy dual-site for enhanced CO photo-production, Adv. Funct. Mater. 33 (2023) 2301729.
[317] H. Sakamoto, M. Maciel, F. Henrique Cardoso, L. Kulay, Energy and environmental contributions for future natural gas supply planning in brazil, Energy Technol. 8 (2019) 1900976.
[318] X. Li, C. Li, Y. Xu, Q. Liu, M. Bahri, L. Zhang, N.D. Browning, A.J. Cowan, J. Tang, Efficient hole abstraction for highly selective oxidative coupling of methane by Au-sputtered TiO_2 photocatalysts, Nat. Energy (2023) 1013–1022.
[319] J. Tang, P.V. Kumar, J.A. Scott, J. Tang, M.B. Ghasemian, M. Mousavi, J. Han, D. Esrafilzadeh, K. Khoshmanesh, T. Daeneke, A.P. O'Mullane, R.B. Kaner, M. A. Rahim, K. Kalantar-Zadeh, Low temperature nano mechano-electrocatalytic CH_4 conversion, ACS Nano 16 (2022) 8684–8693.
[320] S. Wang, V. Fung, M.J. Hülsey, X. Liang, Z. Yu, J. Chang, A. Folli, R.J. Lewis, G. J. Hutchings, Q. He, N. Yan, H_2-reduced phosphomolybdate promotes room-temperature aerobic oxidation of methane to methanol, Nat. Catal. (2023) 895–905.
[321] C. He, S. Wu, Q. Li, M. Li, J. Li, L. Wang, J. Zhang, Constructing matched active sites for robust photocatalytic dry reforming of methane, Chem (2023).
[322] X. Zhang, Y. Xu, Y. Liu, L. Niu, Y. Diao, Z. Gao, B. Chen, J. Xie, M. Bi, M. Wang, D. Xiao, D. Ma, C. Shi, A novel Ni-MoC_xO_y interfacial catalyst for syngas production via the chemical looping dry reforming of methane, Chem 9 (2023) 102–116.
[323] Y. Wang, J. Zhang, W.X. Shi, G.L. Zhuang, Q.P. Zhao, J. Ren, P. Zhang, H.Q. Yin, T.B. Lu, Z.M. Zhang, W single-atom catalyst for CH_4 photooxidation in water vapor, Adv. Mater. 34 (2022) 2204448.
[324] P. Xie, J. Ding, Z. Yao, T. Pu, P. Zhang, Z. Huang, C. Wang, J. Zhang, N. Zecher-Freeman, H. Zong, D. Yuan, S. Deng, R. Shahbazian-Yassar, C. Wang, Oxo dicopper anchored on carbon nitride for selective oxidation of methane, Nat. Commun. 13 (2022) 1375.
[325] X. Yuan, Y. Peng, X. Zhu, H. Wang, Z. Song, W. Si, Y. Wang, J. Li, Anti-poisoning mechanisms of Sb on vanadia-based catalysts for NO_x and chlorobenzene multi-pollutant control, Environ. Sci. Technol. 57 (2023) 10211–10220.
[326] F. Gholami, M. Tomas, Z. Gholami, M. Vakili, Technologies for the nitrogen oxides reduction from flue gas: a review, Sci. Total Environ. 714 (2020).
[327] M. Guo, Q. Liu, C. Liu, X. Wang, Y. Bi, B. Fan, D. Ma, X. Liang, Z. Li, Rational design of novel CrZrO catalysts for efficient low temperature SCR of NO, Chem. Eng. J. 413 (2021) 136712.
[328] S.M. Mousavi, H. Fatehi, X.-S. Bai, Numerical study of the combustion and application of SNCR for NO reduction in a lab-scale biomass boiler, Fuel 293 (2021) 120154.
[329] J. Fragoso, D. Barreca, L. Bigiani, A. Gasparotto, C. Sada, O.I. Lebedev, E. Modin, I. Pavlovic, L. Sánchez, C. Maccato, Enhanced photocatalytic removal of NOx gases by β-Fe_2O_3/CuO and β-Fe_2O_3/WO_3 nanoheterostructures, Chem. Eng. J. 430 (2022) 132757.
[330] V. Khanal, N.O. Balayeva, C. Günnemann, Z. Mamiyev, R. Dillert, D. W. Bahnemann, V. Subramanian, Photocatalytic NO_x removal using tantalum oxide nanoparticles: a benign pathway, Appl. Catal. B-Environ. 291 (2021) 119974.
[331] H. Wang, K. Li, J. Li, Y. Sun, F. Dong, Photochemical transformation pathways of nitrates from photocatalytic NO_x oxidation: implications for controlling secondary pollutants, Environ. Sci. Technol. Lett. 8 (2021) 873–877.
[332] X. Bai, X. Zhao, Y. Zhang, C. Ling, Y. Zhou, J. Wang, Y. Liu, Dynamic stability of copper single-atom catalysts under working conditions, J. Am. Chem. Soc. 144 (2022) 17140–17148.
[333] B.-H. Lee, S. Park, M. Kim, A.K. Sinha, S.C. Lee, E. Jung, W.J. Chang, K.-S. Lee, J. H. Kim, S.-P. Cho, H. Kim, K.T. Nam, T. Hyeon, Reversible and cooperative photoactivation of single-atom Cu/TiO_2 photocatalysts, Nat. Mater. 18 (2019) 620–626.
[334] C. Ban, Y. Wang, Y. Feng, Z. Zhu, Y. Duan, J. Ma, X. Zhang, X. Liu, K. Zhou, H. Zou, D. Yu, X. Tao, L.-Y. Gan, G. Han, X. Zhou, Photochromic single atom Ag/TiO_2 catalysts for selective CO_2 reduction to CH_4, Energy Environ. Sci. (2024).